1976

Surface and Bulk Transport Coefficients in Antimony.

Ching-long Tsai
Louisiana State University and Agricultural & Mechanical College

INFORMATION TO USERS

This material was produced from a microfilm copy of the original document. While the most advanced technological means to photograph and reproduce this document have been used, the quality is heavily dependent upon the quality of the original submitted.

The following explanation of techniques is provided to help you understand markings or patterns which may appear on this reproduction.

1. The sign or "target" for pages apparently lacking from the document photographed is "Missing Page(s)". If it was possible to obtain the missing page(s) or section, they are spliced into the film along with adjacent pages. This may have necessitated cutting thru an image and duplicating adjacent pages to insure you complete continuity.

2. When an image on the film is obliterated with a large round black mark, it is an indication that the photographer suspected that the copy may have moved during exposure and thus cause a blurred image. You will find a good image of the page in the adjacent frame.

3. When a map, drawing or chart, etc., was part of the material being photographed the photographer followed a definite method in "sectioning" the material. It is customary to begin photoing at the upper left hand corner of a large sheet and to continue photoing from left to right in equal sections with a small overlap. If necessary, sectioning is continued again — beginning below the first row and continuing on until complete.

4. The majority of users indicate that the textual content is of greatest value, however, a somewhat higher quality reproduction could be made from "photographs" if essential to the understanding of the dissertation. Silver prints of "photographs" may be ordered at additional charge by writing the Order Department, giving the catalog number, title, author and specific pages you wish reproduced.

5. PLEASE NOTE: Some pages may have indistinct print. Filmed as received.

University Microfilms International
300 North Zeeb Road
Ann Arbor, Michigan 48106 USA
St. John's Road, Tyler's Green
High Wycombe, Bucks, England HP10 8HR

SURFACE AND BULK TRANSPORT COEFFICIENTS IN ANTIMONY

A Dissertation

Submitted to the Graduate Faculty of the
Louisiana State University and
Agricultural and Mechanical College
in partial fulfillment of the
requirements for the degree of
Doctor of Philosophy

in

The Department of Physics and Astronomy

by
Ching-Long Tsai
M.S., Louisiana State University, 1973
December, 1976

ACKNOWLEDGEMENT

The author wishes to express his appreciation to Dr. Claude G. Grenier for his patient guidance throughout the course of this work. The author is especially indebted to Dr. David L. Waldorf for his assistance in the lab and in preparation of this thesis, and to Dr. K. Tanaka for his cooperation in the initial phase of this work.

The author also gratefully acknowledges the contributions from members of the dissertation committee and members of the low temperature group. Thanks are also due to Ms. Jackie Tamas and Ms. Martha Prather who typed this manuscript. In addition, the financial assistance received from the Dr. Charles E. Coates Memorial Fund of the L.S.U. Foundation donated by George H. Coates for preparation of this manuscript is gratefully acknowledged.

At last, the author wishes to thank his parents' encouragement and in particular, his wife's patience and love.

TABLE OF CONTENTS

LIST OF TABLES

LIST OF FIGURES

CAPTION OF FIGURES

Fig. 1 A schematic diagram of the cross-section of a sample with a damaged surface layer.

Fig. 2 Apparent magnetoresistivity at T = 4.21 K of sample #9 as a function of field H. Curve (A) is that for the portion of the sample which was strongly etched while Curve (B) corresponds to the portion for which the surfaces were lapped.

Fig. 3 The apparent conductivities ($1/\rho_{11}$) of the different samples, with various surface treatments, as functions of the reciprocal of their average size (1/d). (□) samples #1 through #12, surfaces roughly lapped. (x) samples #5 through #8, surfaces lightly etched. (O) samples #9 through #12, surfaces strongly etched. (·) samples #1 through #4, surfaces etched for random periods. (+) samples #13 through #16, surfaces electropolished. (Δ) sample #17, surface electropolished and then etched. The broken line marked represents the electropolated bulk conductivity of each sample.

Fig. 4 Apparent conductivities of samples #13 through #16 at H=20KG as a function of the reciprocal of their average size (1/d) at three different

temperatures: T = 1.2K (·), T = 3.0K (+), T = 4.22K (0).

Fig. 5 The apparent deviation from the Bridgmann relation for sample #17 at H = 20KG, given here as as continuous line. The ratio σ_{11}(bulk)/ σ_{11}(expt.) is given by (0).

Fig. 6 Nernst-Ettingshausen effect and Ettinghausen effect in sample #17 at H = 20 KG as a function of temperature. The measured Nernst-Ettingshausen coefficient ε'_{21}(expt.), shown by (Δ), corresponds to the scale on the right side of the figure. The measured Ettingshausen coefficient π'_{21}(expt.), shown by (+), corresponds to the scale on the left side of the figure. For comparison the quantity $T\varepsilon'_{21}$(expt.) is also shown by (o) where it clearly appears that π'_{21}(expt.) $\neq T\varepsilon'_{21}$(expt.).

Fig. 7 A schematic diagram of the Ettingshausen heat current pattern across the sample section.

Fig. 8 The measured magnetoresistivity of sample #17 as a function of temperature for H = 20KG. Curve D(x) gives the adiabatic magnetoresistivity (sample chamber evacuated). Curve A (□) gives the isothermal magnetoresistivity (see text). Curve E, F (o) gives the magnetoresistivity measured with the sample in contact

with liquid helium. The data, shown by (·) (+) and (Δ), are the magnetoresistivities measured when the sample chamber was filled with helium gas at liquid nitrogen temperature with pressure 790 mmHg, 590 mmHg and 260 mmHg respectively. Curve B and C are discussed in the text.

Fig. 9 $\Delta\rho_{11}$ is the change in the magnetoresistivity observed at λ-point for samples immersed in liquid helium. ρ_{11} is the measured resistivity with all data points in a field of 20KG.

Fig. 10 Kapitza resistance R_K versus temperature T for H = 20KG. The data for Si are taken from Johnson and Little (Ref. 34).

Fig. 11 The different regions of phonons in q-space. Region 1: the volume common to "a" and "b". Region 2: the volume of "a" except "1". Region 3: the volume "b" except "1". Region 4: the region outside "a" and "b" (peripheral phonons).

Fig. 12 Thermal conductivity of sample #17 in zero field. The measured values, λ_T, are shown by Curve E. The electronic thermal conductivity, $\lambda_e = \lambda_T - \lambda_g$, is shown by dotted line (...) or Curve F. Lattice conductivity, λ_g, is shown by Curve A. Curve C (— - —), D (—···—)

and B (---) are total, electronic and lattice thermal conductivity respectively which were taken from White and Woods (Ref. 50).

Fig. 13 The product of carrier thermal resistivity, γ_e, and temperature, T, versus T^3. The slope of the straight line is coefficient B. The intersection of straight line and $\gamma_e T$-axis gives ρ_o/L_o. The bending of the curve is attributed to Debye integral, J_5, (see text).

Fig. 14 Lattice conductivity, λ_g, divided by T^2 versus T. λ_g^{en} is the contribution of enclosed phonons (see Ref. 28, Eq. (17)) and $\Delta\lambda_g$ is the mutual drag contribution as estimated by Gurevich et al. (ref. 42).

Fig. 15 The electrical resistivity in zero field, ρ, as a function of temperature, T. The different symbols correspond to the measurements of different runs. The solid curve was determined by a least square fit of the data.

Fig. 16 The ideal resistivity, ρ_{id}, versus temperature. The data is fitted to Eq. (58) with $\textcircled{H}_4^* = 15.7K$.

Fig. 17 The ratio of the "ideal" Lovenz number, $(\lambda_e)id/\sigma_{id}T$, versus T^2. The measured values are given by (.). The solid line is given by Eq. (86) with $\textcircled{H}_4^* = 15.7K$ and $\tilde{\textcircled{H}}_h^* = 25K$.

Fig. 18 The measured Lorenz number in zero field, L, as a function of temperature.

Fig. 19 Thermoelectric power in zero field, $\varepsilon(0)$, versus temperature. The measured values are given by (0), the dashed curve (---) is taken from Bresler and Red'ko (Ref. 10), and the broken line (— - —) corresponds to carrier diffusive term of TEP.

Fig. 20 The ratio of TEP, $\varepsilon(0)$, to T versus T^2. The measured values of this study are shown by (⊙). The data points shown by (+) are taken from Crosby (Ref. 61).

Fig. 21 The lattice conductivity, λ_g, divided by T^2 versus T. The data of this investigation are designated by (+) while the data of Blewer et al. (Ref. 28) are designated by (⊙). Curve A is estimated from Eq. (95) and Curve B is estimated from Eq. (96).

Fig. 22 The measured values of the exponent of lattice conductivity,

$$n = \frac{d(\ell n\ \lambda_g)}{d(\ell n\ T)} ,$$

as a function of temperature.

Fig. 23 The measured values of electronic thermal magnetoconductivity at H = 3KG, as a function of temperature. The data points are shown by (.).

Fig. 24 The apparent electronic thermal magnetoresistivities, $(\gamma_e)_{11}$, at T = 4.2K(+) and T = 2.1K (.) as a function of field H.

Fig. 25 The saturated field for electrons, $H\lambda_e$, versus T^3. The experimental points (.) were determined from Eq. (97), (98) and (99). The upper curve (---) is fit to Eq. (100) for $\textcircled{H}_e^*$ = 29K and lower curve (— - —) for $\textcircled{H}_e^*$ = 28K.

Fig. 26 The saturated field for holes, Hλh, versus T^3, determined by the same procedure as for Hλe. Upper curve is fit for $\textcircled{H}_h^*$ = 26K and lower curve is for $\textcircled{H}_h^*$ = 25K.

Fig. 27 The apparent magnetoresistivity of sample #17 at T = 4.22K, as a function of field H.

Fig. 28 The apparent magnetoresistivity of sample #17 at H = 20KG, as a function of temperature. Curve A gives the isothermal magnetoresistivity. Curve E, F give the magnetoresistivity measured as sample immersed in liquid helium bath. Curve D gives the adiabatic magnetoresistivity. Curves G and H are isothermal and adiabatic magnetoresistivity in the non-drag limit respectively. Curve K is deduced from the zero

field resistivity with application of Kohler's rule.

Fig. 29 The ideal magnetoconductivity, $\sigma_{e-p}(H)$, at H = 20KG versus temperature. The data given by (+) is fitted to Eq. (53) with $\textcircled{H}_e^* = 26K$.

Fig. 30 Lorenz number at high field limit, $H\sigma_e/H\lambda_e$, versus T. The apparent values are shown by Curve A. The bulk values are shown by Curve B. The non-drag limit values are shown by Curve C.

Fig. 31 The "ideal" Lorenz number at high field limit, $H_{\sigma e}^{id}/H_{\lambda e}^{id}$, versus T^2. The data given by (.) are fitted with $\textcircled{H}_e^* = 25K$.

Fig. 32 The apparent density of electronic states at the Fermi surface of S_b, Z_{eff}, versus T^2. The data shown by (+) are determined from $\langle\varepsilon''_{21}\rangle = \langle\sigma_{11}\rangle\lambda_g \langle\varepsilon'_{21}\rangle$ and Eq. (105). The data shown by (.,x) are determined from $\langle\pi''_{21}\rangle = \langle\sigma_{11}\rangle\lambda_g\langle\pi'_{21}\rangle$ and Eq. (105). The data shown by (⊙) and (□) are taken from Crosby (Ref. 61) and Long *et al.* (Ref. 20) respectively.

ABSTRACT

The effect of diverse surface treatments on magnetoresistivity of antimony single crystals of different size has been studied and the contribution of surface and bulk current has been determined, and consequently these results have been used to obtain the bulk transport coefficients. Transport measurements on electropolished samples under the asymptotic high field condition were analyzed empirically. Measurements of adiabatic and isothermal magnetoresistivity, Nernst-Ettingshausen and Ettingshausen effects and thermal resistivity indicate that the experimentally determined coefficients can be related in a simple manner with the bulk coefficients if proper correction for surface effect is applied. Two phenomenological models, referred to in the text as the layer and skin models, were developed with layer model showing good agreement with sample possessing damaged surfaces and the skin model showing good agreement with etched or electropolished surfaces. The fact that resistance measured in superfluid helium is not completely isothermal is used to determine the Kapitza resistance. The analysis of the bulk transport coefficients leads to the following conclusion. The consistency of the Ziman cutoff confirms the proposed mechanisms. The deformation potentials of both carriers were also obtained. There is a strong simple phonon drag effect in Nernst-Ettingshausen effect and a strong mutual drag effect in

magnetoresistivity and Ettingshausen effect. The drag contributions in TEP and ideal resistivity are rather small due to the drag compensation. There is no observable drag effect in either carrier thermal resistivity or lattice conduction.

INTRODUCTION

Antimony, like bismuth and arsenic, is a semimetal. Though its transport properties have been studied by de Haas-van Alphen effect, Shubnikov-de Haas effect, ultrasonic attenuation, cyclotron resonance, radio-frequency size effect (RFSE), magnetoreflection, microwave resonance, resonance Raman scattering, infrared absorption and galvanomagnetic as well as thermomagnetic effects at high and low temperature, there still exists many unsolved problems in this area. Therefore, we will attempt in this thesis to cover some of the principal questions in which useful information can and should be gathered.

Generally speaking, the questions relate to size effect, surface current, Kapitza resistance, electron-phonon scattering and mutual as well as simple drag phenomena. The effects of size and surface current on the transport coefficients at low temperature and high magnetic field are treated in Chapter I of this thesis, the Kapitza resistance between antimony and superfluid helium and its measurement in Chapter II. The third chapter of this thesis includes electron-phonon normal process intravalley scattering and their mutual as well as simple drag effects at zero and high magnetic fields in the helium temperature range.

The Appendix includes thermal conduction measurement and the bridge equations, misalignment and spurious effects, equations of damaged-layer model and the equation of Kapitza

resistance between antimony and superfluid helium surface. The experimental details for the ideal resistivity and thermoelectric power (TEP) at zero field can also be found in the Appendix.

CHAPTER I

EFFECT OF SURFACE LAYER CURRENT ON THE TRANSPORT COEFFICIENTS IN ANTIMONY MONOCRYSTAL AT LOW TEMPERATURES AND HIGH MAGNETIC FIELD

A. Introduction

The transverse magnetoresistance of semi-metals (Bi and Sb) at low temperatures is known to be affected, both in magnitude and magnetic field dependence, by the condition of the surface of the sample.[1-11] Typically, the magnetoresistance of an emery-lapped specimen can be increased several fold by a short chemical etching. The expected quadratic dependence on magnetic field is replaced by a H^{α} dependence, where $\alpha < 2$, wherein, for example, $\alpha \sim 1.6$ describes an emery-lapped specimen and $\alpha \sim 1.9$ is found after the short etching.

The present investigation includes a study of magnetoresistance as well as a study of other transport effects which are likewise affected by the condition of the surface. These results are discussed by recourse to two empirical models of surface conductance.

The sample may have a damaged layer on its surface. The effect of this layer on the measured magnetoresistivity may be described in gross approximation by regarding the specimen as two parallel conductors: a bulk conductance which is strongly reduced by the magnetic field and the damaged surface layer conductance which is only weakly affected by the magnetic field. The relative contribution of the latter to the total conductance will depend on such

parameters as degree of crystalline disorder, thickness of the layer and the magnetic field.

The scattering of charge carriers at the surface and in the adjacent damaged layer is rather different from that in the bulk in the amounts of intra- and intervalley scattering. The electron and hole distributions at the surface will be different from those in the bulk, and the transition from surface to bulk rather than occurring abruptly at the surface or at the damaged/bulk interface occurs smoothly over a length characteristic of some effective bulk scattering such as bulk intervalley or interband scattering. As the surface distribution "diffuses" into the bulk distribution over an effective diffusion length, one may look upon the layer adjacent to the surface (or adjacent to the damaged layer) as having different transport properties from the bulk and particularly in terms of the conduction contribution. What was said about the damaged layer being in parallel with the bulk can also be said about the diffusion layer being in parallel with the bulk. For that matter, one may consider for conduction purposes the system of a damaged layer, a diffusion layer, and the bulk as a system of conductors in parallel.

The diffusion layer contribution is expected to depend on the field and on the type of scattering in the bulk and in the damaged layer or at the surface (i.e. diffuse versus specular scattering contribution of the surface). Also, a completely different condition exists if the sample surface

under consideration is perpendicular to the magnetic field, or if the surface is parallel to both magnetic and electric fields. In the latter case both electrons and holes have the same transverse drift velocity (the Hall velocity) so that hole-electron pairs are created on one surface, drift across the sample and recombine on the other surface through interband scattering. Such a state of affairs has been recognized as a major factor in the "diffusion size effect" observed in bismuth.[2]

If the effective layer thickness is small compared to the dimensions of the sample cross-section in either the case of diffusion or damaged layers, it may then be expected for identically prepared surfaces that the measured magnetoresistivity depends linearly on $P/4A$, where P is the perimeter and A is the area of the cross section.[12] Whenever a transport coefficient, besides conductivity, is to be determined, the presence of the layers gives rise to an inhomogeneous distribution of currents and thereby this measured transport coefficient may show some apparent discrepancy with the relationships expected from crystal symmetry or from the Onsager reciprocal relations.[13] In this respect, the Ettingshausen and Nernst-Ettingshausen effects have been found to be of particular interest. Both of these effects are large enough to be measured accurately, they correspond to fundamental transport processes easily formulated at high magnetic fields and the bulk coefficients are expected to satisfy Bridgmann's relation.[13] The present

investigation reveals an apparent non-compliance of the experimentally determined coefficients with either Bridgmann's or the symmetry relations or both. When this discrepancy is analyzed in terms of difference in distribution of heat current density, $\vec{w}^*$, and electrical current density, $\vec{J}$, in the separate measurements, some interesting information can be obtained relative to surface current properties.

The present surface study is an outgrowth of a more general transport effect study in antimony as it became apparent that a correction for surface conductance should be made for the correct determination of bulk coefficients. Since the original purpose was mainly to obtain corrective terms, the present study is not as systematic as that of Hattori[2] on the bismuth magnetoresistance nor that of Bogod and Drasovitskii[3] on the magnetoresistance of antimony.

Our findings on the influence of damaged layers and the changes resulting from surface treatment by chemical etching and electropolishing on the magnetoresistance are in general agreement with those of other investigators. Our results are reported in part 1 of the section on results and discussion.

The influences of surface currents on the other transport effects are to be found in parts 2, 3, and 4 of the same section. The data relating to this study were in large part measured on an electropolished sample (#17).

Surface treatment other than etching and electropolishing such as coating with diverse substance was also undertaken. It was found that these treatments did not affect significantly the surface conduction effects, and that most of this change could be correlated qualitatively with the effect that coating will have on the thermal contact between the sample and the helium bath. The result of this study will not be given here, instead only those results which pertain to the thermal contact of a clean sample with the bath will be considered. The thermal contact of this sample with liquid He I and liquid He II as well as with vapor and saturated and unsaturated superfluid films is analyzed in terms of the degree of adiabatic/isothermal characteristics displayed by the measured magnetoresistance of the sample.

As a consequence of this study determination of the Kapitza resistance[14] R_K between antimony and superfluid helium is made and the reasonable value found for this resistance seems to indicate that a workable method utilizing Ettingshausen heat can be used for the determination of R_K for material with a large figure of merit. The result and discussion of the Kapitza resistance between antimony and superfluid helium will be reported in Chapter II.

B. Experimental Detail and Transport Coefficients

Sample Preparation

The monocrystalline samples of different sizes were cut by a spark cutter[15] from the same pure antimony ingot.[16]

These samples are at least 6 cm long and have a nearly square cross section. The average section size d = 4 A/P (where A is the area and P the perimeter of the cross section) is for these nearly square sections a good approximation for either width or thickness. The values of l/d for the different samples are given in Table I. These samples all have the same crystallographic orientation. The long dimension, that is, the current direction, is parallel to the bisectrix axis which is denoted as the x or 1-direction. The lateral faces are perpendicular to the binary axis (y or 2) and to the trigonal axis (z of 3) which is always the direction of the applied magnetic field. With this choice of crystallographic orientation, the bulk resistivity, thermoelectric, Peltier and thermal conductivity tensors are reduced to relatively simple forms.

After spark cutting the surface treatment consisted of first lapping on #600 emery paper and then etching just half of the total length of the sample. In this way we created two specimens of nearly identical size and bulk characteristics which differed only in the condition of the surfaces. The etching removed most of the damaged surface layer of thickness 10 to 30 μm, however microscopic observation revealed that the surface was still quite rough. A group of samples (#5 to #8) was partially etched, removing an estimated 10 μm thick layer. A prolonged but uncontrolled etching applied to samples #1 to #4 removed an estimated 10 to 30 μm. The last group, #9 to #12, underwent an even longer and

Table I

#	$\frac{l}{d}$ (b)	Rough Surface (a) $\rho_{11}(H)$ (c)	Rough Surface (a) α (e)	Treated Surface $\rho_{11}(H)$ (c)	Treated Surface α (e)	Surface Treatment
1	2.52	1.331	1.60	5.662	1.96	
2	3.47	1.284	1.57	3.583	1.93	Uncontrolled chemical etching
3	3.85	.890	1.59	2.617	1.92	
4	4.17	.945	1.57	2.922	1.92	
5	2.31	1.402	1.64	2.555	1.90	
6	5.14	.669	1.59	1.044	1.88	Light etching
7	7.70	.547	1.52	.824	1.90	
8	15.12	.286	1.52	.415	1.80	
9	2.65	1.537	1.63	4.792	1.96	
10	4.04	.942	1.59	3.473	1.96	Strong etching
11	5.97	.746	1.58	2.959	1.96	
12	10.77	.458	1.58	1.597	1.95	
13	2.09			8.384	1.97	
14	6.67			4.637	1.97	Electro-polishing
15	2.65			7.663	1.97	
16	4.55			5.869	1.97	
17	3.45			8.081	1.98	(d)

(a) After spark cutting, the samples were lapped on #600 emery paper.

(b) Average size $d = 4\ A/P$ is measured in cm (A is the area of the cross section, P is the perimeter).

(c) ρ_{11} is measured in mΩcm. The number of figures given are not representative of the precision. H = 20 kG and T = 4.22 K.

(d) Same treatment as samples #13 to #16, followed by a light chemical etch.

(e) $\rho_{11}(H) \propto H^{\alpha}$ over the range of field 1 to 24 kG.

controlled etching. Another group of samples, #13 to #17, were, after the spark cutting and lapping operations, electropolished in a basic solution KOH + $C_3H_5(OH)_3$ + H_2O.[17] The resulting surfaces in contrast with those produced by etching, were strikingly mirrorlike. Sample #17 was subsequently cleaned rapidly in the acid etching solution, and contrary to expectation this rapid etching improved the bulk property of the sample instead of bringing its properties more in line with the etched samples #9 to #12.

The Bulk Transport Coefficents

Even though standard measurements of simple transport coefficients were involved here, it will be helpful to examine the general transport equations for bulk material in order to understand some of the problems arising because of the nature of thermal contact between the sample and the liquid He bath as well as the influence of the surface layers.

In the notation used by Jan[18,19] the bulk transport equations can be written in tensor form:

$$\begin{aligned} \vec{J} &= \hat{\sigma}\vec{E}^* - \hat{\varepsilon}''\vec{G} \\ \vec{w}^* &= -\hat{\pi}''\vec{E}^* + \hat{\lambda}''\vec{G} \end{aligned} \tag{1}$$

or

$$\begin{aligned} \vec{E}^* &= \hat{\rho}\vec{J} + \hat{\varepsilon}\vec{G} \\ \vec{w}^* &= -\hat{\pi}\vec{J} + \hat{\lambda}\vec{G} \end{aligned} \tag{2}$$

or

$$\begin{aligned} \vec{E}^* &= \hat{\rho}^a\vec{J} + \hat{\varepsilon}'\vec{w}^* \\ \vec{G} &= \hat{\pi}'\vec{J} + \hat{\gamma}\vec{w}^* \end{aligned} \tag{3}$$

where $\vec{J}$ is the electric current density and $\vec{G}$ is the negative thermal gradient. The quantities $\vec{E}^*$ and $\vec{w}^*$ are the electric field and heat current modified for convenience by terms involving the carrier's chemical potential. For all practical purposes, under the conditions in which the measurements were performed, $\vec{w}^*$ can be replaced by $\vec{w}$, the heat current and $\vec{E}^*$ by $\vec{E}$, the electrostatic potential.

The different transport tensors are: the electrical conductivity $\hat{\sigma}$ and resistivities $\hat{\rho}$, $\hat{\rho}^a$; the thermoelectric $\hat{\varepsilon}$, $\hat{\varepsilon}'$, $\hat{\varepsilon}''$; the Peltier $\hat{\pi}$, $\hat{\pi}'$, $\hat{\pi}''$; the thermal conductivities $\hat{\lambda}''$, $\hat{\lambda}$ and resistivity $\hat{\gamma}$.

With the field H applied in the direction of the trigonal axis, 3, these tensors are expected, by crystal symmetry, to have the form

$$a = \begin{vmatrix} a_{11} & a_{12} & 0 \\ -a_{12} & a_{11} & 0 \\ 0 & 0 & a_{33} \end{vmatrix} \tag{4}$$

and to have the following symmetries relative to the magnetic field

$$\begin{aligned} a_{12}(H) &= a_{21}(-H) = -a_{21}(H) \\ a_{11}(H) &= a_{11}(-H). \end{aligned} \tag{5}$$

Only the coefficients a_{21}, a_{11} are of principal interest in this study because currents and gradients are limited to the basal plane.

Further simplications at very high field are expected as verified in previous work:[20] ε'_{11} is negligible with respect to ε'_{21} and this is also true in the tensors $\hat{\varepsilon}$, $\hat{\varepsilon}''$, $\hat{\pi}$, $\hat{\pi}'$,

and $\hat{\pi}''$. Also ρ_{21} is negligible relative to ρ_{11} so that for most practical matters, the $\hat{\rho}$ tensor is diagonal, and also this is the case for the tensors $\hat{\sigma}$, $\hat{\rho}^a$, $\hat{\lambda}$, $\hat{\lambda}''$ and $\hat{\gamma}$. It may be pointed out that electrical and thermal conduction along the field 3-direction remain at nearly their zero field value, while decreasing several orders of magnitude along the 1 and 2 direction, perpendicular to the field, with $\sigma_{33} >> \sigma_{11}$ as $\sigma_{11} \propto H^{-2}$ and $\lambda_{33} >> \lambda_{11}$ as $\lambda_{11} \to \lambda_g$, the lattice conduction. Corresponding relations will apply to the respective coefficient in $\hat{\lambda}''$, $\hat{\rho}$, $\hat{\rho}^a$ and $\hat{\gamma}$. At 20 kG, $\sigma_{11} \sim 10^{-5}\ \sigma_{33}$ and at T = 2 K, $\lambda_g < 10^{-2}\ \lambda_{33}$. A list of measured coefficients is given in Table II along with the conditions of measurement. Some other coefficients derived from these measured coefficients are

Isothermal electric conductivity $\sigma_{11} = [\rho^{-1}]_{11} \simeq \rho_{11}^{-1}$;

Isothermal thermal conductivity $\lambda_{11} \simeq \lambda_g = [\gamma^{-1}]_{11} \simeq \gamma_{11}^{-1}$

Some relations of interest in our case are

$$\varepsilon'_{21} \sim \rho_{22}\varepsilon''_{21}\gamma_{11} \text{ and } \pi'_{21} \sim \gamma_{22}\pi''_{21}\rho_{11} \quad (6)$$

and

$$\rho_{11} - \rho^a_{11} = -[\hat{\varepsilon}\hat{\pi}']_{11} = -[\hat{\varepsilon}'\hat{\lambda}\hat{\pi}']_{11} \sim -\varepsilon_{12}\lambda_{22}\pi'_{21} \simeq \varepsilon'_{21}\lambda_g\pi'_{21}. \quad (7)$$

Bridgmann's relation $\pi_{21}(-H) = T\varepsilon_{12}(H)$ yields

$$\pi'_{21} = T\varepsilon'_{21}. \quad (8)$$

In all the above expressions use has been made of symmetry (5) and simplification brought about by deletion of negligible terms.

Table II

Isothermal electric resistivity	$\rho_{11} = E_1/J_1$	$J_2=G_2=G_1=0$
Adiabatic electric resistivity	$\rho^a_{11} = E_1/J_1$	$J_2=w^*_2=w_2=w_1=0$
Adiabatic thermal resistivity	$\lambda_{11} = G_1/w_1$	$J_1=J_2=w^*_2=w_2=0$
Adiabatic Ettingshausen coefficient	$\pi'_{21} = G_2/J_1$	$J_2=w^*_1=w_2=w^*_2=0$
Adiabatic Nernst-Ettingshausen coefficient	$\varepsilon'_{21} = E^*_2/w_1$	$J_1=J_2=w_2=w^*_2=0$

The Layer Model Transport Coefficients

The presence of surface layer conductance will alter the measured transport coefficients from their high field bulk values.[21] In order to describe these changes a simple model, sketched in Fig. 1, is introduced which has the following properties:

a) The layer transport properties are identical with those of the bulk, except for larger scattering frequencies in the layers.

b) The thickness of the layer, δ, is large enough so that uniform transport tensors can be defined for the layer with the same symmetries as in Eqs. (4) and (5), but small enough relative to d, the sample cross section size, to allow the model to be limited to the first order in δ/d.

c) The scattering frequency in the layer is much larger than that in the bulk, but small enough so that the asymptotic high field condition is also satisfied. Thus on the one

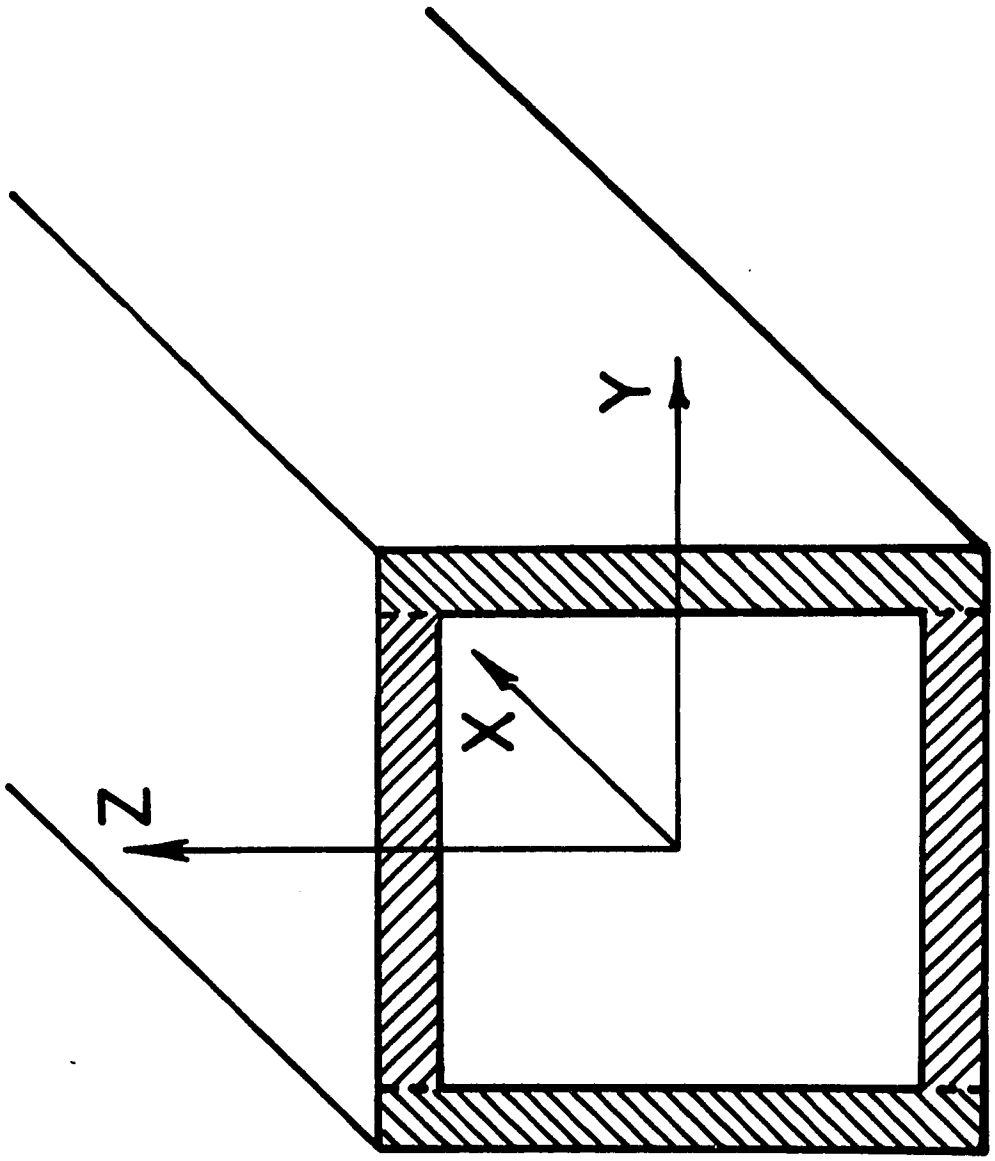

Fig. 1

hand $\sigma_{11s} >> \sigma_{11b}$, on the other γ_{11}, ϵ''_{12}, π''_{12}, etc., are the same in the layer as in the bulk and ρ_{21}, γ_{21}, ϵ_{11}, etc., are negligible everywhere.

d) The length of the sample in the x-direction is large so that the end surfaces may be disregarded and the model reduces to the juxtaposition of a bulk core with 4 surface layers. In this conductor configuration, effective transport coefficients can be calculated (see Appendix A). For the determination of the effective resistivity coefficient in the x-direction $\langle \rho_{11} \rangle$ the bulk core and the 4 layers are in parallel and the equipotential is normal to the x-direction. Under this configuration and the above assumptions one obtains

$$\frac{\langle \sigma_{11} \rangle}{\sigma_{11b}} = \frac{\rho_{11b}}{\langle \rho_{11} \rangle} = p_1 = 1 + \frac{2\delta_y}{d}\left(\frac{\sigma_{11sy}}{\sigma_{11b}} - 1\right) + \frac{2\delta_z}{d}\left(\frac{\sigma_{11sz}}{\sigma_{11b}} - 1\right)$$

$$\text{or} \quad p_1 \sim 1 + \frac{2\delta_y}{d}\frac{\sigma_{11sy}}{\sigma_{11b}} + \frac{2\delta_z}{d}\frac{\sigma_{11sz}}{\sigma_{11b}}. \tag{9}$$

Hereafter the brackets, $\langle\ \rangle$, denote measured or effective quantities; δ_y and δ_z are the thicknesses of layers normal to the y- and z-axes respectively, while σ_{11sy} and σ_{11sz} are the conductivities of these layers. For the conduction in the y-direction one obtains

$$\frac{\langle \sigma_{22} \rangle}{\sigma_{11b}} = \frac{\rho_{11b}}{\langle \rho_{22} \rangle} = p_2 = 1 + \frac{2\delta_y}{d}\left(1 - \frac{\sigma_{11b}}{\sigma_{11sy}}\right) + \frac{2\delta_z}{d}\left(\frac{\sigma_{11sz}}{\sigma_{11b}} - 1\right)$$

$$\text{or} \quad p_2 \sim 1 + \frac{2\delta_z}{d}\frac{\sigma_{11sz}}{\sigma_{11b}}. \tag{10}$$

Similar expressions are found for all other effective transport coefficients(see Appendix A), but these can be expressed with a good approximation in the simple forms, such as

$$\frac{\langle \varepsilon'_{21} \rangle}{\varepsilon'_{21b}} \sim \frac{\langle \pi'_{12} \rangle}{\pi'_{12b}} \sim \frac{\langle \rho_{22} \rangle}{\rho_{11b}} = \frac{1}{p_2}$$
$$\frac{\langle \varepsilon'_{12} \rangle}{\varepsilon'_{12b}} \sim \frac{\langle \pi'_{21} \rangle}{\pi'_{21b}} \sim \frac{\langle \rho_{11} \rangle}{\rho_{11b}} = \frac{1}{p_1} \qquad (11)$$

and $\langle \lambda_{11} \rangle = \langle \lambda_{22} \rangle = \lambda_{11b} = \lambda_g$.

It is interesting to note that this model preserves the Bridgmann relation since

$$\frac{\langle \pi'_{21} \rangle}{T \langle \varepsilon'_{12} \rangle} = \frac{\pi'_{21b}}{T \varepsilon'_{12b}}$$

but the tensor symmetry is broken since

$$-\frac{\langle \varepsilon'_{12} \rangle}{\langle \varepsilon'_{21} \rangle} \simeq -\frac{\langle \pi'_{21} \rangle}{\langle \pi'_{12} \rangle} \simeq \frac{\langle \rho_{22} \rangle}{\langle \rho_{11} \rangle} = \frac{p_1}{p_2}.$$

For the difference between isothermal and adiabatic resistivities we have

$$\langle \rho_{11} \rangle - \langle \rho^a_{11} \rangle = -\frac{\varepsilon'_{12b} \lambda_g \pi'_{21b}}{p_1^2} \simeq \langle \varepsilon'_{21} \rangle \lambda_g \langle \pi'_{21} \rangle \frac{p_2}{p_1}. \qquad (12)$$

This expression can be also reduced to the useful form

$$\frac{\langle \rho_{11} \rangle - \langle \rho^a_{11} \rangle}{\langle \rho_{11} \rangle} \sim -\left(\frac{\varepsilon''_{12} \pi''_{21}}{\lambda_g}\right) \langle \rho_{11} \rangle. \qquad (13)$$

The Skin Model

The layer model will be best suited for describing samples with damaged surface layers, even though the neglect

of proximity effects may restrict its usefulness. The removal of those layers by etching and electropolishing will eliminate surface currents on the faces normal to the z-axis. The damaged layer currents on the y-faces also disappear but currents arising from diffusion of carriers within an effective thickness δ might discernibly alter the measured transport coefficients from their bulk values.[22]

The layer model might be extended to this situation by setting $p_2 = 1$ in the above formulae. However it is doubtful that the layer model could describe diffusion layer condition which is basically a proximity effect. Therefore a model is constructed upon fundamentally different assumptions which are more in line with diffusion layer conduction, namely:

a) The effective thickness of the diffusion layer δ is small compared to the sample width d, it is dependent on the surface condition and bulk properties.

b) The average diffusion current density is proportional to the bulk current density.

c) There is no "skin heat current" in the case of thermal conduction.

d) In the case of thermoelectric phenomena $\vec{E}$ and $\vec{G}$ depend only on $\vec{w}^*$ and $\vec{J}_b$ and are independent of the fraction of the current carried in the skin.

The apparent current density components are related to the "bulk density" by $\vec{J}_1 = q_1\vec{J}_{1b}$ and $\vec{J}_2 = q_2\vec{J}_{2b}$ with $q_2 \sim 1$ and where $q_1 > 1$ and like p_1 in the layer model depends

linearly on (1/d). (A more general assumption such as $\vec{J} = \hat{q}\vec{J}_b$ could be used, but this would involve unnecessary complications.) Under the above assumptions, the fundamental transport equations (1), (2), (3) are altered only by the replacement of J_{1b} by J_1/q_1 and J_{2b} by J_2/q_2 yielding the following relation between the effective and bulk coefficients.

$$\frac{\langle a_{1i}\rangle}{a_{1ib}} = q_1 \text{ and } \frac{\langle a_{2i}\rangle}{a_{2ib}} = q_2 \sim 1 \text{ for } a \equiv \sigma \text{ and } \varepsilon''$$

$$\frac{\langle a_{i1}\rangle}{a_{i1b}} = \frac{1}{q_1} \text{ and } \frac{\langle a_{i2}\rangle}{a_{i2b}} = \frac{1}{q_2} \sim 1 \text{ for } a \equiv \rho,\ \rho^a,\ \pi \text{ and } \pi' \tag{14}$$

$$\frac{\langle a_{ij}\rangle}{a_{ijb}} = 1 \qquad \text{for } a \equiv \varepsilon,\lambda,\varepsilon',\gamma,\pi'',\lambda''.$$

Some of the useful relations are

$$\frac{\langle \rho_{11}\rangle}{\rho_{11b}} = \frac{\sigma_{11b}}{\langle \sigma_{11}\rangle} = \frac{\langle \rho^a_{11}\rangle}{\rho^a_{11b}} = \frac{\langle \pi'_{21}\rangle}{\pi'_{21b}} = \frac{1}{q_1}$$

$$\frac{\langle \rho_{22}\rangle}{\rho_{22b}} = \frac{\sigma_{22b}}{\langle \sigma_{22}\rangle} = \frac{\langle \rho^a_{22}\rangle}{\rho^a_{22b}} = \frac{\langle \pi'_{12}\rangle}{\pi'_{12b}} = \frac{1}{q_2} \sim 1 \tag{15}$$

and

$$\frac{\langle \varepsilon'_{21}\rangle}{\varepsilon'_{21b}} = \frac{\langle \varepsilon'_{12}\rangle}{\varepsilon'_{12b}} = \frac{\lambda_{11}}{\lambda_g} = \frac{\lambda_{22}}{\lambda_g} = 1.$$

These relations show some partial break in the symmetry relations (4) and (5) as well as in Bridgmann relation (8). Another useful relation which can be obtained is

$$\langle \rho_{11}\rangle - \langle \rho^a_{11}\rangle = \langle \varepsilon'_{21}\rangle\langle \pi'_{21}\rangle\lambda_g \tag{16}$$

which also can be formulated:

$$\frac{\langle \rho_{11}\rangle - \langle \rho^a_{11}\rangle}{\langle \rho_{11}\rangle} \sim \left(\frac{\pi''_{21}\varepsilon''_{21}}{\lambda_g}\right)_b \rho_{11b}. \tag{17}$$

Let's note that when we suppose $p_2 = q_2 = 1$ both models yield

$$\frac{\langle \rho_{11} \rangle}{\rho_{11b}} = \frac{\langle \pi'_{21} \rangle}{\pi'_{21b}} = \frac{1}{p_1} \text{ (or } \frac{1}{q_1} < 1) \text{ and } \frac{\langle \varepsilon'_{21} \rangle}{\varepsilon'_{21b}} = 1. \quad (18)$$

However the skin model gives

$$\langle \rho_{11} \rangle - \langle \rho^a_{11} \rangle = \langle \varepsilon'_{21} \rangle \langle \pi'_{21} \rangle \lambda_g$$

while the layer model yields $\langle \varepsilon'_{21} \rangle \langle \pi'_{21} \rangle \lambda_g \, p_1^{-1}$ for the same quantity. Also for the skin model the relative change

$$\frac{\langle \rho_{11} \rangle - \langle \rho^a_{11} \rangle}{\langle \rho_{11} \rangle}$$

should be independent of sample size and surface treatment; whereas it is proportional to $\langle \rho_{11} \rangle$ for the layer model.

Experimental Procedure

The data reported here are limited to the temperature range 1.2 to 4.2 K and the magnetic field up to 24 kG. In the relation with measurement of Ettingshausen and Nernst-Ettingshausen and related effects, field values of 10 and 20 kG were used. The magnetic field was always applied in the trigonal 3-direction.

The techniques of the measurement of transport coefficients are similar to those used in preceding works,[19,20] with experimental procedures chosen to correct for spurious effects (see Appendix E).

The primary currents $\vec{J}$ and $\vec{w}^*$ were applied along the bisectrix 1-direction. The electrical currents, sufficient to give a measured longitudinal potential difference of

$\sim$100 μv, were usually 1 to 5 mA depending on the magnetic field. The applied heat currents were sufficient to give a longitudinal temperature differences of 40 to 60 mK and ranged from $\sim$ 2 mW at 4.2 K and $\sim$2 μW at 1.4 K. The potential difference measurements for the magnetoresistance in the 1-direction and for the Nernst-Ettingshausen coefficient in the 2-direction were made with a Rubicon potentiometer[23] using a 147 Keithley nano-voltmeter as the null detector. Temperature gradient measurements for thermal resistance in the 1-direction and the Ettingshausen coefficients in the 2-direction were made with Allen-Bradley carbon resistors.[24] (See Appendix B and C.)

The Sb sample was soldered with Cd-Bi to an auxilliary heater mounting which in turn was thermally anchored to a 17 mm diameter Cu rod which in turn was in contact with the liquid He bath. For the so-called adiabatic[25] measurements, the sample was enclosed in a vacuum space.

For other measurements, the sample was in contact with the liquid He bath. Several experiments were also carried out with He exchange gas in the sample chamber. This last arrangement enabled also the measurement of magnetoresistance in the presence of unsaturated or saturated He films.

C. Results and Discussion

1. The Effect of Size and Surface Treatment on Magnetoresistance

In general agreement with the results of other investigators,[2,3] we found, for very pure samples, (a) that

the various surface treatments, emery-lapped, partially etched, strongly etched, and electropolished, increases the magnetoresistances in that order; (b) magnetoresistance in the range 1 to 24 kG can be described by $\rho \propto H^{\alpha}$ where $\alpha < 2$; (c) the value of α is the lowest for the most damaged surfaces and approaches 1.98 for the surfaces which gave the greatest magnetoresistance; (d) the value of α is only slightly temperature dependent in the liquid He range; (e) the α values were practically size independent except for the thinnest of the rough surface samples where the size dependence was only slight.

Table I presents the magnetoresistivity and the α values for samples of various sizes and surface conditions for the temperature 4.2 K. The ρ_{11} data corresponds to a 20 kG field.

The field dependence of the magnetoresistance of sample #9 is shown in Fig. 2. Curve B corresponds to the measurements on that part of the sample which was emery lapped and curve A to the other part which was lapped and subsequently etched. At 20 kG the measurements differ by a factor of nearly three with α values of 1.63 and 1.96 respectively.

In Figs. 3 and 4 the conductivities of the various samples are plotted as a function of 1/d. The most striking feature of this plot is the nearly linear dependence of σ upon 1/d for samples which have been given the same surface treatment. The magnetoconductivities of the electropolished samples #13, 14, 15, 16 all with $\alpha \simeq 1.97$ display the linear

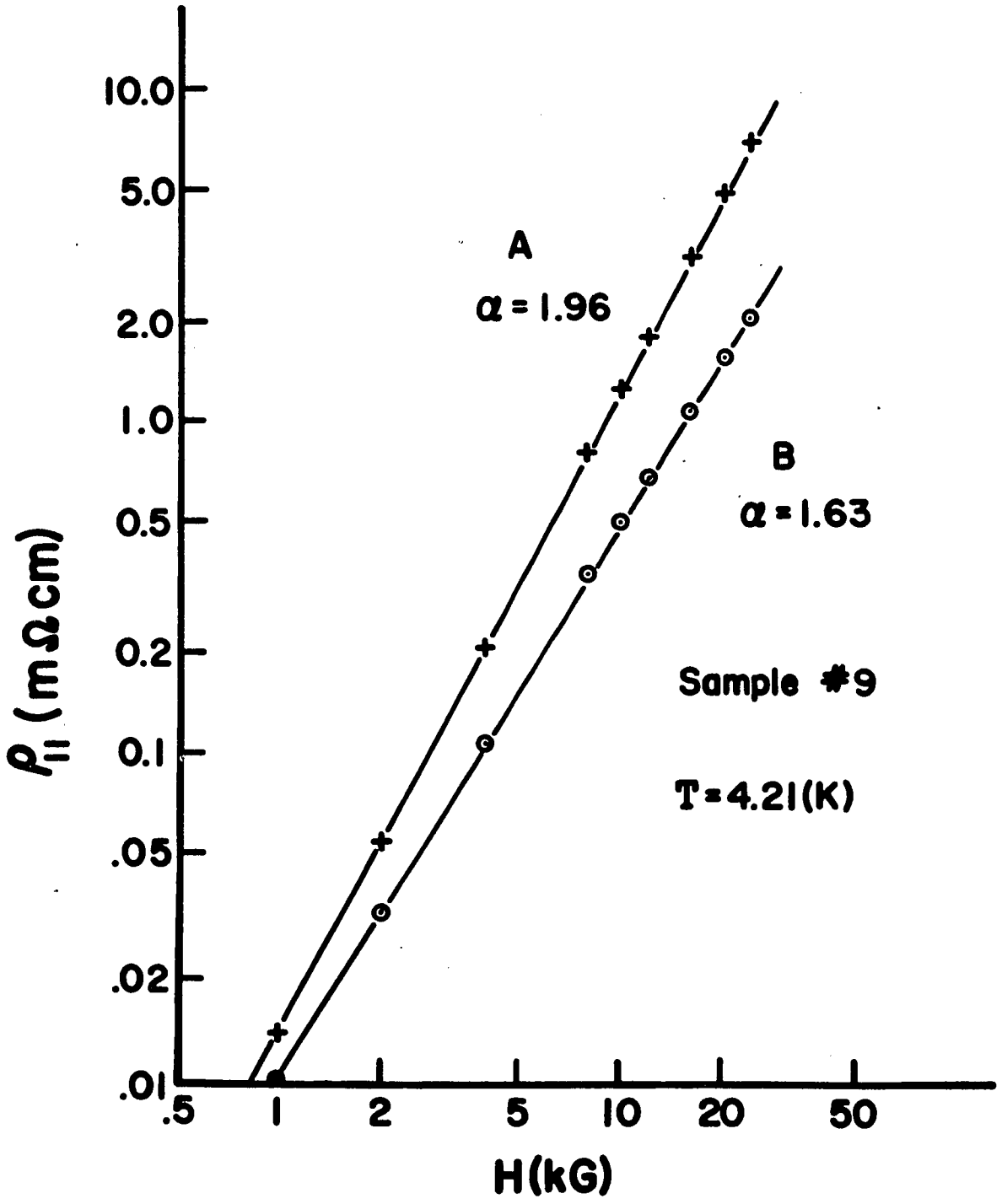
10.0
5.0
2.0
1.0
0.5
0.2
0.1
.05
.02
.01
ρ_{11} (mΩcm)
.5
1
2
5
10
20
50
H(kG)
A
α = 1.96
B
α = 1.63
Sample #9
T = 4.21(K)

Fig. 2

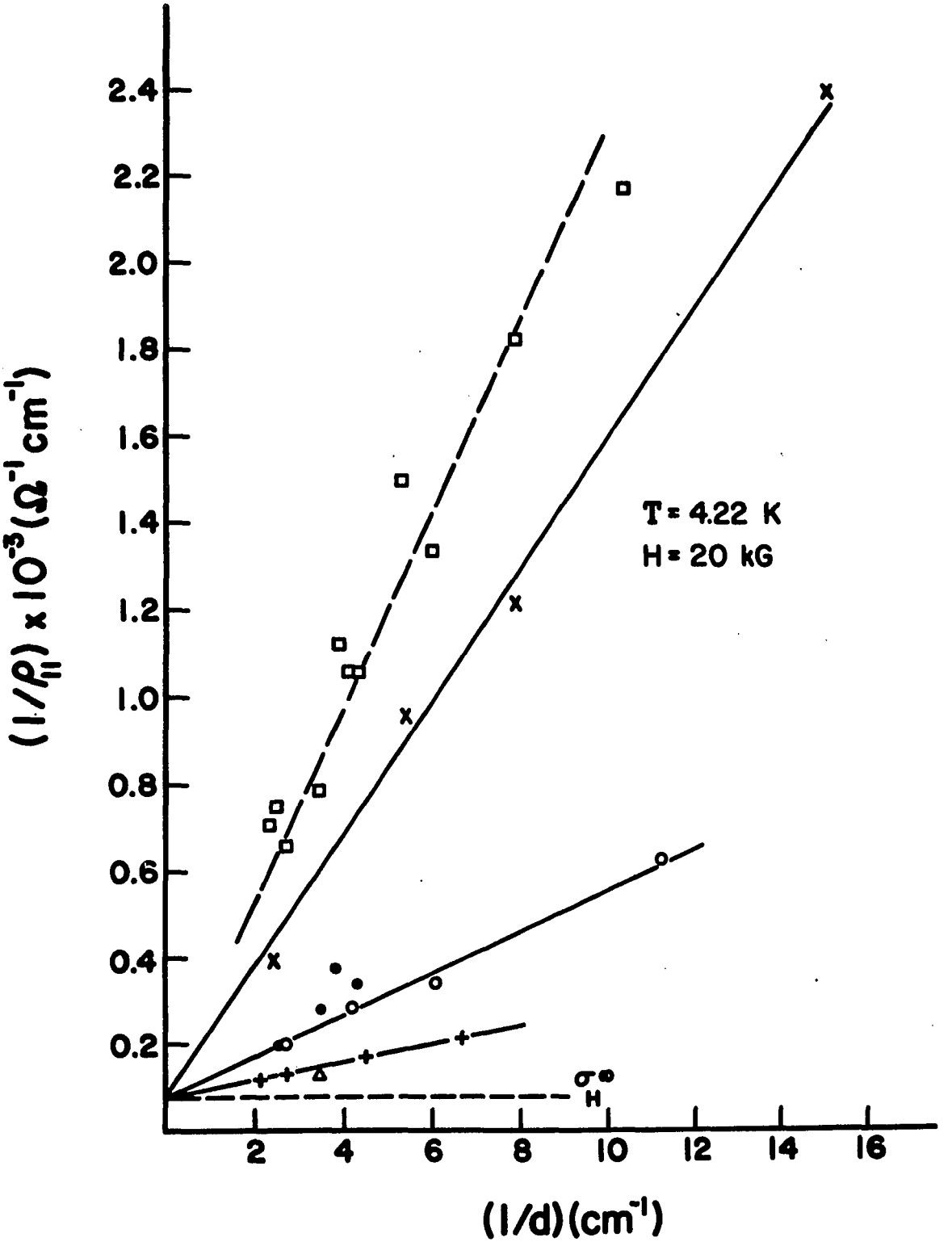
2.4
2.2
2.0
1.8
1.6
1.4
1.2
1.0
0.8
0.6
0.4
0.2
$(1/\rho_{11}) \times 10^{-3} (\Omega^{-1} cm^{-1})$
T = 4.22 K
H = 20 kG
σ_H^{∞}
2
4
6
8
10
12
14
16
(1/d)(cm^{-1})

Fig. 3

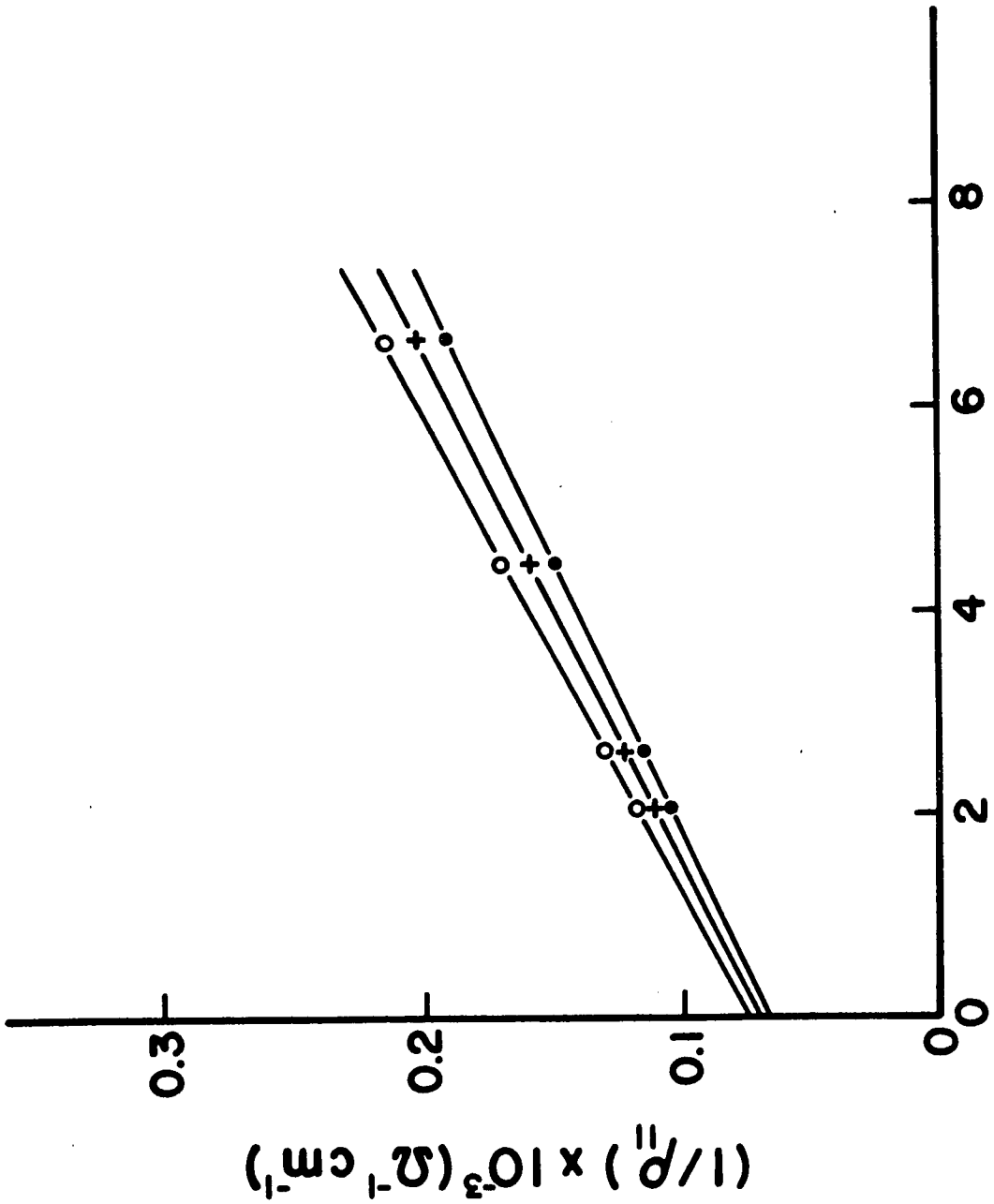

Fig. 4

dependence on 1/d. The set of etched samples #9, 10, 11, 12 all with $\alpha \simeq 1.96$ also showed a good linear 1/d dependence. However the samples #1, 2, 3, 4 treated by uncontrolled etching showed assorted α values and scattered conductivity values. Sample #1 with $\alpha = 1.96$ fell in the preceding category and fit their 1/d dependence. Another set #5, 6, 7, 8 in which the surface treatment involved a light but roughly controlled etching with the exception of the thinnest sample gave $\alpha \sim 1.90$; the measured conductivities also showed an acceptable 1/d dependence.[26] The trend shown by the samples with lapped (rough) surfaces is in accord with that of the etched and polished samples but the α values are lower ($\alpha \sim 1.6$) and show a light dependence on 1/d. For each of the sets of data corresponding to different surface treatments, extrapolation to $1/d = 0$ (i.e. $d \to \infty$) can be made and the extrapolated values for $1/\rho_{11}$ are in rough agreement for the various sets and may be regarded as the bulk conductivity, σ_{11b}. From Fig. 3, $\frac{1}{\rho_{11b}} \sim \sigma_{11b} \sim 70\ \Omega^{-1}\text{cm}^{-1}$ for $H = 20$ kG and $T = 4.21$ K and from Fig. 4 the same extrapolation yields σ_{11b} at three different temperatures. The ratio $q = \frac{\langle \rho_{11} \rangle}{\rho_{11b}}$ (i.e. $\sigma_{11b}/\langle \sigma_{11} \rangle$) between measured resistivity and bulk resistivity can be determined for each sample and the corresponding values for sample #17 are shown on Fig. 5.

It is apparent from these results that the concept of surface layer conductance is consistent with the observed size dependence of the magnetoconductivity. However the nature of the mechanism of surface layer conduction is not

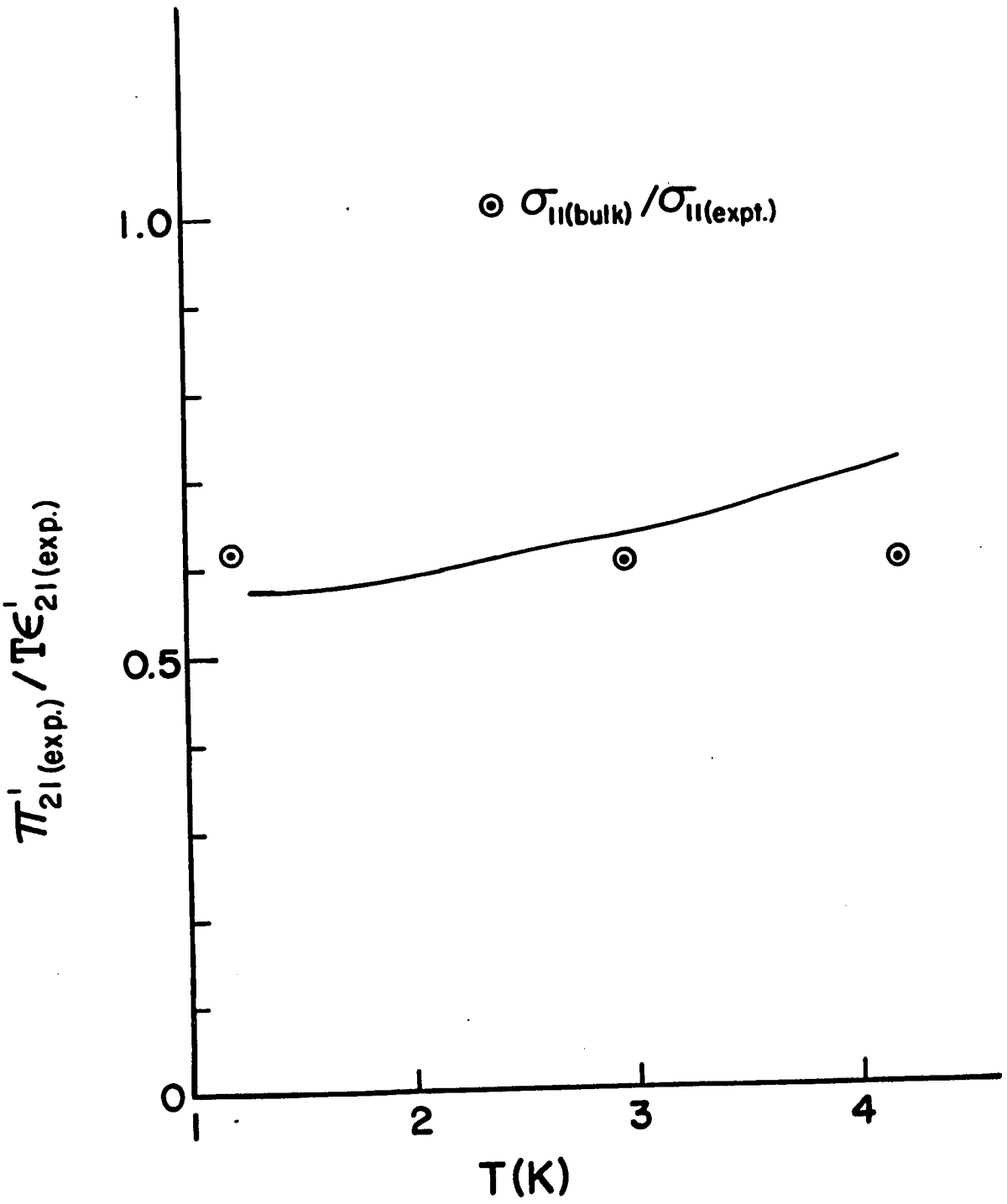

Fig. 5

clear. On the one hand a highly conductive layer must exist on samples with emery lapped surfaces and partially etched surfaces, but on the other hand these layers must have been removed by strong etching or electropolishing. Therefore we could conclude that the excess conduction of the samples with rough surfaces over those with strongly etched or polished surfaces could arise from the diversion of significant fraction of the total current into layers possessing conductivities significantly greater than that of the bulk. Thus, at first glance we have a situation described by the damaged layer model. However, it is mostly unlikely that two parallel conductors of rather different characteristics would both exhibit a nearly perfect H^{α} magnetic field dependence. Even in the cases where the surface conductance exceeds that of the bulk we must expect the proximity of the two parallel conductors to modify the total conductance in a manner which is beyond the scope of the above damaged layer model. For example, in Sb there is no inhibition of the transverse drift of electron-hole pairs because of charge carrier compensation, so hole-electron pairs are created on one surface, drift through the damaged layers and the bulk to the opposite side where they recombine. This interchange provides one possible mechanism which affects both layer and bulk conductances. Other mechanisms, such as intervalley scattering, must also enter. For samples in which the damaged surface layers have been removed, we expect that scattering by the surfaces perpendicular to the magnetic

field corresponds to a simple boundary scattering which makes only a negligible contribution to the total conductance. The surfaces perpendicular to the y- or drift direction can give a type of scattering which has been designated as the "diffusion size effect."[2] If the diffusion processes are confined to a narrow region of the surface we can empirically describe the transport coefficients by equations similar to those for the damaged layer model (7). In the case of Bi, where interband scattering is the principal mechanism of the diffusion size effect, Hattori[2] has derived the following equation for the effective conductivity.

$$\langle \sigma_{11} \rangle = \sigma_{11b} + \frac{n_h ec}{H} \frac{V_e + V_h}{H} \frac{2}{d[\sqrt{D^*/\tau_{eh}} + S]} \qquad (19)$$

where e and h refer to electron and hole properties, $n_h ec/H$ is the high field Hall conductivity $|\sigma_{12e}|$, $(V_e + V_h)/H$ is the high field transverse carrier diffusion coefficient, D^* is the ambipolar diffusion coefficient, τ_{eh} is the bulk electron-hole interband scattering time, and d is the width of the specimen. This equation neglects the contribution of the surfaces normal to the magnetic field. $V_{e,h} = \frac{2}{3}(\xi_{e,h}/e)$ where $\xi_{e,h}$ is the Fermi energy of electrons, holes measured from the band edge. S is the electron-hole surface recombination velocity.

σ_{11b}, the bulk magnetoconductivity, varies as H^{-2}. The diffusive size term depends on d^{-1} and its field dependence will be H^{-2} times the field dependence of $(\sqrt{D^*/\tau_{eh}} + S)^{-1}$. D^* is expected to vary as H^{-2} but τ_{eh} and S are regarded as

having only a very slight field dependence. Thus our results for samples which have been strongly etched or electropolished, indicate the very slight departure of the magnetoresistivity from quadratic field dependence may be regarded as a consequence of the factor $\sqrt{D^*/\tau_{eh}}$ being negligible compared to S, the surface recombination velocity. Thus neglecting $\sqrt{D^*/\tau_{eh}}$ an estimate of S can be made. For sample #17 $S \sim 6.9 \times 10^6$ cm/sec. For the etched samples #1 and #9 through #12 (etched surfaces) $S \sim 1.6 \times 10^6$ cm/sec and for the electropolished samples #13 - #16, $S \sim 4.1 \times 10^6$ cm/sec. These values are of the same order as those found in Bi.[2] It is to be noted that these values are intermediate between the Fermi velocity ($v_F \simeq 2.2 \times 10^7$ cm/sec) and the average sound velocity ($v_s \sim 2.5 \times 10^5$ cm/sec).

Extensive investigations of recombination in semiconductors show that S depends upon the degree of specular reflection occurring at the sample surface,[27] the greater the coefficient of specular reflection the smaller the recombination velocity. It would seem that electropolished surfaces as a matter of course possess a greater coefficient of specular reflection than the chemically etched surfaces, simply because the former surfaces exhibit a more perfect mirror like quality. However our results are not in accord with these preconceptions since our electropolished samples have larger recombination velocity than the etched samples.

The results on the samples with emery lapped surface cannot be understood as a simple extension of diffusive terms alone unless damaged layer conductance is superposed.

In conclusion, the linear dependence of the magnetoconductivity with 1/d (the inverse of the cross section size) strongly supports the concept of thin surface layer current under d.c. current condition. Even though one may conjecture a possible difference between the different models corresponding to emery lapped surface samples versus electropolished samples, one cannot decide between these models on the basis of size dependence alone. Both layer and skin models outlined in the preceding section yield a p_1 (or q_1) coefficient linear in 1/d and that will be true also for models based on some similar assumption. Azbel[7,8] "static skin effect" yields the 1/d dependence and so does the "diffusion size effect" as formulated by Hattori[2] or empirically interpreted by Bogod and Krasovitskii.[3]

2. Lattice Thermal Conduction

With heat flowing in the 1-direction and magnetic field applied along the 3-direction, the thermal conductivity is observed to saturate about 3-5 kG, that is, $\lambda_{11} = \lambda_{11e} + \lambda_g$ tends to λ_g, the lattice thermal conductivity, since λ_{11e}, the carrier contribution, decreases as H^{-2}. The values of λ_g for various crystals[28] are in good agreement; and even though no systematic study of size effect and surface treatment has been performed, all indications are that λ_g will

not show any important size or surface treatment dependence. In other words, $\vec{w}^*$ is uniform over the sample cross section in contrast to the electrical current density $\vec{J}$. Thus $\lambda_g^{-1} = \gamma_{11} = \gamma_{22} = \gamma_{11(bulk)}$ applies for the entire sample cross section regardless of the presence of damaged layers, etc.

3. Nernst-Ettingshausen and Ettingshausen Effects

The Nernst-Ettingshausen effect is measured directly under the conditions $w_2 = w_2^* = J_1 = J_2 = 0$ with the applied heat current w_1^* and we have $E_2^*/w_1^* = \varepsilon'_{21}$ or $E_2^*/G_1 = \varepsilon_{21}$. Experimental procedures correct for the spurious potential, and furthermore no correction needs to be made on the experimental ε'_{21} coefficient for thermocouple effects since the Righi-Leduc effect is negligible (indeed $\gamma_{21} = 0$ yields $G_2 = 0$). The coefficient ε'_{21} was found proportional to the magnetic field and the values for H = 20 kG are given in Fig. 6.

The Ettingshausen effect G_2/J_1 is measured with $w_2, J_2, w_2^* = 0$ and the electrical current density J_1 set along the sample. In principle we would like to have $w_1 = 0$, but small spurious heat flow appears in the sample, and Eq. (3) would yield $G_2 = \pi'_{21}J_1 + \gamma_{21}w_1^*$. Experimental procedure would partially correct for the spurious heat term $\gamma_{21}w_1^*$, but since $\gamma_{21} \sim 0$ this correction can be neglected. Thus G_2/J_1 yields π'_{21}. This coefficient exhibits the expected proportionality with the magnetic field and the values at 20 kG as a function

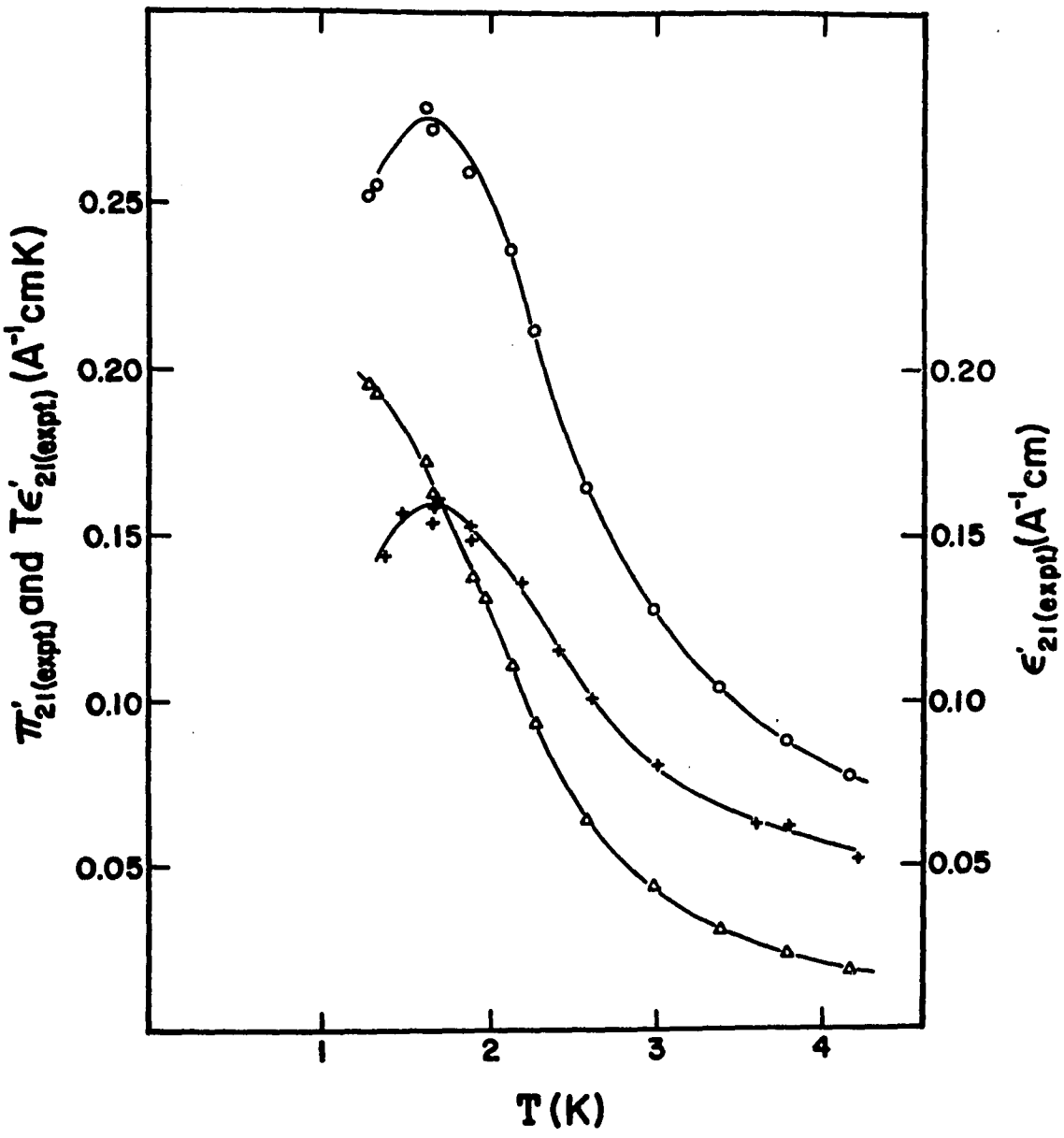
0.25
0.20
0.15
0.10
0.05
1
2
3
4
T(K)
$\pi'_{21(expt)}$ and $T\epsilon'_{21(expt)}$ ($A^{-1}cmK$)
$\epsilon'_{21(expt)}$($A^{-1}cm$)

Fig. 6

of temperature are given in Fig. 6. To test the Bridgmann relation[13] on the bulk form, (Eq. 8) $\pi'_{21} = T\varepsilon'_{21}$, the quantity $T\varepsilon'_{21}$(20 kG) is also presented in Fig. 6. It can be seen, though the temperature dependence of $T\varepsilon'_{21}$ and π'_{21} are very nearly the same, that the former is larger than the latter by a factor of about 1.7. One possible interpretation is that a significant fraction of the total electrical current flows superficially and makes only a negligible contribution to the transverse temperature difference. The resulting temperature difference then arises mostly from the bulk current. It should be noted that the damaged layer model and the skin model both predict the same ratio for $\pi'_{21b}/\langle\pi'_{21}\rangle$, i.e. $\langle\sigma_{11}\rangle/\sigma_{11b}$ (Eqs. 11 and 15). Our size effect measurement in sample #17 yields $\langle\sigma_{11}\rangle/\sigma_{11b} \sim 1.6$ which is within error the same value obtained for $T\varepsilon'_{21}/\langle\pi'_{21}\rangle$. Thus we could explain the apparent discrepancy in the Bridgmann relation by assuming $\langle\varepsilon'_{21}\rangle = \varepsilon'_{21b}$ which is consistent with the skin model, or with the layer model when one supposes $p_2 = 1$, i.e. that the z-layers do not carry surface current.

In Fig. 5 both experimental values $\langle\pi'_{21}\rangle/T\langle\varepsilon'_{21}\rangle$ and $\sigma_{11b}/\langle\sigma_{11}\rangle$ for sample #17 at 20 kG are shown for comparison and are seen to match rather well. It is difficult to know whether the apparent discrepancy in the high temperature range is significant since the mismatch is within experimental error.

In conclusion, the Ettingshausen and Nernst-Ettingshausen effects in an electropolished Sb sample seem in favor of the skin model or possibly a layer-type model with surface current only on the y-faces, i.e. the faces parallel to magnetic field and current.

4. Isothermal and Adiabatic Magnetoresistance

Part 1 of this section was confined to the results of the size effect in magnetoconductivity. Other information is brought to light by investigating the magnetoresistivity under isothermal and adiabatic conditions.

All surface treatments described in part 1 relate to direct treatments such as chemical etching, mechanical and electropolishing. Indirect treatments such as coating the surfaces with either grease or varnish also were made in an exploratory manner so as to check their effects on the magnetoresistance. The result of this study shows that the residual magnetoresistivity of the coated samples (i.e. the value of ρ_{11} extrapolated to T = 0 K) does not deviate by more than 2% from the values obtained on uncoated samples. These discrepancies can be ascribed to uncertainties in the absolute determinations of magnetoresistivities. When, on the other hand, study is made of the effect that surface coating has on the temperature dependent part of the magnetoresistance, it is found consistent with the assumption that only the thermal conductance from the sample to the bath is decreased, thus making the condition of

measurement closer to being adiabatic.

If the electrical current density J_1 flows through the sample under truly isothermal conditions, there will be an Ettingshausen heat current $w_2^* = -\pi_{21}J_1$ according to Eq. (2) flowing across the sample, since $G_2 = 0$. Thus there will be heat current into the sample from the bath on one side and back into the bath on the other side of the sample. If this transverse heat flow is stopped ($w_2 = 0$) then a transverse temperature gradient is generated across the sample as seen from Eq. (3) and the magnetoresistivity takes on its adiabatic value. When the sample is immersed in either liquid or vapor He, the situation is intermediate between isothermal and adiabatic; that is, both G_2 and w_2^* are non-zero. The principal factors determining the heat flow, w_2^*, are the thermal resistance between the sample and its bath and the thermal resistivity of the bath itself. In relation to the effect of coating on the magnetoresistance it was qualitatively determined that the coating was impeding the w_2 heat flow and bringing the magnetoresistivity closer to its adiabatic value. A flow diagram corresponding to this situation is represented in Fig. 7. Because of the trivial outcome of the coating experiments the following study is limited to uncoated samples.

The magnetoresistivity of sample #17, uncoated, measured under the following environmental situations: high vacuum, liquid He I, liquid He II, helium vapor and saturated helium films gave the following results:

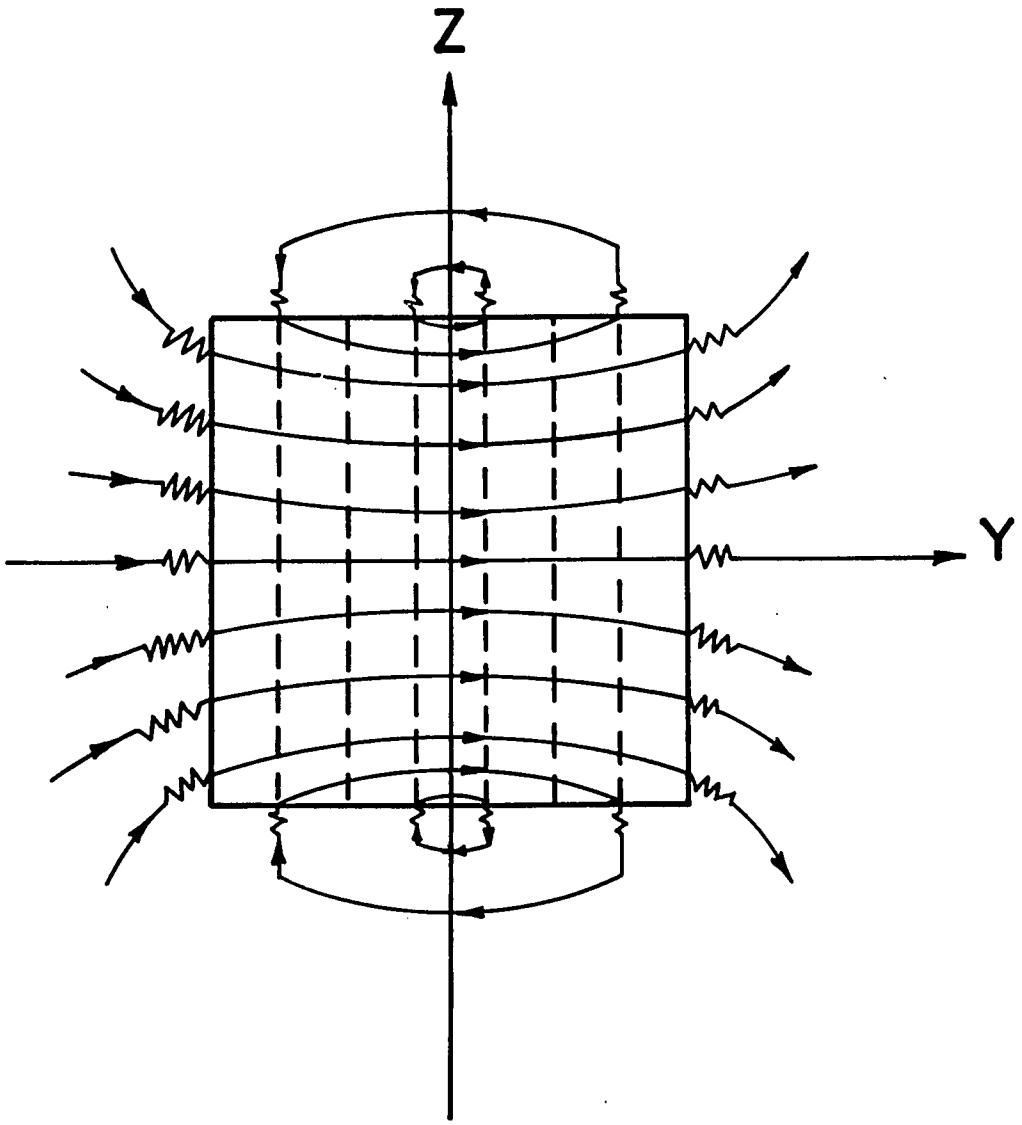

Fig. 7

a) Measurements taken with the sample in high vacuum are adiabatic $\langle \rho_{11}^{a} \rangle$.[25] The results for a magnetic field of 20 kG are shown as curve D of Fig. 8.

b) Measurements taken in the presence of helium vapor are not measurably different from the adiabatic values at the upper range of temperatures. The vapor lacks sufficient thermal conductance to produce a discernible w_2^*.

c) If the sample is immersed in liquid He I, the magnetoresistivity shows a slight increase above that of the adiabatic condition but still well below the isothermal value (see curve E of Fig. 8). Therefore the transport processes in liquid He I are insufficient to carry more than about 10% of the Ettingshausen heat current. These results give an indication of the poor efficiency of He I in maintaining a uniform temperature in a horizontal plane.[29]

d) This situation disappears when the bath is cooled below 2.18 K and the magnetoresistance shows a step increase of approximately 3.5% as the bath changes from He I to He II. The relative change $\Delta\rho/\rho$ is independent of the field, i.e. since ρ is about proportional to H^2 then $\Delta\rho$ is also proportional to H^2. The resistance ρ_{11}(He) increases slightly as the temperature is lowered down to 1.2 K, curve F, Fig. 8. Even though liquid He II is nearly a perfectly isothermal fluid, the electrical conduction is not exactly isothermal because the Kapitza boundary resistance to the flow of the Ettingshausen heat current sets up temperature gradients in the sample. This problem is discussed in the next chapter.

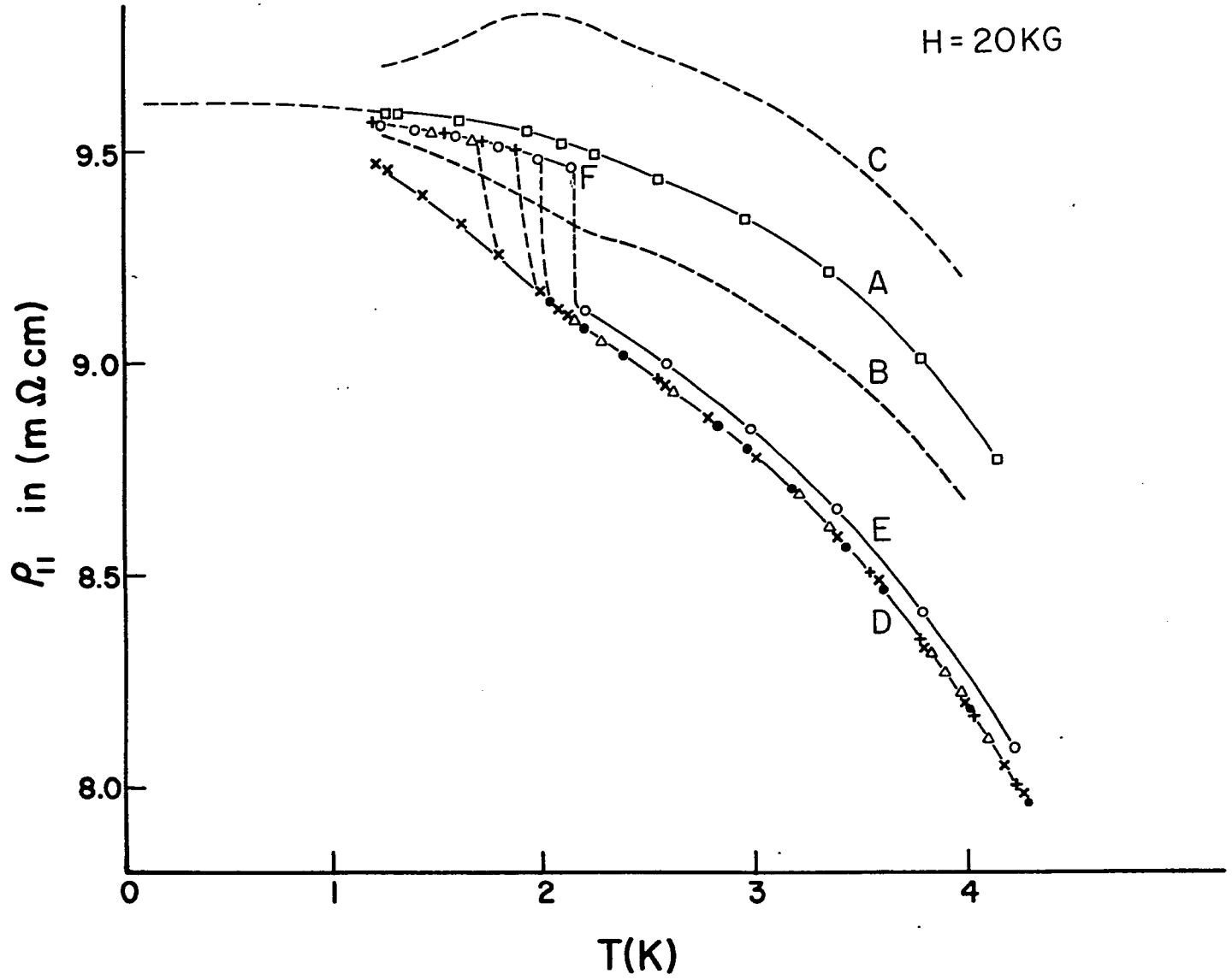

Fig. 8

e) As mentioned in (b) the presence of He vapor in the sample chamber yields a magnetoresistivity indistinguishable from the adiabatic case - except at temperatures well below the λ-point. Measurements were taken with three different quantities of He gas in the sample chamber (the gas pressures at liquid nitrogen temperature were 790, 590 and 230 mm Hg respectively). The dotted lines connecting the adiabatic and isothermal curves of Fig. 8 indicate the temperature range in which the adiabatic-isothermal transition occurred. We may conclude that the helium film on the sample changes from the unsaturated, low thermal conduction film at the higher temperature to the saturated superfluid film at the lower temperature within the respective temperature intervals. Thus, below the λ-point the unsaturated film is unable to provide observable heat transport while the saturated film carries heat as effectively as the bulk superfluid. We should note that the equality of ρ_{11}(He) in the presence of either bulk superfluid or saturated film means that the Kapitza resistance is the same in both cases.

f) When magnetoresistance of a coated sample is measured, the values found are intermediate between the helium bath curve E, F and the adiabatic curve D in agreement with the resulting decrease in thermal contact between the sample and the bath.

g) Since ρ_{11}(He) is not equal to the true isothermal magnetoresistivity ρ_{11}, we can estimate the latter only from $\langle \rho^a_{11} \rangle$ and the corrective term, $[\hat{\varepsilon}\hat{\pi}']_{11}$. For a sample in

which there are no surface effects, the Bridgmann and symmetry relations apply and the corrective term can be written in three equivalent forms

$$\rho_{11} - \rho_{11}^{a} = \lambda_g \varepsilon'_{21b} \pi'_{21b} = \lambda_g \pi'^{2}_{21b}/T = \lambda_g \varepsilon'^{2}_{21b} T.$$

If we substitute in our measured values, the equality no longer holds, thus yielding three different corrective values. The corresponding "isothermal" magnetoresistivity curves are designated A, B, C in Fig. 8 corresponding respectively to the three different corrections. Obviously curve B may be rejected since $\langle \rho_{11}(\mathrm{He}) \rangle$ cannot exceed $\langle \rho_{11} \rangle$. Curve C is rendered unphysical by the maximum at about 2 K. Only curve A follows the behavior expected for the isothermal magnetoresistivity, and strongly suggests the form

$$\langle \rho_{11} \rangle - \langle \rho_{11}^{a} \rangle = \lambda_g \langle \varepsilon'_{21} \rangle \langle \pi'_{21} \rangle .$$

This equation is in agreement with the skin model (Eq. 16). The layer model corresponds to the unacceptable solution B: Indeed in part 3 of this section concerning the interpretation of the ratio $\langle T\varepsilon'_{21} \rangle / \langle \pi'_{21} \rangle$ it was found that $p_2 \sim 1$ (Eq. 12), therefore

$$\langle \rho_{11} \rangle - \langle \rho_{11}^{a} \rangle = \lambda_g \frac{\langle \varepsilon'_{21} \rangle \langle \pi'_{21} \rangle}{p_1} = \lambda_g \frac{\langle \pi'_{21} \rangle^{2}}{T},$$

i.e., the B curve.

The difference $\langle \rho_{11} \rangle - \langle \rho_{11}^{a} \rangle$ was determined only for sample #17, however measurements of the step $\Delta\rho_{11}$ due to the transition of liquid He from normal to superfluid were made on many of the samples tabulated in Table I. This step from

an almost adiabatic to almost isothermal resistance is for sample #17 better than 80% of $\langle \rho_{11} \rangle - \langle \rho_{11}^{a} \rangle$ (see Fig. 8). If we suppose that the ratio, $k = \langle \Delta\rho_{11} \rangle / \langle \rho_{11} \rangle - \langle \rho_{11}^{a} \rangle$, may be regarded as constant for all specimens, then the layer model will predict from Eq. (13),

$$\frac{\langle \Delta\rho_{11} \rangle}{\langle \rho_{11} \rangle} = k\left(\frac{\varepsilon''_{21}\pi''_{21}}{\lambda_g}\right)_b \langle \rho_{11} \rangle ,$$

a proportionality of the relative step with the experimental resistance.

The skin model predicts from Eq. (17)

$$\frac{\langle \Delta\rho_{11} \rangle}{\langle \rho_{11} \rangle} = k\left(\frac{\varepsilon''_{21}\pi''_{21}}{\lambda_g}\right)_b \rho_{11b}$$

that the relative step will be independent of the field as well as independent of surface condition and size.

In Fig. 9 we present a plot of the step ratio $\langle \Delta\rho_{11} \rangle / \langle \rho_{11} \rangle$ vs. $\langle \rho_{11} \rangle$. Two distinct regions of behavior are apparent: The low resistance samples (rough surface and weak etching) show a proportionality to $\langle \rho_{11} \rangle$ as expected from the layer model with the slope almost exactly matching the value $k(\varepsilon''_{21}\pi''_{21}/\lambda_g)$ and therefore these results strongly support the damaged layer model, especially with regards to the assumption that $\varepsilon''_{21}, \pi''_{21}, \lambda_g$ are the same in the layer as in the bulk.

The high resistance samples (strongly etched and electropolished) show a value for $\langle \Delta\rho_{11} \rangle / \langle \rho_{11} \rangle$ independent of $\langle \rho_{11} \rangle$, a result which is in agreement with the skin model.

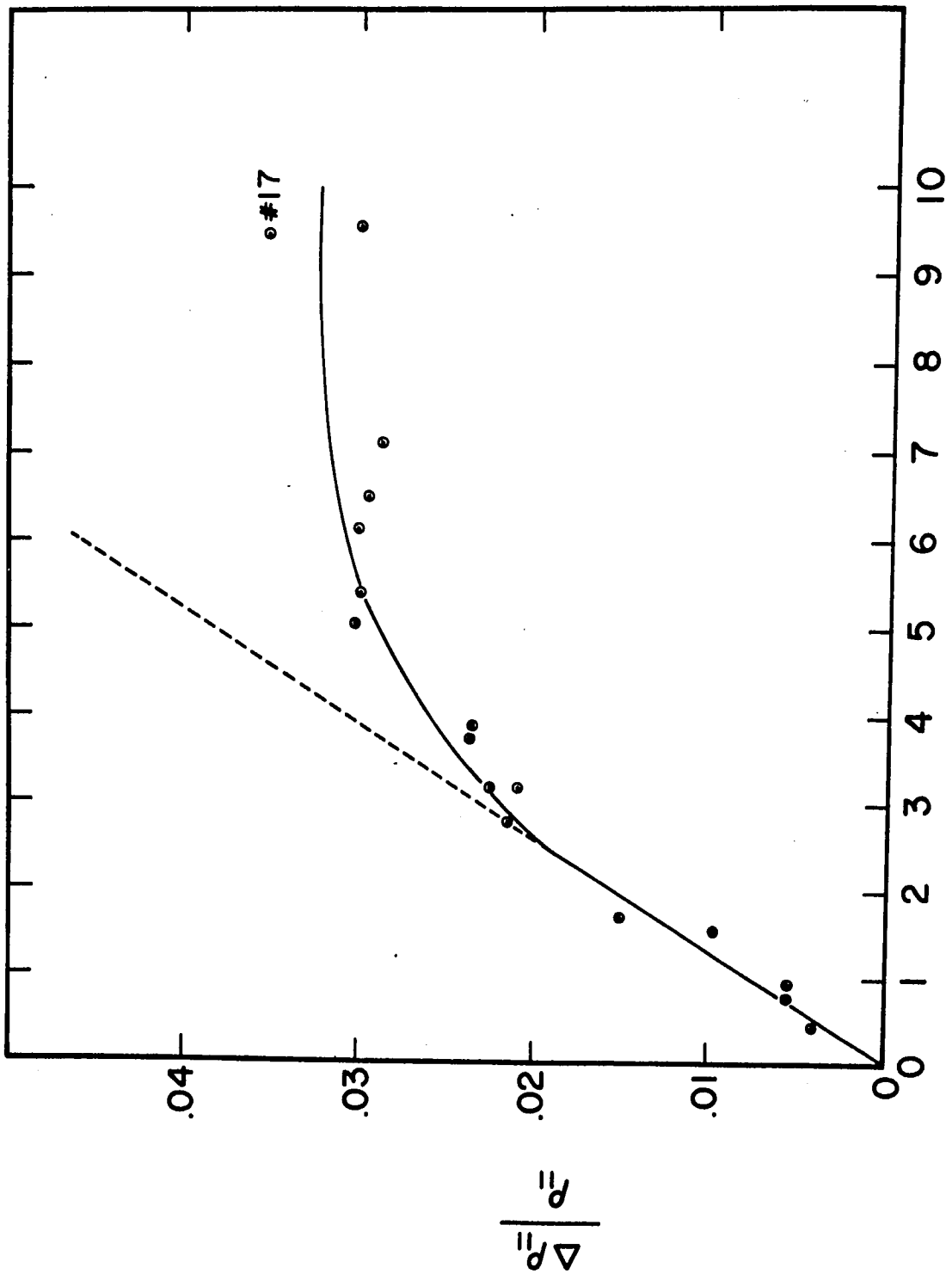
#17
0
.01
.02
.03
.04
0
1
2
3
4
5
6
7
8
9
10
$\frac{\Delta\rho_{11}}{\rho_{11}}$
ρ_{11} (mΩcm)

Fig. 9

To summarize, some behavior expected from damaged layer-models is found on those samples which are indeed expected to have a damaged surface. Those samples, freed of damaged layer by electropolishing or strong etching, tend to follow the skin model. This model has been over simplified for the sake of easy formulation of the effect and it is quite possible that the results may fit some other skin-type model. The hypotheses, introduced in the skin model, are based on the empirical assumption that the transport Eq. (1) can be extended to include Hattori[2] diffusion term. These equations will be:

$$\begin{aligned} \vec{J}_i \mp e\hat{D}\cdot\vec{\nabla}n_i &= \hat{\sigma}_i\cdot\vec{E}^* - \hat{\varepsilon}''_i\cdot\vec{G} \\ \vec{w}_i &= -\pi''_i\cdot\vec{E}^* + \hat{\lambda}''_i\cdot\vec{G}, \end{aligned} \tag{20}$$

where i denotes the i^{th} valley. It is assumed that the gradient of carrier density, $\vec{\nabla}n_i$, depends primarily on the current $\vec{J}_i$, it is also assumed that $\vec{\nabla}n_i$ would have a negligible effect on second equation. No attempt has been made to justify theoretically these hypotheses.

CHAPTER II

KAPITZA RESISTANCE DETERMINATIONS

A. Introduction

As noted in part 4, section C of Chapter I, the magnetoresistivity, measured in the presence of either superfluid bulk helium or the saturated film, is intermediate between the adiabatic and isothermal resistivities (see Fig. 8). Let us define the degree of adiabaticity Δ, as

$$\Delta = \frac{\rho_{11} - \rho_{11}(\mathrm{He})}{\rho_{11} - \rho_{11}^{a}} \tag{21}$$

where $\rho_{11}(\mathrm{He})$ is the magnetoresistivity measured in the presence of superfluid helium. As can be seen in Fig. 8, the value of Δ is about 20% over the measured temperature range. Thus, in spite of the perfectly isothermal environment provided by superfluid helium, the electrical conduction is not isothermal. That is, a temperature gradient arises within the specimen because of the temperature jump at the metal-helium interface which is due to the Kapitza boundary resistance.

From Eqs. (2) we note

$$w_2^* = +\pi_{12}J_1 + \lambda_g G_2.$$

Thus, for the isothermal case $G_2 = 0$ and $w_2^* = \pi_{12}J_1$. However because of the Kapitza resistance at the boundary, the surface temperature must be either above or below the bath temperature in order that heat flow may occur across the

metal-liquid helium interface. This flow pattern is schematically diagramed in Fig. 7. For conduction in a sample immersed in superfluid helium, we will have both $w_2^* \neq 0$, $G_2 \neq 0$. Our method of measuring the Kapitza resistance involves the analysis of the "Ettingshausen heat current," $w_2^* = \pi_{12} J_1$, flowing in the specimen, and particularly its influence upon the measured magnetoresistivity. This indirect method is in contrast with the more commonly employed techniques of steady heat flow[14] or the transmission of second sound.[30] In support of our hypothesis, we did take measurements on samples whose surfaces were coated with vacuum grease or varnish. The measured magnetoresistivity was lower for samples with coated surfaces than for samples with clean surfaces in qualitative agreement with the corresponding increases in thermal contact resistance between sample and liquid helium bath. Therefore we assume for samples with clean surfaces, such as #17, that deviation from perfect isothermal conduction arises only from the Kapitza resistance which we determine by means of the following analysis.

In order to derive a value of R_K, the Kapitza resistance, from the measured values of Δ we must have recourse to a specific model of conduction within the specimen. The simplest analytical procedure starts with the assumption of a current density, J_1, which is uniform over the sample cross section. As discussed above, there are compelling reasons for concluding that J_1 is not uniform. In fact, the

distribution of J_1 will most probably be different for all three environments: adiabatic, truly isothermal and superfluid helium. However, let us note that the measured resistivity differs from the bulk by a factor of roughly 0.62 (for sample #17) while the difference $(\rho_{11} - \rho_{11}^a)/\rho_{11}$ is only about 4.5% at the λ-point. Thus, to this extent we may regard q_1 (see Eq. 14) as the same for measurements in all three environments (see Appendix D) and thereby Δ can be evaluated by substituting into (21) the experimentally determined magnetoresistivities.

B. Results and Discussion

Following Callen[13] we note $\nabla\cdot\vec{w}_E = 0$ where $\vec{w}_E$ is the total energy current. With $\vec{w}^* = \vec{w}_E - \mu\vec{J}$ where μ is the electrochemical potential, then $\nabla\cdot\vec{w}^* = \vec{E}^*\cdot\vec{J}$. Substituting the bulk equations defining $\vec{E}^*$ and $\vec{w}^*$ into the above equation yields

$$\nabla\cdot(\hat{\lambda}\cdot\vec{G}) = \vec{J}\cdot\hat{\rho}\cdot\vec{J} + \vec{G}\cdot(\hat{\varepsilon} - \frac{\partial\hat{\pi}}{\partial T})\cdot\vec{J}. \qquad (22)$$

One can disregard gradient in the 1-direction and thereby reduce the problem to two dimensions, and neglect terms which are of second degree in the temperature gradients. Then,

$$-\lambda_g \frac{\partial^2 T}{\partial y^2} - \lambda_{33} \frac{\partial^2 T}{\partial z^2} = \rho_{11} J_1^2 - (\varepsilon_{12} - \frac{\varepsilon\pi_{12}}{\partial T}) J_1 \frac{\partial T}{\partial y} \qquad (23)$$

since $w_3^* = [-\hat{\pi}\vec{J}]_z + [\hat{\lambda}\vec{G}]_z$ reduces to $\lambda_{33}G_3$, then

then $\lambda_{33} \frac{\partial^2 T}{\partial z^2} = - \frac{\partial w_3^*}{\partial z}$. This physical situation possesses certain symmetries which are inferred in the flow diagram, Fig. 7, namely,

$$T(y,z) - T_o = T(y,-z) - T_o \tag{24}$$

$$T(y,z) - T_o = -[T(-y,z) - T_o], \tag{25}$$

where T_o is the bath temperature. From the former equation, $w_3^*(y,z) = -w_3^*(y,-z)$ hence $w_3^*(y,0) = 0$. The latter equation means that $T(y,z) - T_o$ is anti-symmetric about $y = 0$, so that $w_2^*(y,z) = w_2^*(-y,z)$. We may then restrict our discussion to the positive quadrant, $0 \le y \le \frac{b}{2}$, and $0 \le z \le \frac{c}{2}$.

$$-\lambda_g \frac{\partial^2 T}{\partial y^2} + \frac{\partial w_3^*}{\partial z} = \rho_{11} J_1^2 - (\varepsilon_{12} - \frac{\partial \pi_{12}}{\partial T}) J_1 \frac{\partial T}{\partial y}. \tag{26}$$

Since $\lambda_{33} >> \lambda_g$, we may expect $T(y,z)$ to be nearly independent of z[31] and thus only $\partial w_3^*/\partial z$ depends upon z. Thus integrating from $z = 0$ to $z = c/2$ we have

$$-\lambda_g \frac{\partial^2 T}{\partial y^2} + \frac{2}{c} w_3^*(y,\tfrac{c}{2}) = \rho_{11} J_1^2 - (\varepsilon_{12} - \frac{\partial \pi_{12}}{\partial T}) J_1 \frac{\partial T}{\partial y}. \tag{27}$$

Further we have the boundary condition $w_3^*(y,\frac{c}{2}) = \frac{T(y)-T_o}{R_K}$, where R_K is the Kapitza resistance on the $z = \frac{c}{2}$ surface.

Neglecting Joule and Thomson heating we obtain[32]

$$\lambda_g \frac{\partial^2 T}{\partial y^2} - \frac{T(y) - T_o}{\frac{c}{2} R_K} = 0. \tag{28}$$

This equation is easily solved with the boundary condition at $y = b/2$,

$$\frac{T(b/2) - T_o}{R_K} = w_2^*(\frac{b}{2}) = [-\pi_{21}J_1] - \lambda_g \left.\frac{\partial T}{\partial y}\right|_{\frac{b}{2}} \tag{29}$$

we find

$$\frac{dT}{dy} = - \frac{\pi_{21}J_1}{\lambda_g} \frac{\alpha}{M} \cosh(\alpha y) \tag{30}$$

where $\alpha = [\frac{2}{cR_K\lambda_g}]^{\frac{1}{2}}$ and $M = \frac{\sinh(\frac{\alpha b}{2})}{R_K\lambda_g} + \alpha\cosh(\frac{\alpha b}{2})$. We have assumed the same Kapitza resistance on all faces. Now the actual field E_1^* is given by

$$E_1^* = \rho_{11}J_1 - \varepsilon_{12}\frac{dT}{dy} = (\rho_{11} + \frac{\varepsilon_{12}\pi_{21}\alpha\cosh(\alpha y)}{\lambda_g M})J_1 \tag{31}$$

and since E_1^* is uniform in the z,y plane, the effective conductivity is

$$\bar{\sigma}_{11} = \frac{1}{\rho_{11}(He)} = \frac{1}{b\rho_{11}} \int_{-b/2}^{+b/2} [1 + \frac{(\varepsilon'_{12}\lambda_g\pi'_{21})\alpha\cosh(\alpha y)}{\rho_{11}M}]^{-1} dy. \tag{32}$$

The second term in the integrand is small, allowing a first order expansion and

$$\frac{\rho_{11}}{\rho_{11}(He)} - 1 = - \frac{\varepsilon'_{12}\lambda_g\pi'_{21}}{\rho_{11}}[(\frac{c}{b})(\frac{\alpha b}{2})^2 + (\frac{\alpha b}{2})\coth(\frac{\alpha b}{2})]^{-1} \tag{33}$$

with $-\varepsilon'_{12}\lambda_g\pi'_{21} = \rho_{11} - \rho_{11}^a$, one obtains

$$(\frac{\rho_{11}}{\rho_{11}(He)})\frac{\rho_{11}-\rho_{11}(He)}{\rho_{11} - \rho_{11}^a} = [(\frac{c}{b})(\frac{\alpha b}{2})^2 + (\frac{\alpha b}{2})\coth(\frac{\alpha b}{2})]^{-1}, \tag{34}$$

so that $\Delta \sim [(\frac{c}{b})(\frac{\alpha b}{2})^2 + (\frac{\alpha b}{2})\coth(\frac{\alpha b}{2})]^{-1}$. All of the quantities on the left are determined experimentally. The

solution of the transcendental equation (34) yields the values of $\alpha b/2$ from which R_K can be determined. The values of R_K are presented in Fig. 10.[33]

To the best of our knowledge there are no data published on Kapitza resistance of Sb nor of other semimetals. It is therefore difficult to judge the reliability of the method employed here or the validity of the assumptions regarding the estimation of the isothermal magnetoresistance. The Kapitza resistances presented here are larger than those generally obtained for other metals.[14] One possible reason would be that the estimate of ρ_{11} is too large, that is, $(\varepsilon'_{12}\lambda_g\pi'_{21})_{exp}$ may be larger than the appropriate corrective term $\Delta\rho_{11}$. The values of R_K obtained here are more comparable with those of semiconductors as can also be seen in Fig. 10 which includes the results of Johnson and Little[34] for pure Si. Since in Sb we have thermal conduction by only phonons in the y-direction in high fields, we could ascribe the close similarity of R_K in Si and Sb to the similarity of conduction processes.

Determination of R_K above the λ-point is made difficult by the fact that the helium bath is not isothermal,[29] and this fact contributes to most of the degree of adiabaticity that was found. Since the heat transport in liquid He I involves rather more complicated processes than simple thermal conduction,[35] no attempt has been made to determine the Kapitza resistance in this range.

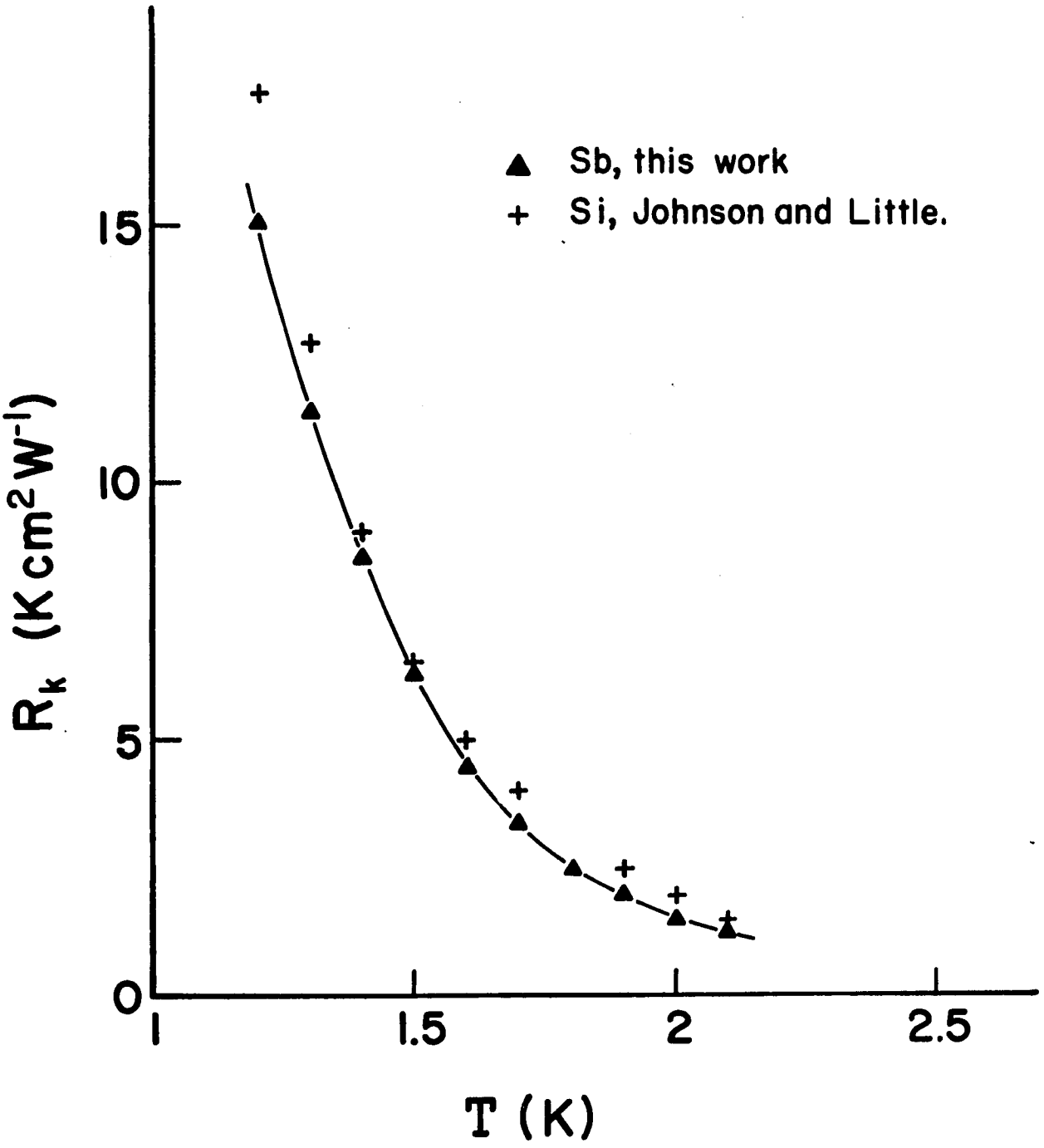
▲ Sb, this work
+ Si, Johnson and Little.
15
10
5
0
R_k (K cm^2 W^{-1})
1
1.5
2
2.5
T (K)

Fig. 10

CHAPTER III

ELECTRON-PHONON INTERACTION AND DRAG EFFECTS IN BULK TRANSPORT COEFFICIENTS AT LOW TEMPERATURE

A. Introduction

In Chapter I we have studied the effects of size and surface, etc., on transport coefficients at high magnetic field. The corrections of these effects allow one to study the bulk transport phenomena. The most interesting features of transport properties in the helium temperature range are electron-phonon normal, that is, intravalley scattering and mutual as well as simple drag effects.

The transport coefficients covered in this study include ideal resistivity, thermal resistivity, thermoelectric power, magnetoresistance, thermal magnetoresistance, Ettingshausen and Nernst-Ettingshausen effects. Lattice conductivity was also measured and analyzed as part of this study.

There are several models used in transport theory. In this thesis, one attempts to analyze the results in terms of effective-scattering-Debye-temperature, that is, Ziman's cutoff temperature, the matrix elements of the electron-phonon interaction, that is, deformation potentials and drag contributions. They will be discussed in more detail in the following sections.

All measurements show an excellent correlation with Ziman's cutoffs and qualitative agreement with the proposed scattering mechanisms. This consistency allows the

estimation of the scattering parameters such as the deformation potential.

Information about the surface and size effects which properly allows for correction of the high field transport coefficients is lacking in the zero field; and the correction for size and surface effect at zero field can only be worked out under certain assumptions as it is done, for example, in the case of the ideal resistivity.

Although there have been several theoretical and experimental investigations of phonon drag effect since L. E. Gurevich pointed out the importance of taking into account the influence of the non-equilibrium character of the phonon subsystem on the electron subsystem in the thermoelectric power phenomena, there has been no systematic work on electron-phonon simple and mutual drag effects in antimony. Therefore, it is important to examine and to separate "drag" and "diffusive" effects. As is noted elsewhere the influence of the non-equilibrium character of the phonon subsystem on the electron subsystem is called simple phonon drag effect. Furthermore, a non-equilibrium character of phonon subsystem, which is due to the non-equilibrium character of electron subsystem, affects the electron in turn is called an electron-phonon mutual drag effect. In any semimetal, such as antimony, there are electrons and holes in the charge carrier system. Quite often the phonon will (will be) drag (dragged by) an electron in one direction and

a hole in the opposite, such phenomenon is usually referred to as compensated drag effect.

The results covered in this thesis show that there is strong simple phonon drag effect in Nernst-Ettingshausen effect at helium temperature, and strong mutual drag effects in magnetoresistance and Ettingshausen effects. The drag effect is weak in both the ideal resistivity and in the thermoelectric power because of drag compensation. The consistency of the effective-scattering-Debye-temperature is also found in the drag case. This agreement provides one with the understanding of electron-phonon scattering mechanisms.

B. Theoretical Consideration of Drag Effect in the Bulk Transport Coefficients

General Consideration

As noted in Chapter I the kinetic equations are usually written as:[18]

$$\vec{J} = \hat{\sigma}\vec{E}^* + \hat{\varepsilon}''\vec{\nabla}T \tag{35}$$

$$\vec{W}^* = -\hat{\pi}''\vec{E}^* - \hat{\lambda}''\vec{\nabla}T \tag{36}$$

where $\vec{J}$ and $\vec{W}^*$ are the electrical and thermal current densities, $\vec{E}^*$ and $\vec{\nabla}T$ are the electrochemical and temperature gradients. These coefficients are named as follows: $\hat{\sigma}$, the electrical conductivity; $\hat{\lambda}''$, the thermal conductivity; $\hat{\varepsilon}''$, the thermoelectric tensor; and $\hat{\pi}''$, the Peltier tensor.

In the case of the bulk transport properties, the well known Onsager-Kelvin relations[13] are valid, thus

$$\sigma_{ij}(\vec{H}) = \sigma_{ji}(-\vec{H})$$
$$T\varepsilon_{ij}(\vec{H}) = \pi_{ji}(-\vec{H}).$$

Therefore one can minimize the number of transport coefficients to be calculated. In this section, we will derive some equations describing the contributions of drag effect to the transport coefficients, such as $\sigma(0)$, $\sigma_{11}(H)$, $\varepsilon''_{11}(0)$, $\pi''_{11}(0)$, $\varepsilon''_{21}(H)$ and $\pi''_{21}(H)$ in the helium temperature range based on the assumption of ellipsoidal Fermi surfaces. The other transport coefficients, such as $\sigma_{12}(H)$, $\varepsilon''_{11}(H)$, $\pi''_{11}(H)$, and $\lambda''_{12}(H)$, etc., are comparatively smaller,[20] and are not interesting for this study.

The Fermi surfaces of antimony have been studied through theoretical[36] and experimental[37] investigations, and have been found that there are six hole pockets and three electron pockets, neither electron nor hole Fermi surfaces are ellipsoidal and that neither their distributions are quadratic.[37b] However, the introduction of ellipsoidal and quadratic model approximations doesn'tlead to a significant error in the calculation. In some instance spherical models will also be used, so as to allow some simplifications in the calculation. The fact that these results can be extended to ellipsoidal case with a proper anisotropic correction factor has been successfully tested in bismuth,[38] graphite,[39] even in antimony.[20,40]

As is noted in the investigation of lattice conductivity from liquid helium temperature down to 0.4°K,[28]

the carrier-phonon scattering dominates the "enclosed" phonon (see the next section) scattering mechanisms, in addition, the phonon-electron scattering is more frequent than phonon-hole scattering. Consequently the fact that the mean free path of hole due to scatter with phonon is much longer than that of an electron scattering with phonon is also concluded in Long, et al.,[20] investigation of antimony. In short,

$$\frac{6L}{L^+} + \frac{3L}{L^-} \simeq 1, \; L^+ >> L^-, \; \ell_f^+ >> \ell_f^-$$

where L is the total mean free path of the phonon, L^+ is the mfp of the phonon scattering with the hole, L^- is the mfp of the phonon scattering with the electron, and $\ell_f^{\pm}$ is the mfp of the hole (electron) scattering with the phonon. These considerations simplify some of the complicated calculations in the transport coefficients.

The carrier-phonon interaction takes the form:[41]

$$H_{e-p}^{\pm} = \sum_q V_{\vec{q}}^{\pm} (b_{\vec{q}} \, e^{i\vec{q}\cdot\vec{r}} - b_{\vec{q}}^{*} \, e^{-i\vec{q}\cdot\vec{r}})$$

and

$$V_{\vec{q}}^{\pm} = i\varepsilon_{e,h} \sqrt{\frac{\hbar}{2\rho V \omega_q}} \, (\vec{e}_{\vec{q}} \cdot \vec{q})$$

where $\varepsilon_{e,h}$ are deformation potentials of the electron and the hole respectively, ρ is the density, V is the volume, e_q is the polarization vector, and b_q, b_q^* are the creation and annihilation operators respectively.

The calculation to be presented in this section is based on the assumption that there is no distinction between

longitudinal and transverse phonons. It is also assumed that there is no optical phonon-carrier interaction in the helium temperature range. Furthermore, the intervalley and interband scattering are also neglected. The sound speed, s, is considered as a constant for every branch of phonons and every direction of propagation.

The general coupled Boltzmann equations are:

$$\left(\frac{\partial f_{\vec{k}}}{\partial t}\right)_{\text{scatt}} + \left(\frac{\partial f_{\vec{k}}}{\partial t}\right)_{\text{diff}} + \left(\frac{\partial f_{\vec{k}}}{\partial t}\right)_{\text{field}} = 0 \qquad (37)$$

$$\left(\frac{\partial N_{\vec{q}}}{\partial t}\right)_{\text{scatt}} + \left(\frac{\partial N_{\vec{q}}}{\partial t}\right)_{\text{diff}} = 0 \qquad (38)$$

$f_{\vec{k}}$ and $N_{\vec{q}}$ are the distribution functions of the carrier and the phonon with the wave vector $\vec{k}$ and $\vec{q}$ respectively. It is usual that the solutions of these coupled Boltzmann equations are:[42]

$$f_{\vec{k}} = f^{o}_{\vec{k}} - (\vec{V}(\varepsilon)\cdot\vec{k})\,\frac{\partial f^{o}_{\vec{k}}}{\partial \varepsilon} \qquad (39)$$

$$N_{\vec{q}} = N^{o}_{\vec{q}} - (\vec{U}(\omega)\cdot\vec{q})\,\frac{\partial N^{o}_{\vec{q}}}{\partial \hbar\omega} \qquad (40)$$

$f^{o}_{\vec{k}}$ and $N^{o}_{\vec{q}}$ are the equilibrium distribution functions; $\frac{1}{\hbar}\vec{V}(\varepsilon)$ and $\frac{1}{\hbar}\vec{U}(\omega)$ are the drift velocities of the carrier and the phonon respectively.

If we disregard the interband and intervalley scatterings, the rate of change of the carrier distribution function due to the scattering by phonons is given by Ziman:[43]

$$\left(\frac{\partial f_{\vec{k}}}{\partial t}\right)_{e\leftarrow p} = -\frac{1}{(2\pi)^3}\frac{1}{k_B T}\iint\{[\vec{V}(\varepsilon)\cdot\vec{k}-\vec{V}(\varepsilon')\cdot\vec{k}'+\vec{U}(\omega)\cdot\vec{q}]P^{\vec{k}'}_{\vec{k}\vec{q}} + [\vec{V}(\varepsilon)\cdot\vec{k}-\vec{V}(\varepsilon')\cdot\vec{k}'-\vec{U}(\omega)\cdot\vec{q}]P^{\vec{k}',\vec{q}}_{\vec{k}}\}d^3\vec{k}'d^3\vec{q} \tag{41}$$

and

$$\left(\frac{\partial f_{\vec{k}}}{\partial t}\right)_{scatt} = \left(\frac{\partial f_{\vec{k}}}{\partial t}\right)_{e\text{-}p} + \left(\frac{\partial f_{\vec{k}}}{\partial t}\right)_{imp.etc.}$$

or

$$\left(\frac{\partial f_{\vec{k}}}{\partial t}\right)_{scatt} = \left(\frac{\partial f_{\vec{k}}}{\partial t}\right)_{e\text{-}p} + \frac{|\vec{v}_k|}{\ell_{imp.etc.}}(\vec{V}(\varepsilon)\cdot\vec{k})\frac{\partial f^o_{\vec{k}}}{\partial \varepsilon}$$

where $P^{\vec{k}'}_{\vec{k}\vec{q}}$ or $P^{\vec{k}',\vec{q}}_{\vec{k}}$ describes the transition probability in which a phonon is annihilated or created respectively. Generally the expressions of them are given by:[44]

$$P^{\vec{k}'}_{\vec{k}\vec{q}} = \frac{\pi\varepsilon^2}{\rho\omega_{\vec{q}}}(\vec{e}_q\cdot\vec{q})\delta_{\vec{k}+\vec{q},\vec{k}'}\delta(\varepsilon_{\vec{k}}-\varepsilon_{\vec{k}'}+\hbar\omega_q)N^o_{\vec{q}}f^o_{\vec{k}}(1-f^o_{\vec{k}'}) \tag{43}$$

$$P^{\vec{k}',\vec{q}}_{\vec{k}} = \frac{\pi\varepsilon^2}{\rho\omega_{\vec{q}}}(\vec{e}_q\cdot\vec{q})\delta_{\vec{k},\vec{k}'+\vec{q}}\delta(\varepsilon_{\vec{k}}-\varepsilon_{\vec{k}'}-\hbar\omega_q)(N^o_{\vec{q}}+1)f^o_{\vec{k}'}(1-f^o_{\vec{k}}). \tag{44}$$

The other terms in Boltzmann equation for charge carrier are:

$$\left(\frac{\partial f_{\vec{k}}}{\partial t}\right)_{diff} = -(\vec{v}_k\cdot\vec{\nabla}T)T\frac{\partial(\varepsilon-\xi)}{\partial T}\frac{\partial f^o_{\vec{k}}}{\partial\varepsilon} \tag{45}$$

$$\left(\frac{\partial f_{\vec{k}}}{\partial t}\right)_{field} = -e(\vec{E}\cdot\vec{v}_k)\frac{\partial f^o_{\vec{k}}}{\partial\varepsilon} + \frac{e}{\hbar c}\vec{v}_{\vec{k}}\cdot(\vec{H}\times\vec{V}(\varepsilon))\frac{\partial f^o_{\vec{k}}}{\partial\varepsilon}. \tag{46}$$

While those two terms of the Boltzmann equation for phonon are:

$$\left(\frac{\partial N_{\vec{q}}}{\partial t}\right)_{scatt} = \left(\frac{\partial N_{\vec{q}}}{\partial t}\right)_{p\text{-}e} + \left(\frac{\partial N_{\vec{q}}}{\partial t}\right)_{bound.iso.etc.} \tag{47}$$

$$\left(\frac{\partial N_{\vec{q}}}{\partial t}\right)_{p\text{-}e} = -\frac{1}{(2\pi)^3}\frac{1}{k_B T}\sum_{\pm}\iint\{[\vec{V}^{\pm}(\varepsilon)\cdot\vec{k}-V^{\pm}(\varepsilon')\cdot\vec{k}'+\vec{U}(\omega)\cdot\vec{q}]P^{\pm k'}_{\vec{k}\vec{q}}\ d^3\vec{k}d^3\vec{k}' \tag{48}$$

$$\left(\frac{\partial N_{\vec{q}}}{\partial t}\right)_{\text{bound.iso.etc.}} = \frac{s(\vec{U}(\omega)\cdot\vec{q})}{L_r}\,\frac{\partial N^{o}_{q}}{\partial \hbar\omega} \tag{49}$$

and

$$\frac{1}{L_r} = \frac{1}{L_b} + \frac{1}{L_{iso}} + \ldots$$

where L_b and L_{iso} are mfp of phonon limited by phonon-boundary and phonon-isotope scatterings respectively.

$$\left(\frac{\partial N_{\vec{q}}}{\partial t}\right)_{\text{diff}} = (\vec{s}\cdot\vec{\nabla}T)\,\frac{\hbar\omega}{T}\,\frac{\partial N^{o}_{\vec{q}}}{\partial \hbar\omega}. \tag{50}$$

It is necessary to evaluate the integrals before solving coupled Boltzmann equations. The procedures of integration can be found in many references.[45] We will not repeat this calculation here. Further, if we use the concept of mean free paths to express $V(\varepsilon)$ and $U(\omega)$, then $V(\varepsilon)$ and $U(\omega)$ are given by:

$$\vec{V}^{\pm}(\varepsilon) + \frac{e^{\pm}\ell^{\pm}}{cp^{\pm}}[\vec{H}x\vec{V}^{\pm}(\varepsilon)] - \frac{\ell^{\pm}}{\ell_f^{\pm}J_5\left(\frac{\Theta^{*}_{e,h}}{T}\right)} \int_0^{\frac{\Theta^{*}_{e,h}}{T}} \vec{U}(x)\frac{x^5 e^x}{(e^x-1)^2}dx \tag{51}$$

$$= \frac{\ell^{\pm}}{p^{\pm}}\left(e^{\pm}\vec{E} - \frac{(\varepsilon-\xi^{\pm})}{T}\,\vec{\nabla}T\right)$$

$$\vec{U}(\omega) = -\frac{6L}{L^{+}}\int_{\varepsilon^{+}(q/2)}^{\infty} \vec{V}^{+}(\varepsilon)\,\frac{\partial f^{o+}_{\vec{k}}}{\partial\varepsilon}d\varepsilon - \frac{3L}{L^{-}}\int_{\varepsilon^{-}(q/2)}^{\infty} \vec{V}(\varepsilon)\,\frac{\partial f^{o-}_{\vec{k}}}{\partial\varepsilon}d\varepsilon - \frac{\hbar L s}{T}\vec{\nabla}T \tag{52}$$

where $\ell^{\pm}$ is mfp of the hole (electron)

$\ell_f^{\pm}$ is mfp of the hole (electron) due to scattering with a phonon

$p^{\pm}$ is the momentum of a hole (electron)

$J_5(\frac{\Theta}{T})$ is the Debye integral of the form

$$J_5(\frac{\Theta}{T}) = \int_0^{\frac{\Theta}{T}} \frac{x^5 e^x}{(e^x-1)^2}\, dx$$

L, L^+ and L^- are defined previously.

Θ^* is defined as $(\frac{2k_f}{q_D})\Theta_D$ (see the next section for more detail)

$x = \frac{\hbar sq}{k_B T}$ s is the speed of sound

k_B is Boltzmann constant.

In addition,

$$\frac{1}{\ell^\pm} = \frac{1}{\ell_f^\pm} + \frac{1}{\ell_{\text{imp. etc.}}^\pm}$$

$\frac{1}{L_1} = \frac{6}{L^+} + \frac{3}{L^-} + \frac{1}{L_r}$ if the phonon scatters with both carriers

$\frac{1}{L_2} = \frac{6}{L^+} + \frac{1}{L_r}$ if the phonon scatters with only a hole

$\frac{1}{L_3} = \frac{3}{L^-} + \frac{1}{L_r}$ if the phonon scatters with only an electron

and

$$\frac{1}{\ell_f^{\pm}} = \frac{3\pi h^2 \varepsilon_{e,h}^2 \, Nn}{16\rho s \xi_{p,h}^2 \beta P_f^{\pm}} \left(\frac{\Theta_D}{\Theta_{e,h}^*} \right)^2 \left(\frac{T}{\Theta_D} \right)^5 J_5\left(\frac{\Theta_{e,h}^*}{T} \right) \tag{53}$$

where $\beta = 1$ for electron, $\beta = 2$ for hole.

Calculation of $\sigma(0)$ the Zero Field Electrical Conductivity

Because the Fermi temperatures of electrons and holes for antimony are about 1022°K and 1319°K respectively,[46] it is permissible to consider that carriers in antimony are highly degenerate at the helium temperature. As one calculates $\sigma(0)$, it is usually assumed that $\vec{H} = 0$, $\vec{\nabla}T = 0$. Therefore the drift velocities $\vec{V}^{\pm}(\varepsilon_f)$ and $\vec{U}(\omega)$ are given by:

$$\vec{V}^{\pm}(\varepsilon_f) - \frac{\ell^{\pm}}{\ell_f^{\pm} J_5\left(\frac{\Theta_{e,h}^*}{T} \right)} \int_0^{\frac{\Theta_{e,h}^*}{T}} \vec{U}(x) \frac{x^5 e^x}{(e^x - 1)^2} \, dx = \frac{\hbar \ell^{\pm}}{P_f^{\pm}} e^{\pm} \vec{E} \tag{54}$$

$$\vec{U}(\omega) = \frac{6L_1}{L^+} \vec{V}^+(\varepsilon_f) + \frac{3L_1}{L^-} \vec{V}^-(\varepsilon_f) \qquad q \ \varepsilon \text{ region 1} \tag{55a}$$

$$\vec{U}(\omega) = \frac{6L_2}{L^+} \vec{V}^+(\varepsilon_f); \ \frac{6L_2}{L^+} \simeq 1 \qquad q \ \varepsilon \text{ region 2} \tag{55b}$$

$$\vec{U}(\omega) = \frac{3L_3}{L^-} \vec{V}^-(\varepsilon_f); \ \frac{3L_3}{L^-} \simeq 1 \qquad q \ \varepsilon \text{ region 3} \tag{55c}$$

$$U(\omega) = 0 \qquad q \in \text{region } 4 \qquad (55d)$$

In the first three cases, $1/L_r$ is regarded as negligible. If referring to the next section, we call "a" a ellipsoidal volume of q space which corresponds to the phonons scattered by the hole (i.e. the hole "enclosed phonon") and "b" the similar volume for electron "enclosed phonon," the regions 1, 2, 3 and 4 as sketched in Fig. 11 correspond to:

region 1: the volume common to "a" and "b"
region 2: the volume "a" except "1"
region 3: the volume "b" except "1"
region 4: the region outside "a" and "b" (peripheral phonons).

Let's note that there are six hole-pockets and three electron-pockets in antimony, thus Fig. 11 should add another 5 "a" and another 2 "b".

From Eqs. (54) and (55) along with the condition of highly degenerate carrier distributions and negligible inter-valley scattering, [i.e., $U(\omega) = 0$ for region 1], the drift velocities of carriers become:

$$V^{\pm}(\varepsilon_f)\left(1 - \frac{\ell^{\pm}}{\ell_f^{\pm} J_5\left(\frac{\Theta^*_{e,h}}{T}\right)} \int_{\frac{\Theta_4}{T}}^{\frac{\Theta^*_{e,h}}{T}} \frac{x^5 e^x}{(e^x-1)^2}\, dx\right) = \frac{\hbar e^{\pm} \ell^{\pm}}{P_f^{\pm}} E \qquad (56)$$

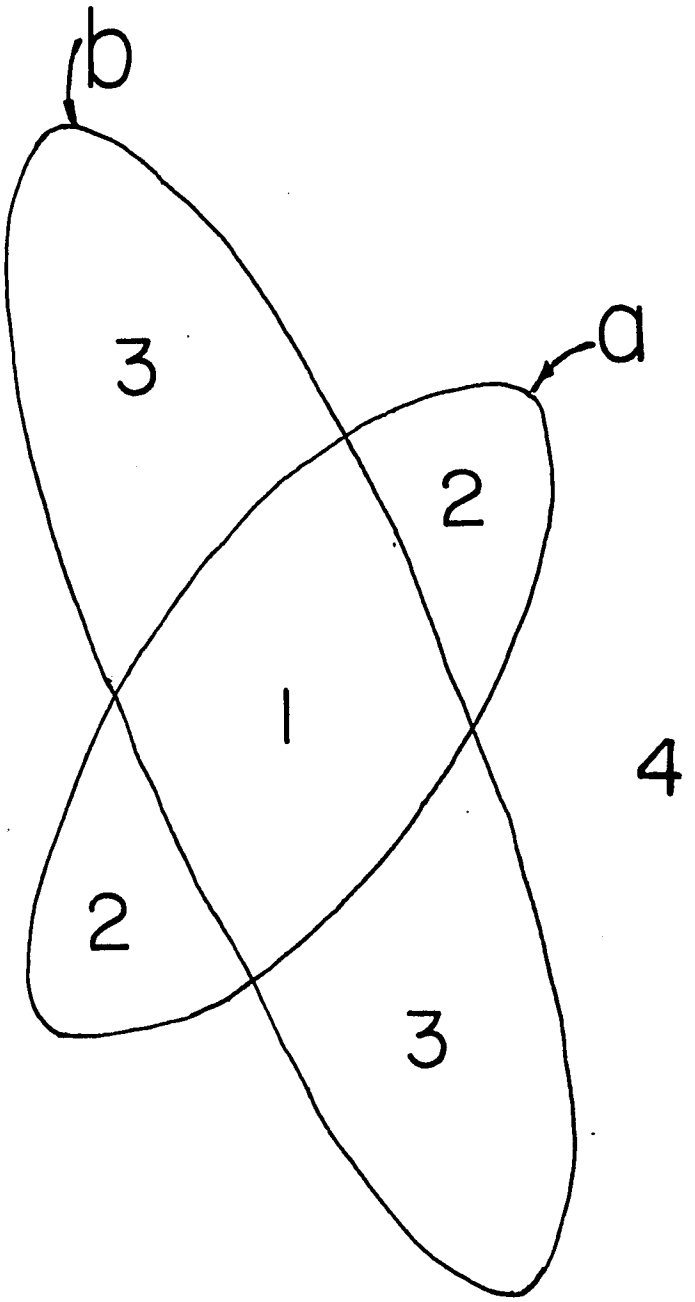

Fig. 11

where

$$\Theta_4^* = \frac{2\hbar s\, k_4}{k_B}$$

k_4 is the "radius" of region 1 as we approximate this region by a sphere.

Or

$$V^{\pm}(\varepsilon_f) = \frac{\frac{\hbar e^{\pm}}{P_f^{\pm}} E}{\frac{1}{\ell^{\pm}_{\text{imp. etc.}}} + \frac{J_5(\frac{\Theta_4^*}{T})}{\ell_f^{\pm} J_5(\frac{\Theta_{e,h}^*}{T})}} \tag{56a}$$

Consequently, one obtains the current density,

$$\vec{J} = ne^+\left(\frac{1}{\hbar}\vec{\nabla}^+(\varepsilon_f) - \frac{1}{\hbar}\vec{\nabla}^-(\varepsilon_f)\right)$$

or

$$\sigma(0) = \frac{ne^2}{P_f^+}\,\frac{1}{\frac{1}{\ell^+_{\text{imp. etc.}}} + \frac{J_5(\frac{\Theta_4^*}{T})}{\ell_f^+ J_5(\frac{\Theta_h^*}{T})}} + \frac{ne^2}{P_f^-}\,\frac{1}{\frac{1}{\ell^-_{\text{imp.}}} + \frac{J_5(\frac{\Theta_4^*}{T})}{\ell_f^- J_5(\frac{\Theta_e^*}{T})}}$$

In antimony, $\ell^+ >> \ell^-$, thus

$$\sigma(0) \simeq \frac{ne^2}{P_f^+} \frac{1}{\frac{1}{\ell^+_{\text{imp. etc.}}} + \frac{J_5(\frac{\Theta^*_4}{T})}{\ell_f^+ J_5(\frac{\Theta^*_h}{T})}} \tag{57}$$

or

$$\rho = \rho_o + \rho_{id}$$

where

$$\rho_o = \frac{P_f^+}{ne^2 \ell^+_{\text{imp. etc.}}}$$

and

$$\rho_{id} = \frac{3\pi h^2 \varepsilon_h^2 N}{32\rho s e^2 \xi_h^2} \left(\frac{\Theta_D}{\Theta^*_h}\right)^2 \left(\frac{T}{\Theta_D}\right)^5 J_5\left(\frac{\Theta^*_4}{T}\right) \tag{58}$$

where $\Theta^*_4 \simeq 16^\circ K$ from theoretical consideration because the shortest axes of both electron and hole ellipsoids are $\sim 4.1 \times 10^6$ 1/cm, therefore $q_1 \sim 8.2 \times 10^6$ 1/cm or $\Theta^*_4 \simeq 16^\circ K$.

Thermoelectric Power $\varepsilon_{11}(0)$ at Zero Field

In order to simplify the calculations, we will determine $\pi''_{11}(0)$ instead of $\varepsilon''_{11}(0)$. According to kinetic equation (35),

$$W_1 = -\pi''_{11}(0)\, E_1 - \lambda''_{11} \nabla_x T$$

under the condition of isothermal measurements, $\nabla_x T = 0$, thus

$$W_1 = -\pi''_{11}(0)\, E_1$$

This heat current corresponds to the heat carried by the electrons, the holes as well as the phonons which interact with (or are dragged by) electrons and/or holes. The phonon's part can be written as

$$W_q = -\frac{1}{(2\pi)^3} \int \hbar\omega_q (\vec{U}(\omega)\cdot\vec{q})\, s\, \frac{\partial N_q^o}{\partial \hbar\omega}\, d^3q \qquad (59)$$

where the non-equilibrium part (or drift velocity) of the phonon is, from previous calculation at a first order approximation,

$$\vec{U}(\omega) = \frac{6L_1}{L^+}\frac{\hbar e^+ \ell^+}{P_f^+} E + \frac{3L_1}{L^-}\frac{\hbar e^- \ell^-}{P_f^-} E \qquad q \in \text{region 1}$$

$$\vec{U}(\omega) = \frac{6L_2}{L^+}\frac{\hbar e^+ \ell^+}{P_f^+} E \qquad q \in \text{region 2}$$

$$\vec{U}(\omega) = \frac{3L_3}{L^-}\frac{\hbar e^- \ell^-}{P_f^-} E \qquad q \in \text{region 3}$$

$$U(\omega) = 0 \qquad q \in \text{region 4}$$

47

In region 1 our result of TEP is similar to that obtained by Gurevich and Korenblit.[42] The results of the TEP in regions 2 and 3 are not easy to calculate exactly. It can be approximated by the assumption that one can transform the ellipsoidal Fermi surface into a spherical one. After such a transformation, one can compute the heat current carried by these phonons which interact with the carriers. This heat current is given by

$$W_q = (W_q)_1 + (W_q)_2 + (W_q)_3$$

where

$$(W_q)_1 = -\frac{3Nk_BT}{ne}\left(\frac{T}{\Theta_D}\right)^3 E \int_0^{\frac{\Theta_4^*}{T}} \left(\sigma_h \frac{6L_1}{L^+} - \sigma_e \frac{3L_1}{L^-}\right) \frac{x^4 e^x}{(e^x-1)^2}\, dx$$

$$(W_q)_2 = -\frac{3Nk_BT}{ne}\left(\frac{T}{\Theta_D}\right)^3 E \int_{\frac{\Theta_4^*}{T}}^{\frac{\Theta_h^*}{T}} \alpha_h\sigma_h \frac{6L_2}{L^+} \frac{x^4 e^x}{(e^x-1)^2}\, dx$$

$$(W_q)_3 = -\frac{3Nk_B}{ne}\left(\frac{T}{\Theta_D}\right)^3 E \int_{\frac{\Theta_4^*}{T}}^{\frac{\Theta_e^*}{T}} \alpha_e\sigma_e \frac{3L_3}{L^-} \frac{x^4 e^x}{(e^x-1)^2}\, dx$$

where α_h and α_e are the parameters used in the transformation.

Because

$$W_q = -\pi''_{11}(0)\, E\ .$$

In the zero field, $\pi''_{12}(0) = 0$, let's neglect the subscripts in $\pi''_{11}(0)$ and $\varepsilon''_{11}(0)$, and

$$\pi(0) = T\varepsilon(0) = \frac{\pi''(0)}{\sigma(0)}$$

Therefore if

$$\varepsilon(0) = \varepsilon_d(0) + \varepsilon_g(0)$$

$\varepsilon_d(0)$ is the diffusive term of the TEP

$$\varepsilon_g = \frac{1}{\sigma(0)} \left\{ \frac{3Nk_B}{ne} \left(\frac{T}{\Theta_D}\right)^3 \left[\int_0^{\frac{\Theta_4^*}{T}} \left(\sigma_h \frac{6L_1}{L^+} - \sigma_e \frac{3L_1}{L^-}\right) \frac{x^4 e^x}{(e^x-1)^2}\, dx \right.\right.$$

$$\left.\left. + \int_{\frac{\Theta_4^*}{T}}^{\frac{\Theta_h^*}{T}} \sigma_h\sigma_h \frac{6L_2}{L^+} \frac{x^4 e^x}{(e^x-1)^2}\, dx - \int_{\frac{\Theta_4^*}{T}}^{\frac{\Theta_e^*}{T}} \sigma_e\sigma_e \frac{3L_3}{L^-} \frac{x^4 e^x}{(e^x-1)^2}\, dx \right] \right\} \tag{60}$$

The first term of Eq. (60) is similar to the term obtained by Gurevich, et al., for which they obtained

$$\varepsilon_g(0) = \frac{4k_B}{3e^+} \frac{1}{(\ell^+ + \ell^-)} \left[\frac{\ell^+A^+ - \ell^-A^-}{(1-\gamma^+-\gamma^-)(1+D)} \right] \tag{61}$$

according to their notations, for one electron pocket and one hole pocket, then

$$A^{\pm} = \frac{3}{8k_f^3} \int_0^{2k_f} \frac{L}{L^{\pm}} q^3 dq$$

In our notation for six-hole pockets and three-electron pockets:

$$A^{+} = \frac{9N}{4n} \left(\frac{T}{\Theta_D}\right)^3 \int_0^{\frac{\Theta_4^*}{T}} \frac{6L_1}{L^{+}} \frac{x^4 e^x}{(e^x-1)^2} dx$$

$$A^{-} = \frac{9N}{4n} \left(\frac{T}{\Theta_D}\right)^3 \int_0^{\frac{\Theta_4^*}{T}} \frac{3L_1}{L^{-}} \frac{x^4 e^x}{(e^x-1)^2} dx$$

If the intervalley scattering is very weak, $\varepsilon_g(0)$ can be rewritten as

$$\varepsilon_g(0) = \frac{1}{\sigma(0)} \left[\frac{3Nk_B}{ne} \left(\frac{T}{\Theta_D}\right)^3 \int_0^{\frac{\Theta_4^*}{T}} \left(\sigma_h^{imp} \frac{6L_1}{L^{+}} - \sigma_e^{imp} \frac{3L_1}{L^{-}}\right) \frac{x^4 e^x}{(e^x-1)^2} dx\right] \tag{62}$$

It has to be mentioned that, due to the mutual drag effect which we neglected in our calculation, the residual conductivities should be used in Eq. (60). Thus, the difference between Eq. (62) and the first term of Eq. (60) apparently is caused by the neglect of the mutual drag effect in our calculation.

Isothermal Magnetoresistivity $\rho_{11}(H)$

If the cyclotron frequency of the carrier is ω_c where $\omega_c = \frac{eH}{m_c^* C}$, the high field condition implies that $\omega_c \tau_c >> 1$. The saturated field is then defined as $H_o = \frac{m_c^* C}{e\tau_c}$, where τ_c is the relaxation time of the carrier. In antimony, the saturated field was found about 10^2 gauss or less.[20,40] Thus, if $H >> H_o$, the carriers are at the high field condition, that is, $\omega_c \tau_c >> 1$, then the drift velocities $\vec{V}^{\pm}$ and $\vec{U}$ can be written down as:

$$\vec{V}^{\pm}(\varepsilon_f) + \frac{e^{\pm}\ell^{\pm}}{c\, P_f^{\pm}} [\vec{H} \times \vec{V}^{\pm}] - \frac{\ell^{\pm}}{\ell_f^{\pm}\, J_5(\frac{\textcircled{H}^*_{e,h}}{T})} \int_o^{\frac{\textcircled{H}^*_{e,h}}{T}} \vec{U}(x)\, \frac{x^5 e^x}{(e^x-1)^2}\, dx = \frac{\not{H} e^{\pm}\ell^{\pm}}{P_f^{\pm}} E \tag{63}$$

$$\vec{U}(\omega) = -\frac{6L}{L^+} \int_{\varepsilon^+(\frac{q}{2})}^{\infty} \vec{V}^+(\varepsilon)\, \frac{\partial f_{\vec{k}}^{o+}}{\partial \varepsilon}\, d\varepsilon - \frac{3L}{L^-} \int_{\varepsilon^-(\frac{q}{2})}^{\infty} \vec{V}^-(\varepsilon)\, \frac{\partial f_k^{o-}}{\partial \varepsilon}\, d\varepsilon \tag{64}$$

It is easier to use iteration to solve these simultaneous equations. In this study magnetic field is always applied in the trigonal axis, so that the drift velocities of the carriers and phonons are in basal plane. If E is applied along the x direction (or bisectrix axis), then if $\vec{U}(\omega) = 0$, the solutions of $\vec{V}^{\pm}(\varepsilon_f)$ are

$$\vec{V}^{\pm}(\varepsilon_f) = [(\frac{c}{H})^2 \frac{\hbar P_f^{\pm}}{e^{\pm}\ell^{\pm}} E, -\frac{\hbar cE}{H}, 0] \tag{65}$$

From $\vec{V}^{\pm}(\varepsilon_f)$ we can obtain $\vec{U}(\omega)$ as

$$\vec{U}(\omega) = [(\frac{c}{H})^2 \frac{\hbar E}{e^{+}} (\frac{6L_1 P_f^{+}}{L^{+}\ell^{+}} - \frac{3L_1 P_f^{-}}{L^{-}\ell^{-}}), -(\frac{6L_1}{L^{+}} + \frac{3L_1}{L^{-}}) \frac{\hbar cE}{H}, 0]$$

q ε region 1 (66a)

$$\vec{U}(\omega) = [(\frac{c}{H})^2 \frac{\hbar E}{e^{+}} \frac{6L_2 P_f^{+}}{L^{+}\ell^{+}}, -\frac{6L_2}{L^{+}} \frac{\hbar cE}{H}, 0]$$

q ε region 2 (66b)

$$\vec{U}(\omega) = [(\frac{c}{H})^2 \frac{\hbar E}{e^{-}} \frac{3L_3 P_f^{-}}{L^{-}\ell^{-}}, -\frac{3L_3}{L^{-}} \frac{\hbar cE}{H}, 0]$$

q ε region 3 (66c)

$$\vec{U}(\omega) = 0 \qquad \text{q } \varepsilon \text{ region 4} \tag{66d}$$

As is noted previously that the carrier-phonon scattering dominates in the "enclosed phonon" scattering mechanisms. The frequencies of the phonon-boundary and phonon-isotope scatterings are only a small fraction of the scattering frequency of enclosed phonons. For simplicity we assume that

$$\gamma_1 = \frac{6L_1}{L^{+}} + \frac{3L_1}{L^{-}} \qquad \text{as q } \varepsilon \text{ region 1}$$

$$\gamma_2 = \frac{6L_2}{L^+} \qquad \text{as q } \varepsilon \text{ region 2}$$

$$\gamma_3 = \frac{3L_3}{L^-} \qquad \text{as q } \varepsilon \text{ region 3}$$

then, $\gamma_1 \simeq \gamma_2 \simeq \gamma_3 = \gamma$ so long as q is in regions 1, 2 and 3. The introduction of this parameter γ does not lead to a significant error because γ_1, γ_2 and γ_3 are all nearly unity due to the strong phonon-carrier scattering at the helium temperature with $1/L_r$ negligible.

If the deviations (or drag term) of $V^{\pm}(\varepsilon_f)$ are $\delta V^{\pm}(\varepsilon_f)$, then $\delta V^{\pm}$ are given by

$$\delta V^{\pm} \simeq [-(\frac{c}{H})^2 \gamma \frac{\hbar P^{\pm}}{e^{\pm} \ell_f^{\pm}} E \ , \ 0 \ , \ 0 \ ] \tag{67}$$

to the second order of magnetic field, as q is in the regions 1, 2 and 3. From Eqs. (65) and (67) one obtains

$$J \simeq \frac{ne^+}{\hbar} [(V^+ + \delta V^+) - (V^- + \delta V^-)]$$

or

$$\sigma_{11}(H) = n(\frac{c}{H})^2 \left[\frac{P_f^+}{\ell_{imp.}^+} + \frac{P_f^-}{\ell_{imp.}^-} + \frac{(1-\gamma)P_f^+}{\ell_f^+} + \frac{(1-\gamma)P_f^-}{\ell_f^-} \right] \tag{68a}$$

Because $\ell^+ >> \ell^-$, hence,

$$\sigma_{11}(H) \simeq \left(\frac{c}{H}\right)^2 n\left(\frac{P_f^-}{\ell_{imp.}^-} + \frac{P_f^-}{\ell_f^-}(1-\gamma)\right)$$

$$= [\sigma_{imp}(H)]_{11} + (1-\gamma)[\sigma_{e-p}(H)]_{11} \tag{68b}$$

where

$$[\sigma_{imp}(H)]_{11} = \left(\frac{c}{H}\right)^2 \frac{nP_f^-}{\ell_{imp.}^-}$$

$$[\sigma_{e-p}(H)]_{11} = \left(\frac{c}{H}\right)^2 \frac{P_f^-}{\ell_f^-}$$

or

$$\rho_{11}(H) \simeq \left(\frac{H}{c}\right)^2 \frac{1}{n\left(\frac{P_f^-}{\ell_{imp.}^-}\right) + n\frac{P_f^-}{\ell_f^-}(1-\gamma)} \tag{69}$$

Equation (69) is in general agreement with Kagan and Flerov calculation,[48] as well as Gurevich and Korenblit.[42]

Ettingshausen Coefficient $\pi''_{21}(H)$ and Nernst-Ettingshausen Coefficient $\varepsilon''_{21}(H)$

Although the conventional definitions of Ettingshausen and Nernst-Ettingshausen coefficients are $\pi'_{21}(H)$ and $\varepsilon'_{21}(H)$, we will still calculate $\pi''_{21}(H)$ and $\varepsilon''_{21}(H)$ instead of $\pi'_{21}(H)$ and $\varepsilon'_{21}(H)$.

From the obtained drift velocities $V^{\pm}(\varepsilon_f)$ and $U(\omega)$ in Eqs. (65) and (66), one can obtain the heat current density consisting of carriers and phonons flow. If W_q is the heat current carried by phonons, then its y-component is given by:

$$(W_q)_y = \frac{1}{(2\pi)^3}\frac{1}{kT}\int (\vec{U}(\omega)\cdot\vec{q})\, s\hbar\omega\, N_q^o(N_q^o+1)d^3q$$

$$\simeq -\frac{cE}{H}\cdot\frac{\gamma T}{3}C_g\left(\frac{\Theta_1^*}{T}\right) \qquad (70)$$

where $\Theta_1^* = \frac{2\hbar s k_1}{k_B}$ and k_1 is the "radius" of regions 1, 2 and 3 as we approximate this by a sphere. And

$$C_g\left(\frac{\Theta_1^*}{T}\right) = 3Nk_B\left(\frac{T}{\Theta_D}\right)^3 \int_0^{\frac{\Theta_1^*}{T}} \frac{x^4 e^x}{(e^x-1)^2}\,dx$$

Furthermore, the heat current density, W_e, carried by carriers is given by

$$(W_e)_y = -\sum_{\pm}\frac{(2m_{e,h}^*)^{3/2}}{3\pi^2\hbar^3}\int \frac{cE}{H}\,\varepsilon^{3/2}(\varepsilon-\xi^{\pm})\,\frac{\partial f_k^{o\pm}}{\partial\varepsilon}\,d\varepsilon$$

$$= -\frac{cE}{H}C_e\,T \qquad (71)$$

where

$$C_e = \frac{\pi^2 k_B^2 T}{3}(Z_e + Z_h)$$

Z_e and Z_h are the densities of states of electrons and holes at the Fermi surface.

Combining Eqs. (70) and (71), we have

$$W_2 = - \frac{cE}{H} T[C_e + \frac{\gamma}{3} C_g(\frac{\Theta^*}{T})]$$

or

$$\pi''_{21}(H) = \frac{cT}{H} [C_e + \frac{\gamma}{3} C_g(\frac{\Theta^*}{T})] \tag{72}$$

or

$$\varepsilon''_{21}(H) = \frac{c}{H} [C_e + \frac{\gamma}{3} C_g(\frac{\Theta^*}{T})] \tag{73}$$

Adiabatic Magnetoconductivity $\sigma^a_{11}(H)$

If one measured $\sigma^a_{11}(H)$ under the adiabatic condition, i.e., $W^*_y = 0$, then $\sigma^a_{11}(H)$ should be different from $\sigma^{is}_{11}(H)$ which is obtained previously. For the sake of solving this problem, let's assume that the temperature gradient generated by Ettingshausen heat current is so small that the electron and hole distributions are negligibly changed and the superposition principle of carrier's and phonon's drift velocities due to both electrical and temperature gradient is also true. Then, we can write

$$U_y(\omega) = \gamma \frac{cE}{H} - \frac{\hbar L s}{T} \nabla_y T \tag{74}$$

where $\nabla_y T = \frac{\pi''_{21}}{\lambda_g} E$ because $W_y = 0$, therefore

$$U_y(\omega) = \gamma \frac{cE}{H} - \frac{c}{H} \frac{\lambda_g^{eN}}{\lambda_g} \left(\gamma + \frac{3C_e}{C_g(\frac{\Theta^*}{T})}\right) E$$

then one can have

$$\sigma_{11}^a(H) = [\sigma_{imp.}(H)]_{11} + (1-\gamma)[\sigma_{e-p}(H)]_{11} + \frac{\lambda_g^{eN}}{\lambda_g} \left(\gamma + \frac{3C_e}{C_g(\frac{\Theta^*}{T})}\right)[\sigma_{e-p}(H)]_{11} \tag{75}$$

where

$$\lambda_g^{eN} = \frac{1}{3} C_g(\frac{\Theta^*}{T}) \langle L \rangle s$$

and C_e is the specific heat of the carrier

$C_g(\frac{\Theta^*}{T})$ is the specific heat of enclosed phonons

s is the speed of sound.

C. Ziman's Cutoff in the Electron-Hole System

The carrier-phonon normal process intravalley scattering, carrier-phonon drag effect and their contributions in the transport coefficients have been discussed in the previous section, while the quantity which is defined as $\Theta^* = (\frac{2k_f}{q_D})\Theta_D$

has not yet been clearly discussed. It will be the purpose to define this quantity Θ^*, that is, the "effective-scattering-Debye-temperature" or "Ziman's cutoff temperature."

The electron-phonon normal (intra valley) process with $\vec{k} + \vec{q} = \vec{k}'$ and $\varepsilon_{\vec{k}} + \hbar\omega_{\vec{q}} = \varepsilon_{\vec{k}'}$, involved phonons which, to a good approximation, obey the relation $\vec{q} = \vec{k}'_F - \vec{k}_F$ and belongs to a group said to be "enclosed" phonons. In the case of a Fermi sphere of radius k_F, electrons will be solely scattered by the phonons enclosed in a sphere of radius $2k_F$ and if the phonon-phonon interaction is weak, the effective scattering (Debye temperature) appearing in the transport effects in the relation with electron-phonon scattering will be $\Theta^* = \frac{2k_f}{q_D}\Theta_D$,[49] q_D is the Debye-radius, Θ_D is Debye temperature.

In case of a Fermi "ellipsoid," the "enclosed" phonons are contained in a similar ellipsoid of double dimension. The phonons outside this limit will be called "peripheral" phonons and will not scatter the electrons. The scattering cutoff will be referred to as "Ziman's Cutoff." In order to estimate an effective cutoff temperature, it is necessary to use an approximation which averages the anisotropy of electron distribution and phonon velocity, it is possible to introduce an effective scattering temperature.

In the case of antimony with three electron pockets and three pairs of hole pockets, one can define several elementary cutoffs. According to the discussion in previous

section, the "drift velocity" of phonons and the resistive scattering frequency of phonons depend on the external fields, the size and the orientation of Fermi surfaces, and the types of phonons. In short, one can obtain several cut-offs from both size and orientation of Fermi surfaces and from drag effects.

(1) The cutoff associates with those phonons that are enclosed by either electron or hole. These phonons have the same drift velocity as charge carriers at the high field limit. This cutoff is corresponding to those phonons which are in region 1, 2 and 3 of Figure 11 (see previous section).

(2) The cutoff associates with the phonon that is enclosed to the electron. These phonons will scatter with electrons and exhibit a characteristics along with the resistivity of the electron. This cutoff is corresponding to those phonons of "b" ellipsoid of Figure 11.

(3) The cutoff associates with the phonon that is enclosed to the hole. This cutoff is corresponding to those phonons of "a" ellipsoid of Figure 11.

(4) The cutoff associates with those phonons that are enclosed to both electron and hole simultaneously. These phonons can scatter with both electron and hole. In particular, such as in the ideal resistivity case, the net momenta of these phonons gained from scattering with charge carriers are nearly canceled when electron and hole drift in opposite directions. This cutoff is corresponding to

those phonons in region 1 of Figure 11.

The same subdivision valid for the electron-phonon scattering can be applied to the simple and mutual drag effects. It is obvious that only those phonons which scatter (or are scattered by) electrons drag (are dragged by) electrons. In short, the Ziman's cutoffs are exhibited not only in resistive scattering but also in the drag effect.

The same type of cutoff appearing in different kind transport coefficients may exhibit apparently quite different value. For instance, the first type of cutoff, Θ_1^*, appearing in Ettingshausen effect shows an apparent difference from that which appears in lattice conductivity. The cutoff, Θ_1^*, of Ettingshausen effect is about 29°K, while the cut-off, Θ_1^*, of lattice conductivity is about 24°K. This can be understood in such a way that the Fermi surfaces of both electrons and holes are ellipsoids. The cutoff temperature is proportional to some sort of average of the wave vectors for a specific group of enclosed phonons. However, the average usually tends to be that involving the predominant carriers. The predominant phonons yielding Ettingshausen heat current are those phonons with larger wave vectors because of their greater energy; however, the predominant heat carrier in the peripheral phonon heat conduction are those phonons with smaller wave vectors because of less scattering frequency and therefore more mobile. Therefore the cutoff of Ettingshausen is 29°K and larger than that of

lattice conductivity, that is, about 24°K. Such effects may also show in the second and third type of cutoffs.

Though Ziman's cutoffs as well as the selective drag cutoffs are very complicated in some aspects, they provide with the details of electron-phonon scattering mechanisms, and allow one to understand more about transport phenomena.

D. Result and Discussion

Thermal and Electrical Resistivity in Zero Magnetic Field

The measured values of the total thermal conductivity, λ_T, for sample #17 are shown in Fig. 12 along with values of the lattice conductivity, λ_g, measured with the application of a 20 kG magnetic field. The dotted line represents $\lambda_e = \lambda_T - \lambda_g$. Curves B, C, and D were taken from White and Woods.[50] While curves G and H are the curves interpolated from this measurement (curves A, E, F) to White and Woods measurement (B, C, D) using Makinson's formula.[51] These measurements display several notable features: first the thermal conduction below 3°K is almost entirely by charge carriers while above the lattice contributes significantly; the maximum at ~2°K is due to the competition of carrier-phonon and carrier-impurity scattering processes, the maximum at ~5.5°K is due to the superposition of carrier and lattice conduction.

In considering electronic thermal conductivity, λ_e, we assume Matthiessen's rule is valid for lower temperature

limit, then

$$\gamma_e = \frac{1}{\lambda_e} \simeq \frac{\rho_o}{L_o T} + BT^2 \tag{76}$$

where

ρ_o is the residual electrical resistivity

L_o is the Lorenz number, $L_o = 2.45 \times 10^{-8}$ $J^2/coul^2K^2$

B is a constant depending on electron-phonon coupling.

One may obtain ρ_o and B by plotting $\gamma_e T$ against T^3, which is shown in Fig. 13. For sample #17,

$$\rho_o = 4.7 \times 10^{-9} \text{ cm}$$

$$B = 1.13 \times 10^{-4} \text{ m w}^{-1} .$$

The value, ρ_o, obtained from this measurement is consistent with the directly measured value (see section on electrical resistivity).

The parameter B, following Wilson's theory,[49] is for $T \to 0$ limit

$$B = \frac{27h^2 N\epsilon_h^2}{64\pi^3 k_B^2 \xi_h^2 \rho S} \left(\frac{1}{\Theta_D}\right)^3 J_5(\infty) \frac{1}{a_h} \tag{77}$$

where N is the number of atoms in a unit volume

ϵ_h is deformation potential of the hole

ξ_h is the Fermi energy

ρ is the density, s is the speed of sound

Θ_D is the Debye temperature

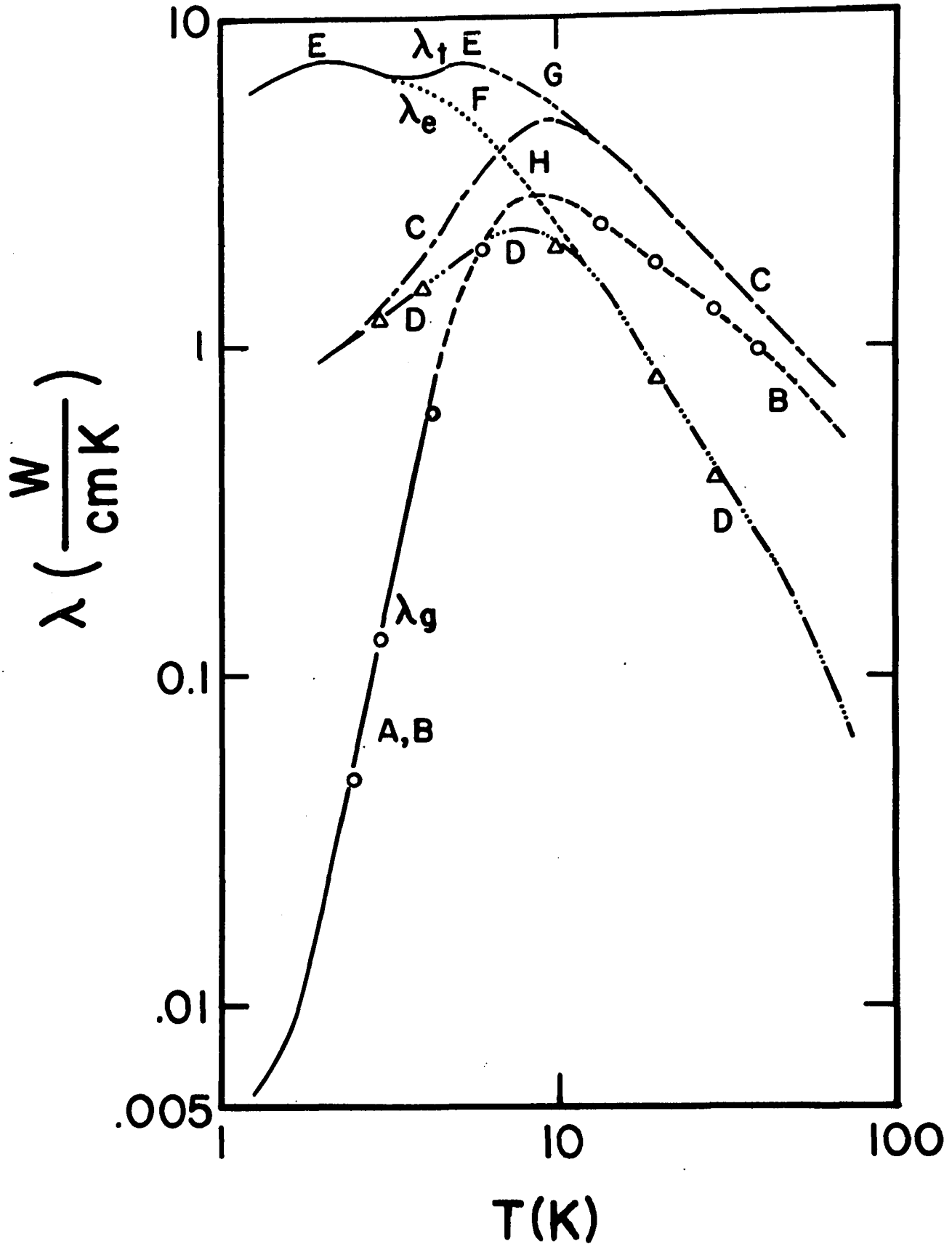

Fig. 12

a_h is the anisotropic parameter.[20]

The scattering parameter (deformation potential) of the high mobility carrier (it is a hole[20]) deduced from this measurement is about 1.615 eV. However, Kleimen[43,52] has shown that there is a correction factor of .68 for B, thus giving deformation potential $\varepsilon_h = 1.96$ eV. This value is in good agreement with that deduced from the RFSE measurement[53] (about 1.9 eV). In the higher temperature range, the deviation of $\gamma_e T$ from Eq. (76) can be understood by the substitution of $J_5(\frac{\Theta_h^*}{T})$ for $J_5(\infty)$ in Eq. (77). The value of Θ_h^* required to fit this experimental curve is 25^oK (see Fig. 13). This is an example of a type 3 cutoff (see Section C) which is about 24.4^oK from theoretical calculation.[28]

Starting at sufficiently high temperature $\lambda_e \sim T^{-2}$ because of the dominance of electron-phonon scattering, but as temperature decreases electron-impurity processes become increasingly more important until they dominate giving $\lambda_e \sim T$. The temperature at which the maximum of λ_e occurs is given by $T_{max} = (\frac{\rho_o}{2L_oB})^{1/3}$ and T_m for #17 is 2 K, which is obvious from Fig. 12. Using our value for B(T), the sample of White and Woods yields $T_m = 6\ 8^oK$,[53] which is slightly lower than the peak shown in Fig. 12. The difference is due to the superposition of the maximum in the lattice thermal conductivity which occurs ~8 K.

To a good approximation for the isotropic sample, the thermal conductivity is generally given by

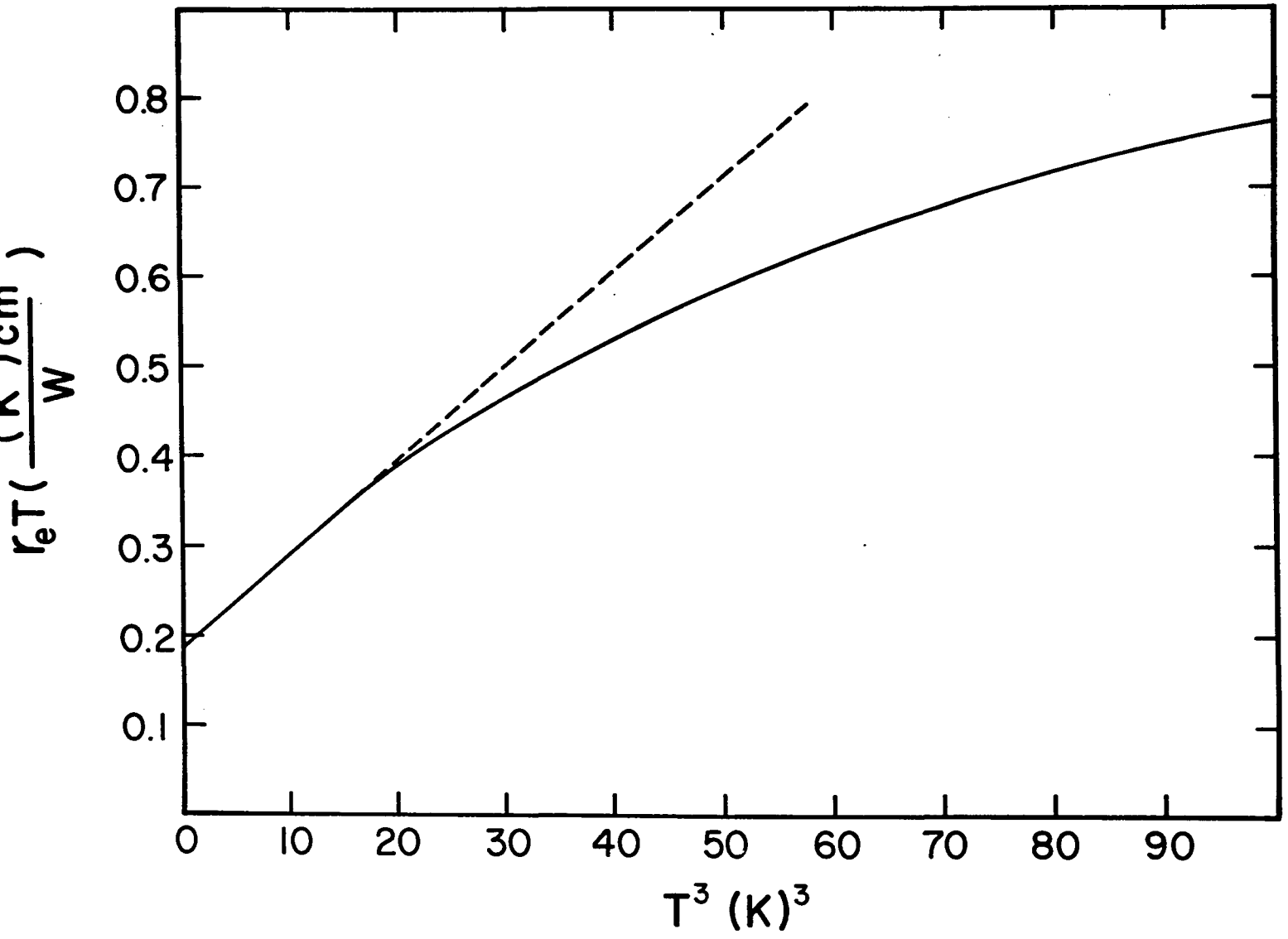
0.8
0.7
0.6
0.5
0.4
0.3
0.2
0.1
0
10
20
30
40
50
60
70
80
90
$r_e T\left(\frac{(K^2)cm}{W}\right)$
$T^3\ (K)^3$

Fig. 13

$$\lambda_e \simeq \frac{1}{3} C U_F \ell \tag{78}$$

where C, U_F and ℓ are specific heat, Fermi velocity and total mean free path of carriers respectively. In the case of antimony one knows that the mean free path of more mobile carriers, holes, is much longer than that of less mobile carriers while because $CU_F = \frac{n\pi^2 k_B^2 T}{P_F}$ thus this term of hole is still slightly larger than that of electron. Therefore, λ_e is approximately given by

$$\lambda_e \simeq \frac{1}{3} C_h U_F^h \ell^+ = \frac{\pi^2 k_B^2 T}{3P_F^+} \ell^+$$

or

$$\frac{1}{\ell_T^+} = \frac{3P_F^+ J_5(\infty)}{n\pi^2 k_B^2 B J_5(\frac{\Theta^*}{T})} \tag{79}$$

where ℓ_T^+ is the mean free path of hole limited by the hole-phonon scattering.

With the numbers $P_F^+ = 6.78 \times 10^{-26}$ Kg m/s and $B = 1.13 \times 10^{-4}$ m/w, the Eq. (79) yields

$$\ell_T^+ = \frac{218.65}{T^3 J_5(\frac{\Theta^*}{T})} \text{ (cm)} \tag{80}$$

It might be of interest to compare this mean free path with the one deduced from RFSE measured by Gantmahker, et al.[53] Both mean free paths are dominated by the small angle electron-phonon scattering. They are in fairly good agreement in higher temperature range but have an apparent discrepancy in the lower temperature range (see Table III). This apparent discrepancy at lower temperature range is probably due to the difference in extrapolation of the calculation. The temperature dependence of ℓ_T^+ is about T^{-3} at lower temperature range, the apparent power dependence will slightly decrease as temperature increases, because the Debye integral weakens the temperature dependence of ℓ_T^+ . Thus ℓ_T^+ looks like T^{-2} dependence at higher temperature range, which was observed by the RFSE.

Table III

The mean free path of a hole (cm)

T	1.5°K	2°K	2.5°K	3°K	3.5°K	4°K
This work	.521	.198	.120	.072	.054	.042
Gantmakher	.302	.170	.109	.075	.056	.043

Another interesting feature which should be made is the scattering mechanism in the thermal conductivity. In the lower temperature, such as helium temperature, the thermal resistivity is proportional to the square of the temperature, and not the fourth power as one would deduce from the electrical resistivity and the Wiedemann-Franz law. This

confirmed that the small angle scatterings dominate the thermal resistivity. One can know that when the phonon energy is comparable with $k_B T$ at low temperature ($T < \Theta_D$) scattering through large angle merely turn a hot electron going one way into a cold electron going the opposite way, and thus the large angle scattering has very little effect on the heat current. But inelastic scattering through small angle is very effective in reducing the heat current, for it can change a hot electron into a cold one, or vice versa at a single scattering. Because only the long wavelength phonons are available in helium temperature for scattering, the angle of scattering must be small in this temperature range.

There is no direct evidence for the mutual or simple drag effects to thermal resistivity. This absence may occur because the scattering of electrons by phonons is not altered by the presence of a thermal current. That is, to a first approximation, the flux of phonons helps the "hot" electrons moving in the flow direction as much as it hinders "cold" electrons moving in the opposite direction, and thus electron-phonon drag phenomena has very little effect on the electronic heat current. The theoretical studies about this only Gurevich, et al., and the calculated value from their equation shows in Fig. 14, and is too small to compare with either electronic conductivity or even lattice conductivity.

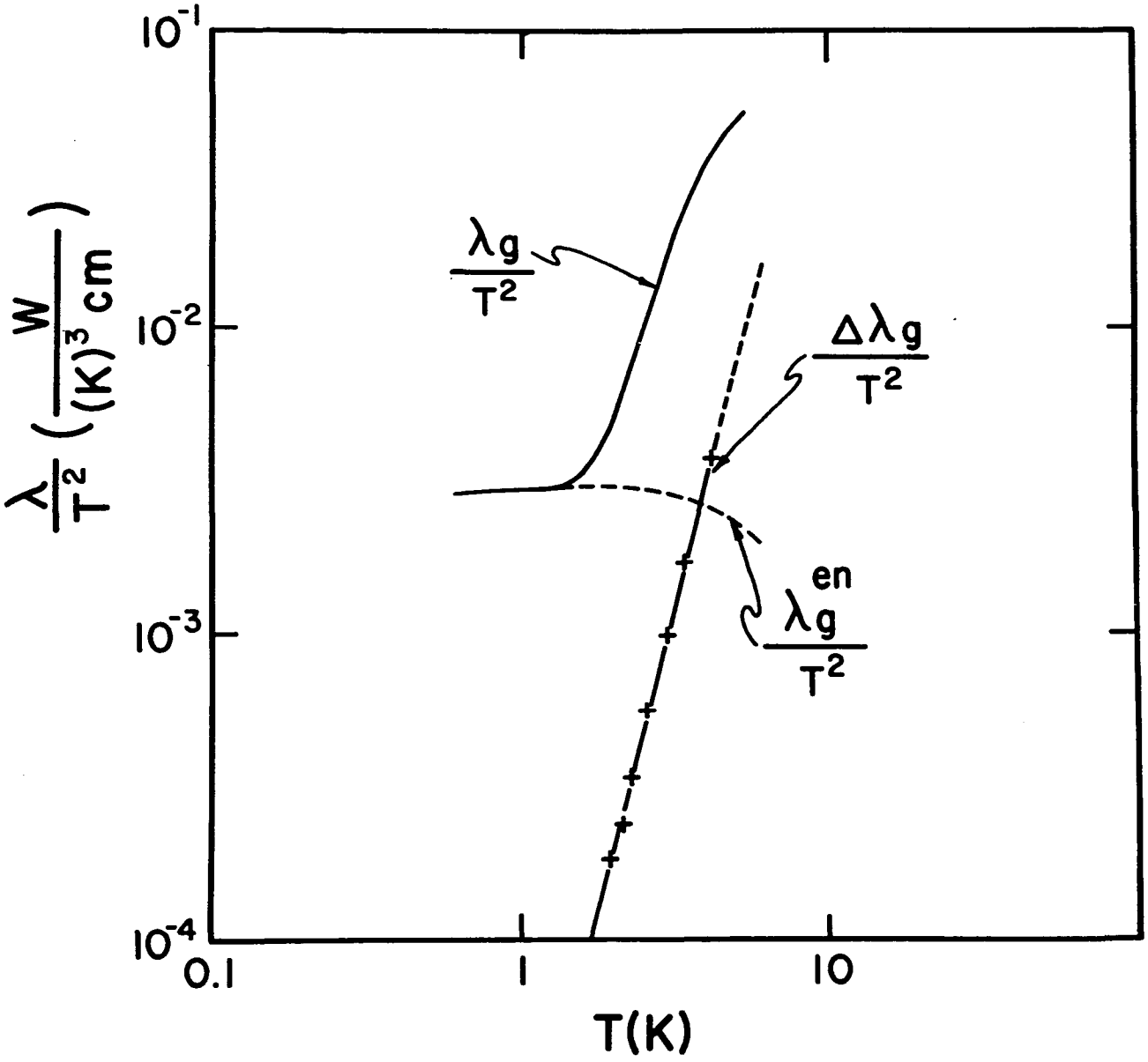
10^{-1}
10^{-2}
10^{-3}
10^{-4}
$\frac{\lambda}{T^2}\left(\frac{W}{(K)^3 cm}\right)$
$\frac{\lambda g}{T^2}$
$\frac{\Delta\lambda g}{T^2}$
$\frac{\lambda g^{en}}{T^2}$
0.1
1
10
T(K)

Fig. 14

The measured values of electrical resistivity, ρ, are shown in Fig. 15. The ideal resistivity $\rho_{id} = \rho - \rho_o$, is shown in log-log plot in Fig. 16, where ρ_o is residual electrical resistivity. For this sample #17, $\rho_o \simeq 4.8 \times 10^{-9}$ Ω cm, which is within 2% of the same value deduced from residual thermal resistivity (see previous section). The temperature dependence of the ideal resistivity apparently obeys the Bloch-Gurneisen T^5 law at lower temperature. This bending of the temperature dependence can be explained by the Debye integral with a small cutoff of drag-compensation which is about 15.7°K. This measured cutoff is in good agreement with theoretical consideration (see section B) and with Long, et al., measurements.[20]

In considering the ideal conductivity, the main contribution comes from the more mobile carriers, i.e. the holes. According to Wilson's theory, the ideal conductivity, σ_{id}, is given by[49]

$$\frac{1}{\sigma_{id}} = \rho_{id} = \frac{3\pi N h^2 \epsilon_h^2}{16 e^2 \rho S \xi_h^2 a_h} \left(\frac{\Theta_D}{\Theta_h^*}\right)^2 \left(\frac{T}{\Theta_D}\right)^5 J_5\left(\frac{\Theta_h^*}{T}\right) \qquad (81)$$

The slope of ρ_{id} against T^5 can be used to calculate the deformations potential. The experimental data yields the deformation potential of hole about 2.87 eV which is higher than the same quantity obtained by either thermal conductivity or RFSE. This discrepancy may be due to the possibility that the experimentally determined coefficient

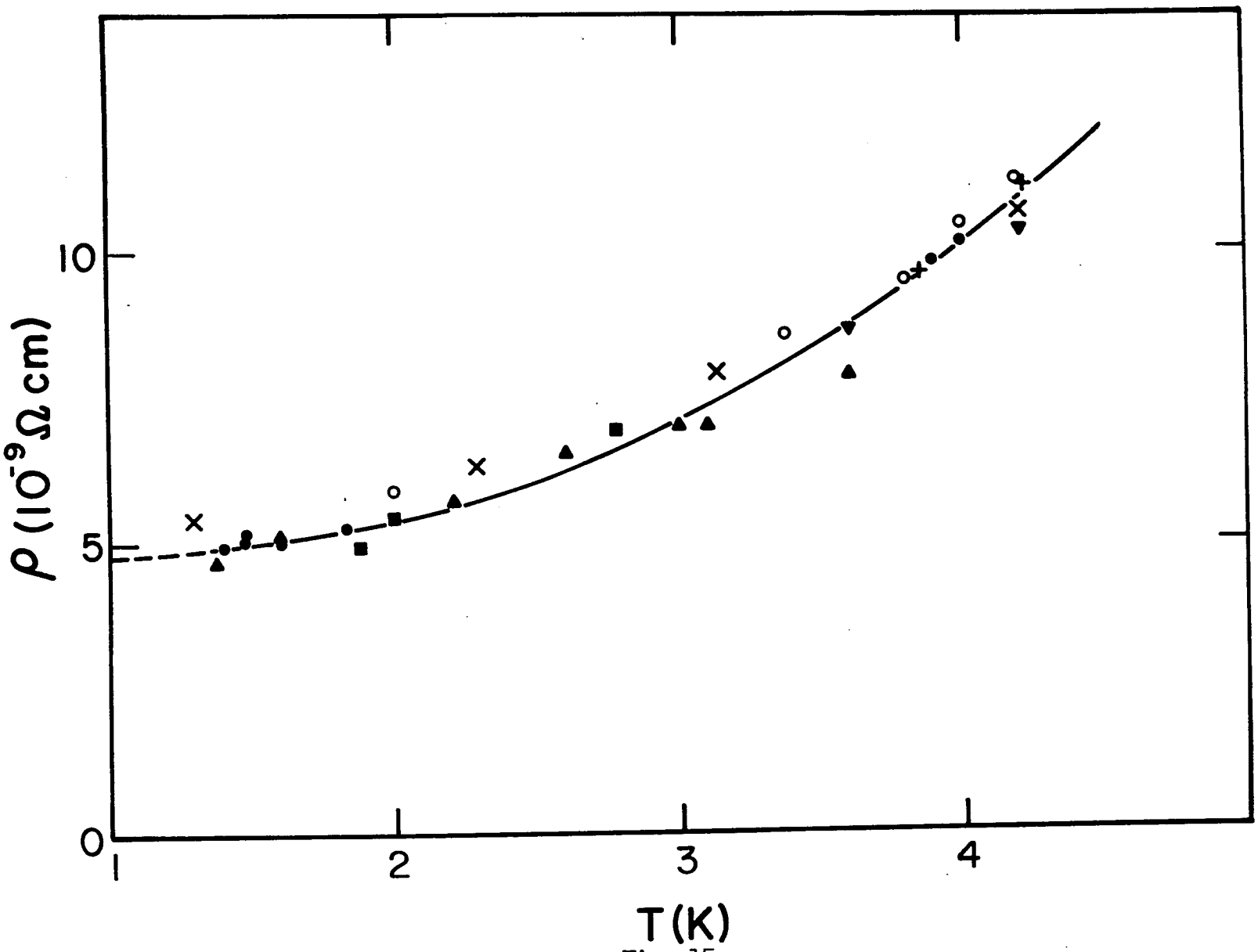

Fig. 15

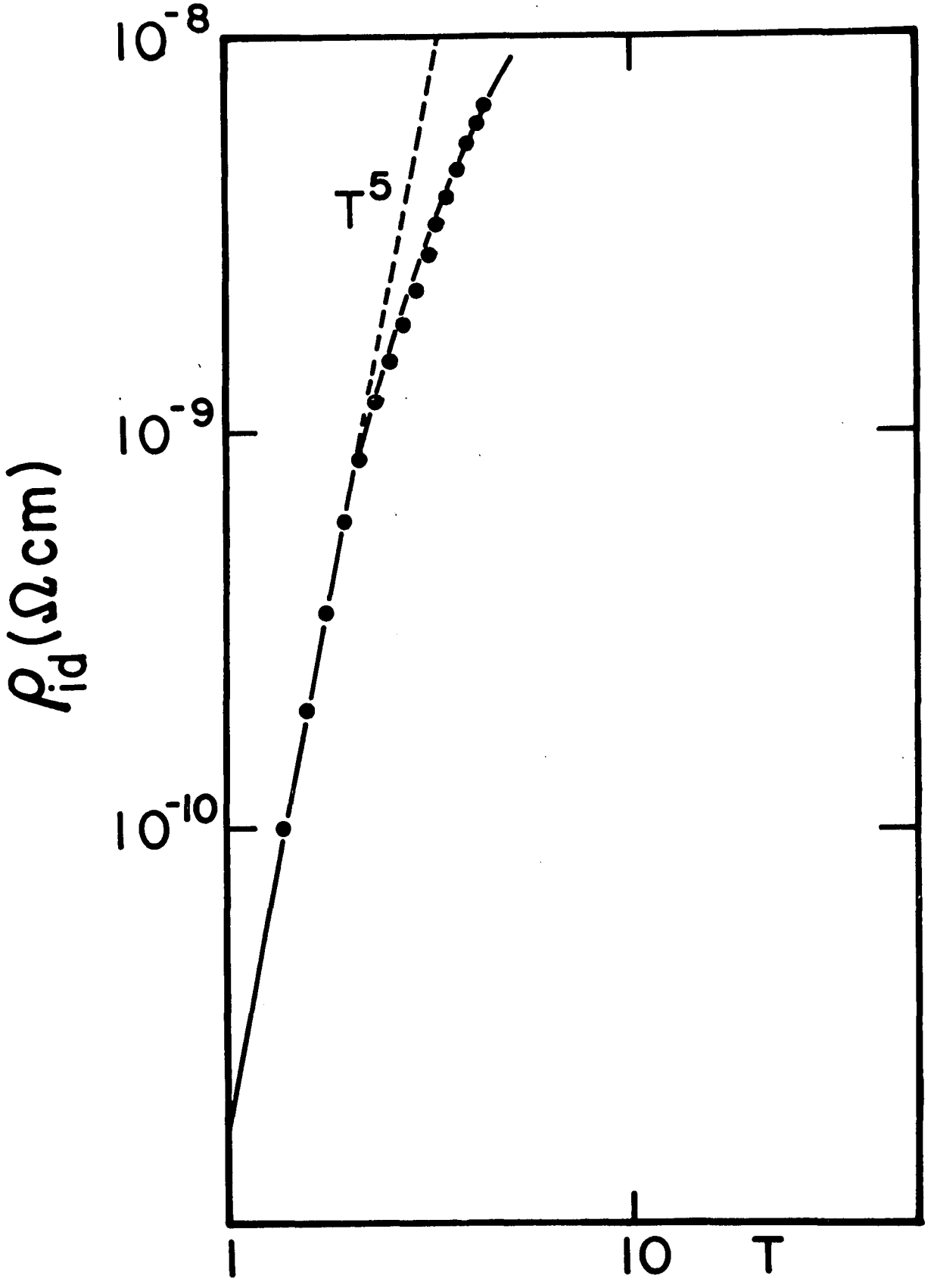

Fig. 16

ρ_{id} has to be corrected from size effect before being analyzed as a bulk coefficient. According to the work by Aleksandrov, et al.,[4] on size effect in antimony the diffusive scattering of charge carrier against boundary of sample yields very strong size dependence. If one is allowed to use Dingle's equation[54]

$$\rho_d = \rho_\infty(1 + \frac{\alpha\lambda}{d}) \tag{82}$$

Aleksandrov, et al., found[4] that $\alpha\rho_\infty\lambda = 3.32 \times 10^{-9}\ \Omega\ cm^2$ and $\lambda \sim 3.4$ mm.

Using Eq. (82) and $\lambda = 3.4$ mm, then the bulk ideal resistivity of sample #17 is about 52% of the measured value which yields the deformation potential about 2.1 eV. This value of deformation potential is more consistent with the other measurements. It is important to note that the thickness does not influence the temperature dependence of the antimony.

The most important feature in ideal resistivity is the temperature dependence. As is noted elsewhere that the T^5 law confirms carrier-phonon small angle scattering dominates the scattering mechanisms of charge carrier system. But electron-phonon large angle scattering is the only effective mechanism to yield electrical resistivity. Because the small angle scattering yields the thermal resistivity at low temperature, thus the ratio of $(\lambda_e)_{id}/\sigma_{id}T$, that is, ideal

Lorenz number is given by a T^2 law. Following Wilson's theory, the ideal thermal resistivity is written as

$$\frac{1}{(\lambda_e)_{id}} = \gamma_{id} = \frac{27Nh^2\varepsilon_{\lambda h}^2}{64\pi^3 k_B \rho S \xi_h^2 a_h} \frac{1}{\Theta_D} \left(\frac{T}{\Theta_D}\right)^2$$

$$x \left\{ J_5\left(\frac{\Theta_h^*}{T}\right) + \frac{2}{3}\left(\frac{T}{\Theta_h^*}\right)^2 \cdot \left(2\pi^2 J_5\left(\frac{\Theta_h^*}{T}\right) - J_7\left(\frac{\Theta_h^*}{T}\right)\right)\right\} \qquad (83)$$

Therefore the "ideal" Lorenz number is given as

$$L_{id} = \frac{(\lambda_e)_{id}}{\sigma_{id} T} \simeq L_o \frac{4\pi^2}{3} \left(\frac{T}{\Theta_h^*}\right)^2 \frac{\varepsilon_{\sigma h}^2}{\varepsilon_{\lambda h}^2} \left(\frac{1}{1 + \frac{2}{3}\left(\frac{T}{\Theta_h^*}\right)^2 \left(2\pi^2 - \frac{J_7\left(\frac{\Theta_h^*}{T}\right)}{J_5\left(\frac{\Theta_h^*}{T}\right)}\right)} \right)$$

(84)

where $\varepsilon_{\sigma h}$, $\varepsilon_{\lambda h}$ are the apparent deformations in electrical and thermal conduction. For lower temperature limit

$$1 + \frac{2}{3}\left(\frac{T}{\Theta^*}\right)^2 \left(2\pi^2 - \frac{J_7\left(\frac{\Theta_h^*}{T}\right)}{J_5\left(\frac{\Theta_h^*}{T}\right)}\right) \simeq 1$$

The Eq. (82) is thus written as

$$\frac{L_{id}}{L_o} = \frac{4\pi^2}{3} \left(\frac{T}{\Theta_h^*}\right)^2 \left(\frac{\varepsilon_{\sigma h}}{\varepsilon_{\lambda h}}\right)^2 \qquad (85)$$

The term of $(\frac{T}{\Theta_h^*})^2$ is from the difference of efficiently scattering mechanisms between electrical and thermal conductivity.

The measured value of L_{id}/L_o is shown in Fig. 17. The important features in this figure are that the "ideal" Lorenz number is quadratic dependence of T below 2^oK, and starts to deviate from the quadratic dependence above that temperature.

This apparent deviation from the quadratic dependence of L_{id} is due to the Debye integrals in both electrical and thermal conductivity with different cutoff temperatures. The effective-scattering-Debye temperature (see Section C for detail) of the former is the one associated with the drag compensation. That of the latter is the one associated with the hole. Therefore, the ideal Lorenz number should be written as

$$\frac{L_{id}}{L_o} = \frac{4\pi^2}{3} \left(\frac{T}{\Theta_h^*}\right)^2 \frac{\varepsilon_{\sigma h}^2}{\varepsilon_{\lambda h}^2} \frac{J_5(\frac{\Theta_4^*}{T})}{J_5(\frac{\Theta_h^*}{T})} \tag{86}$$

where $\Theta_h^* = 25^oK$ and $\Theta_4^* = 15.7^oK$ fit the experimental curve very well.

As one noted in Section B, the mutual drag effect decreases the ideal resistivity and the apparent characteristics of this effect appears in the effective-scattering-Debye-temperature. The observed value of effective-scattering-

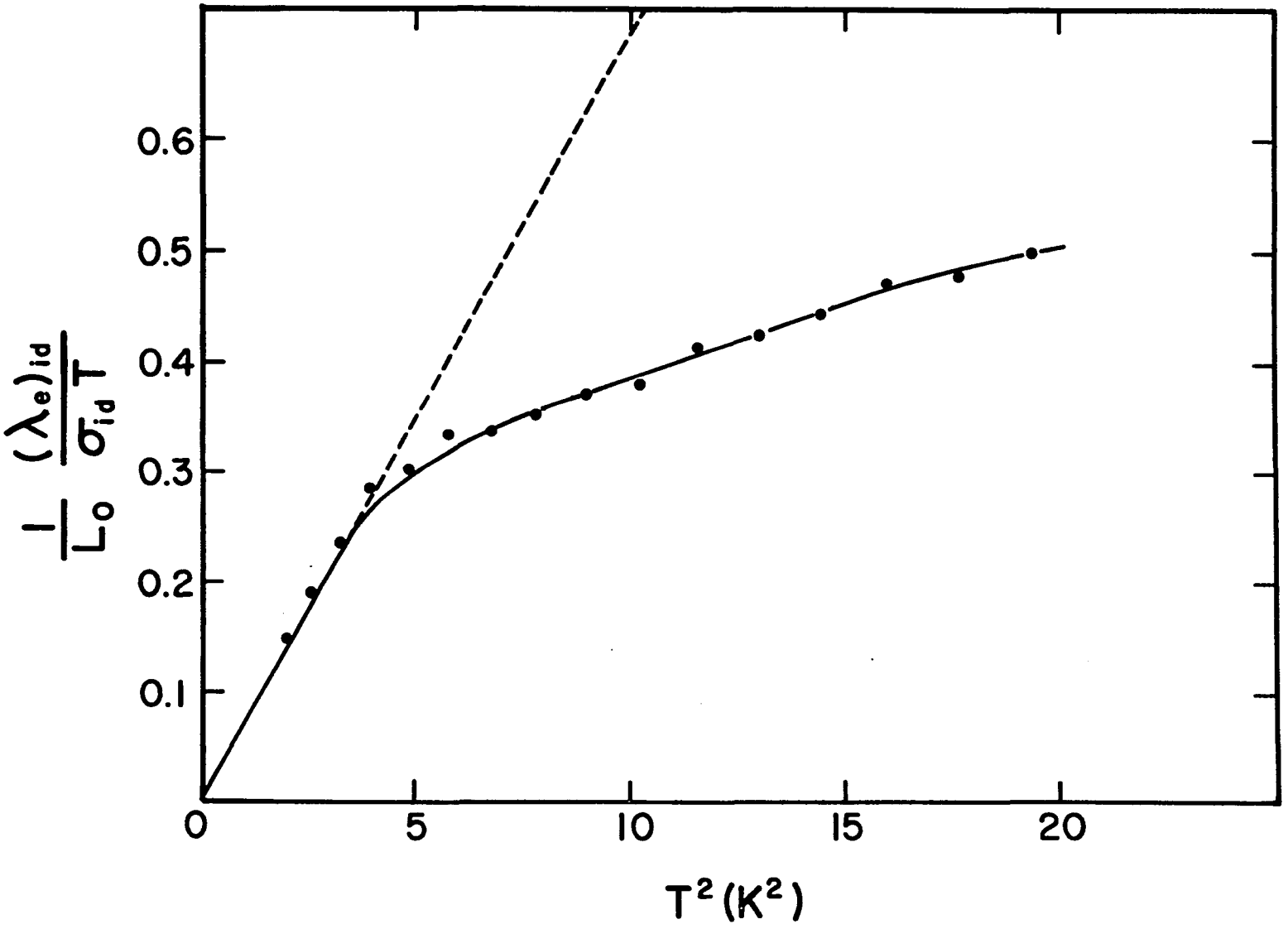
$\frac{1}{L_o}\frac{(\lambda_e)_{id}}{\sigma_{id}T}$
0.6
0.5
0.4
0.3
0.2
0.1
0
5
10
15
20
$T^2(K^2)$

Fig. 17

Debye-temperature of electrical resistivity is corresponding to the volume of phonons (in q-space) which are "enclosed" to both electron and hole, while the measured value of the cutoff of thermal resistivity is corresponding to the volume of phonons which is "enclosed" to hole. In other words, every hole-phonon scattering yields thermal resistivity, while only a part of hole-phonon scattering yield electrical resistivity. Those phonons which only scatter with hole will have the same drift velocity as the hole; therefore, those phonon-hole scatterings are no longer resistive scatterings.[44b]

Finally, it will be worthwhile to mention another characteristic in zero field, the Wiedemann-Franz law. The "total" Lorenz number is shown in Fig. 18. The minimum which occurs at ~ 3.6°K characterizes the carrier-phonon intravalley scattering. The rising of L as temperature decreases below 3°K indicates the relative increase in the carrier-impurity or other elastic scattering mechanisms to play some non-negligible role; the increasing of L as temperature increases from 4°K shows that the carrier-phonon scattering becomes more efficient in relation with the electrical resistivity determination.

Thermoelectric Power (TEP) at Zero Field

Direct measurement of the thermoelectric power (TEP) was performed with $w_2 = w_2^* = J_2 = J_1 = 0$, the heat flow was set along with bisectrix direction and $w_1 = w_1^*$. Since using picovoltmeter system and the niobium superconductor potential

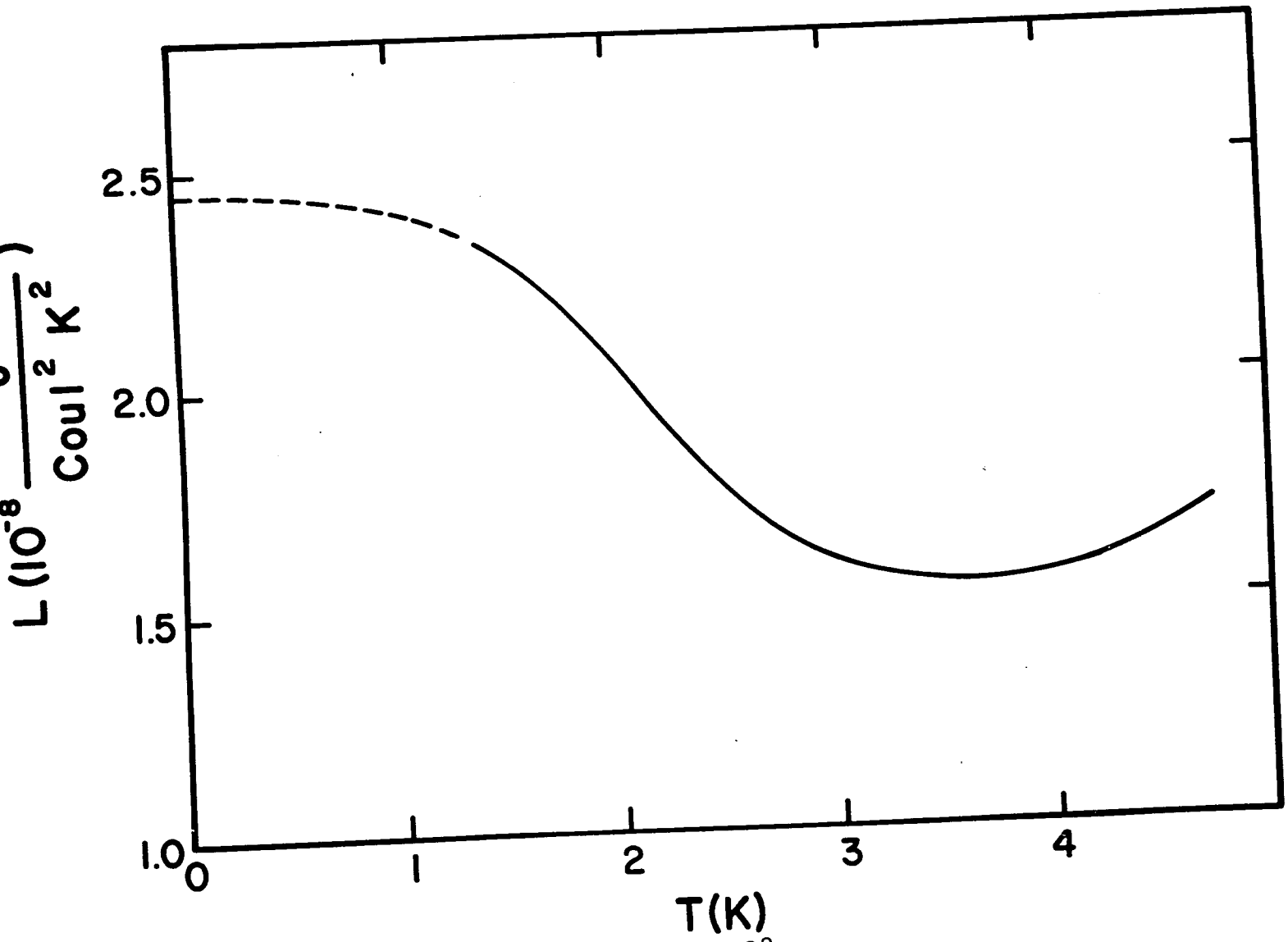

Fig. 18

leads, the longitudinal potential measurement would not be affected by the thermocouple effect from the potential leads even though there is a temperature difference between them. The temperature dependence of the TEP measured along the bisectrix axis at zero magnetic field within the helium temperature range is shown in Fig. 19. The data above $5^{o}K$ is estimated from Bresler and Red'ko measurement[10] in the same orientation. The data of this measurement is in general agreement with other works.[55] The important features in the TEP are the anomalous temperature dependence below $3^{o}K$ and the nearly cubic dependence above that temperature.

Owing to the lack of several important details such as the size effect, etc., the analysis of the TEP is limited to a qualitative discussion.

As one noted above the TEP is conventionally separated into two terms -- a "diffusive" term and a "drag" term. Thus the TEP is usually written as

$$\varepsilon(0) = \varepsilon_d(0) + \varepsilon_g(0) \tag{86}$$

where ε_d is the "diffusive" term; in general, it is linearly dependent on T. ε_g is the "drag" term which displays a cubic dependence on T. So the previous equation can be rewritten as

$$\varepsilon(0) = aT + bT^3 \tag{87}$$

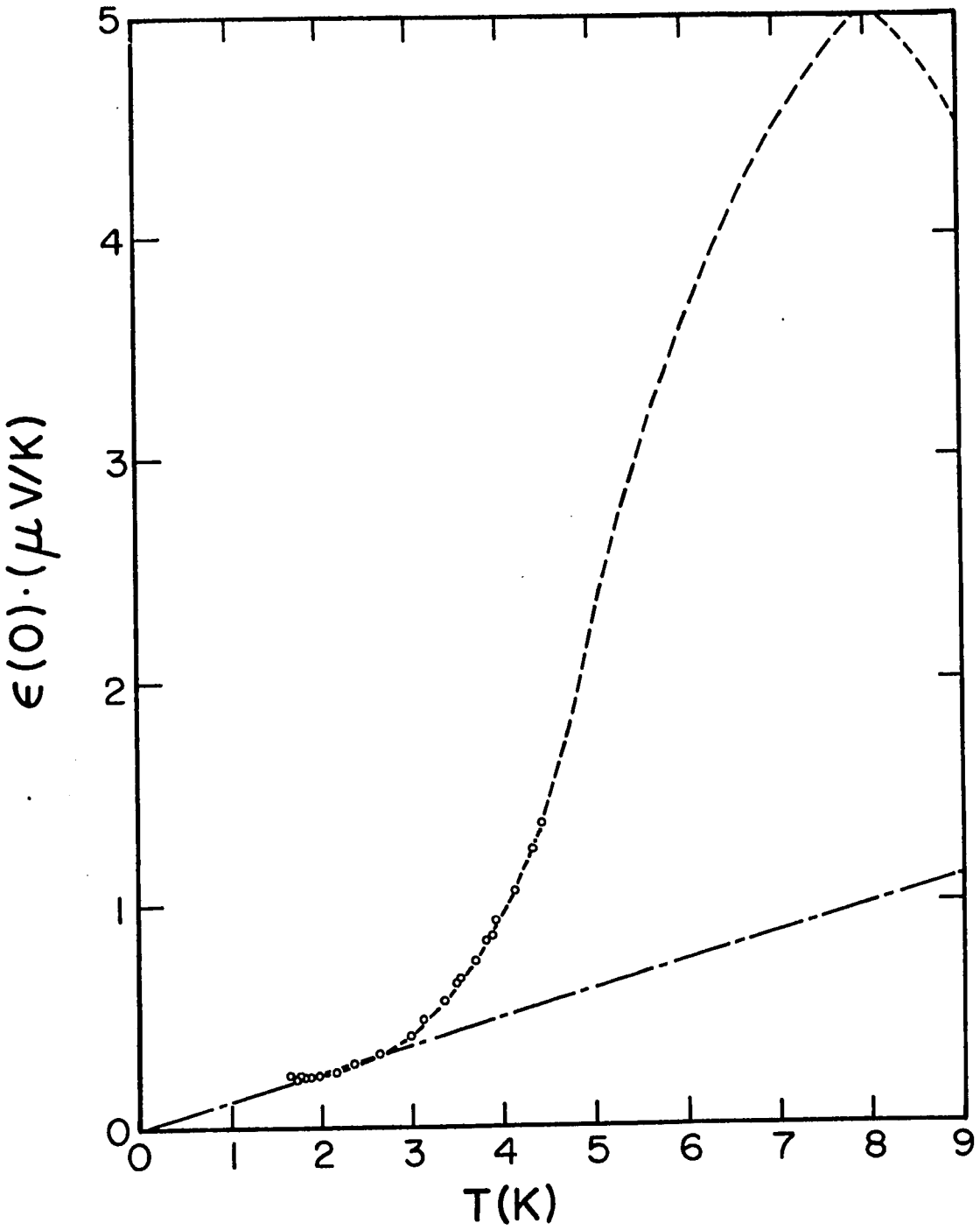

Fig. 19

for lower temperature limit.[56]

These two constants a and b can be obtained by plotting $\varepsilon(0)/T$ vis T^2. For sample #17 (see Fig. 20) at $T \gtrsim 3^{\circ}K$

$$a \simeq -.02\ \mu V/(^{\circ}K)^2 \qquad b = .0157\ \mu V/(^{\circ}K)^4$$

while below $3^{\circ}K$, the temperature dependence of the TEP apparently deviates from Eq. (87).

Above $3^{\circ}K$, the measured value $\varepsilon(0) \sim .0157\ T^3$ is almost entirely from "drag" term. In Section B the drag term is given by

$$\varepsilon_g(0) = \frac{1}{\sigma(0)} \left\{ \frac{3Nk_B}{ne} \left(\frac{T}{\Theta_D}\right)^2 \left[\int_0^{\frac{\Theta_4^*}{T}} \left(\sigma_h \frac{6L_1}{L^+} - \sigma_e \frac{3L_1}{L^-}\right) \frac{x^4 e^x}{(e^x-1)^2} dx \right.\right.$$

$$\left.\left. + \int_{\frac{\Theta_4^*}{T}}^{\frac{\Theta_h^*}{T}} \sigma_h \alpha_h \frac{6L_2}{L^+} \frac{x^4 e^x}{(e^x-1)^2}\, dx - \int_{\frac{\Theta_4^*}{T}}^{\frac{\Theta_e^*}{T}} \sigma_e \alpha_e \frac{3L_3}{L^-} \frac{x^4 e^x}{(e^x-1)^2}\, dx \right] \right\} \tag{88}$$

As one will know in the section on thermal and electrical magnetoresistance and lattice conductivity that $\sigma_h >> \sigma_e$, $\frac{6L_2}{L^+} \sim 1$ $\frac{3L_3}{L^-} \sim 1$ as $T \gtrsim 3^{\circ}K$. Therefore the above equation can be simply rewritten as

$$\varepsilon_g(0) \simeq \frac{\sigma_h(0) \frac{C_g(\frac{\Theta_h^*}{T})}{3ne} - \sigma_e(0) \frac{C_g(\frac{\Theta_e^*}{T})}{3ne}}{\sigma_e(0) + \sigma_h(0)} \tag{89}$$

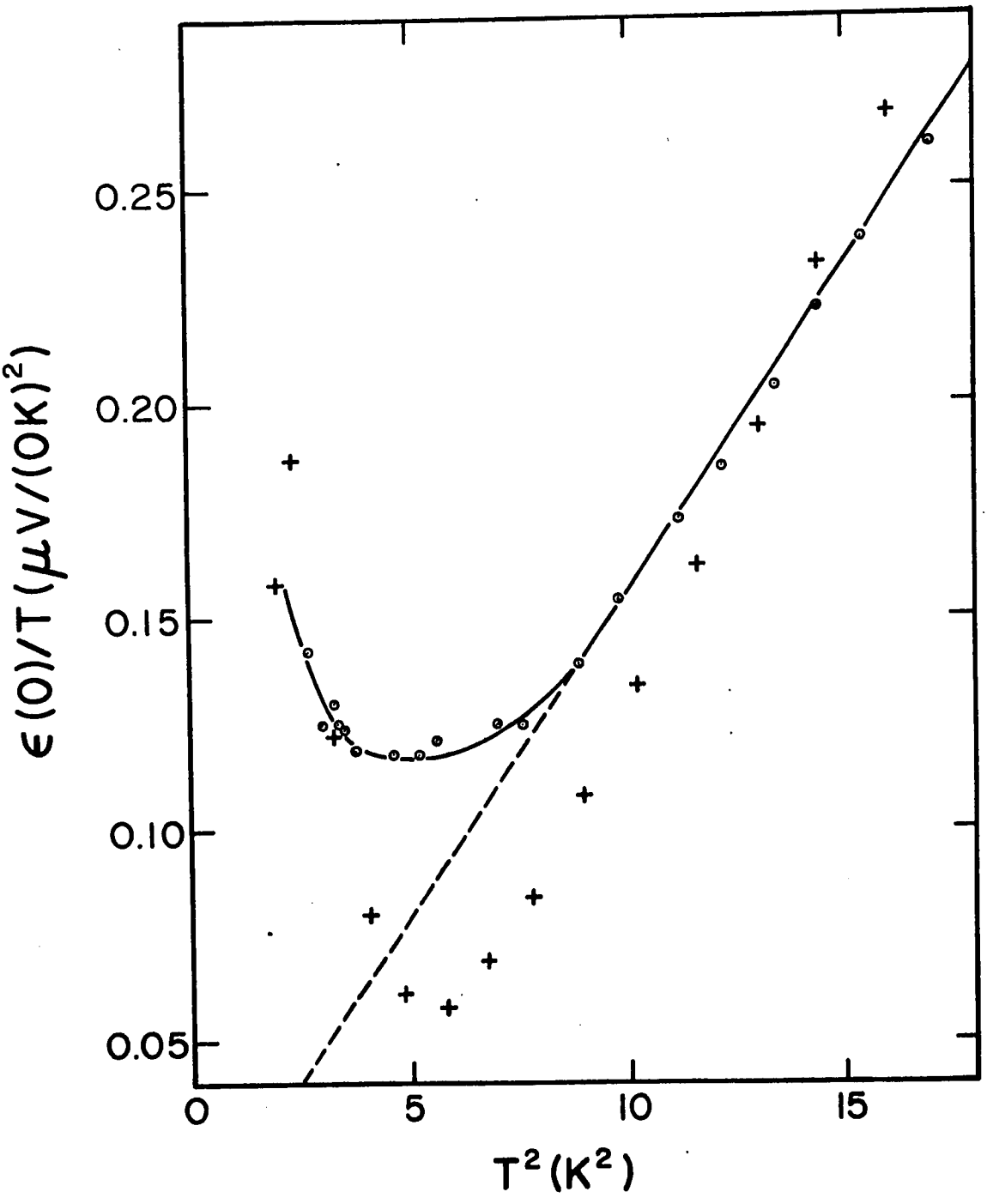

Fig. 20

where

$$C_g\left(\frac{\Theta^*}{T}\right) = 9Nk_B \left(\frac{T}{\Theta_D}\right)^3 \int_0^{\frac{\Theta^*}{T}} \frac{x^4 e^x}{(e^x-1)^2}\, dx \qquad (90)$$

As stated before we are not able to make a quantitative analysis of $\varepsilon_g(0)$ because as a consequence of the size effect which we lack a detailed knowledge about $\sigma_e(0)$, $\sigma_h(0)$, etc. But from the experimentally observed results for lattice conductivity, it has been concluded that the scattering of "enclosed" phonons by carriers begins to prevail over all other scattering mechanisms of "enclosed" phonons system below 10^oK. This effect is more pronounced in the helium temperature range. Due to the strong phonon-carrier interaction, the phonon drag on the carriers and their mutual drag effect would enhance the TEP of Sb below 10^oK on the one hand, and on the other hand due to the competition of the contribution from holes and electrons, the effect of drag-compensation would decrease the TEP. The measured value $\varepsilon_g = .0157\ T^3$ is therefore (due to compensation) much smaller than the absolute values of either drag component of the TEP. But the increase of the TEP above 3^oK and the maximum at $T \sim 8^oK$ can be understood qualitatively from the phonon drag effect. This conclusion is indeed consistent with the observation of Nernst-Ettingshausen and Ettingshausen effects .

Besides drag term, there is a "diffusive" term in the TEP. In general, the "diffusive" term of TEP for semimetals such as Bi and Sb, is generally given by

$$\varepsilon_d(0) = \frac{\sigma_e(0)\varepsilon_d^e(0) + \sigma_h(0)\varepsilon_d^h(0)}{\sigma_e(0) + \sigma_h(0)}$$

where $\sigma_{e,h}(0)$ and $\varepsilon_d^{e,h}(0)$ are the appropriate electrical conductivity and partial TEP of electron and hole respectively.

The partial TEP is expressed as[43]

$$\varepsilon_d^{e,h} = \frac{\pi^2 k_B^2 T}{3e^{\pm}} \left(\frac{\partial \ell n\, \sigma_{e,h}}{\partial \varepsilon} \right)_{\varepsilon=\xi_{e,h}} \tag{91}$$

To a first order approximation one may use

$$\varepsilon_d^{e,h} = \frac{\pi^2 k_B^2 T}{3e^{\pm}\xi_{e,h}} \tag{92}$$

With the values obtained by the above equation and the mobility ratio of σ_h/σ_e (see the section on magnetoresistance), $\varepsilon_d(0) \sim .121$ T which is not enough to interpret the negative value of constant a and the anomalous character of the TEP below 3^oK. It is apparent that there are several other factors included in the TEP below 3^oK, such as diffusive size effect, the decreasing in frequency of phonon-hole scattering, etc. But the more important factors will be the competition of hole and electron contribution and

the so-called "phony phonon drag effect" which takes into account the second order effect of the virtual phonon process in the carrier-phonon and carrier-impurity scattering, proposed by Nielsen and Taylor.[57]

As we discussed in Section B, at a sufficiently low temperature, the phonon will only span in a small q space such that those phonons are enclosed to both electron and hole. At such low temperature the first term of Eq. (88) will yield a negative value because

$$\frac{\sigma_h}{\sigma_e} \sim \frac{\sigma_h^{imp.}}{\sigma_e^{imp.}} \sim 4.5$$

(see the section on magnetoresistance), while

$$\frac{6L^-}{3L^+} \sim \frac{6(m_h^*)^2\varepsilon_h^2}{3(m_e^*)^2\varepsilon_e^2} \simeq \frac{1}{7}$$

Secondly, Nielsen and Taylor have predicted a temperature dependence of TEP which is similar to that predicted by phonon drag effect at low temperature. N-T theory is based on the second order effects of virtual phonon process in the carrier-phonon and carrier-impurity scattering. If one follows their equations, one would obtain a negative sign of TEP in antimony within the helium temperature range because the mobility of holes is higher than that of electrons.

Even though these considerations help to obtain a qualitative understanding of TEP, quantitive conclusion will require a more careful study.

Lattice Conductivity

The thermal conductivity of antimony exhibits several interesting features at low temperature. The electronic thermal conduction has been discussed in Section D of Chapter III. The lattice conductivity has another important feature which will be discussed here. Generally speaking, the fact that the strong magnetic field quenches the electronic conductivity allows the study of the lattice conductivity and its temperature dependence. With the application of magnetic field up to 20 kG, we have measured lattice conductivity from $4.4^{\circ}K$ down to $1.3^{\circ}K$. The measured values are shown in Fig. 21. These values are in good agreement with the values found by other investigators. We have measured the thermal magnetoresistance γ_{11} in the region of intermediate fields in order to determine the electronic contribution which was found to be negligible compared to lattice conductivity above 10 kG.

Lattice conductivity has been studied by several authors.[20,28,50] In an exhaustive investigation, Blewer, et al.[28] concluded:

1) The behavior of the lattice thermal conduction in the lowest range of temperature indicates that the main scattering of phonons is due to the electrons, whereas the

the enhancement in this conductivity above 1.4 K seems to be related to the inability for the phonons with $q > 2k_F$ (perpheral phonons) to be scattered by the electrons, and the validity of a characteristic scattering Debye temperature $\Theta^* = \frac{2k_F}{q_D}\Theta_D$ is verified.

2) The deformation potential of electron-phonon interaction is about 1.8 eV if there is no distinction made between electron and hole, and between transverse and longitudinal phonons.

3) The average cutoff temperature of electrons and holes is about 25°K.

In spite of this exhaustive investigation there are still several unsolved questions such as: the role of 3-phonon normal scattering; the difference between the interaction of carriers with transverse and longitudinal phonons; the difference between hole-phonon and electron-phonon scattering, etc. These problems have to be clarified in order to have a better understanding of the carrier-phonon drag effects.

The measured values of lattice conductivity of this study is shown in Fig. 21 plotted as a function of temperature, while the exponent of the temperature dependence of λ_g is shown in Fig. 22. It can be seen that the lattice conductivity is very strongly temperature dependent, varying as $T^{4.8}$ in the region 2.2 to 4.5 K. This exponent decreases with decreasing temperature until it reaches the value 2 at

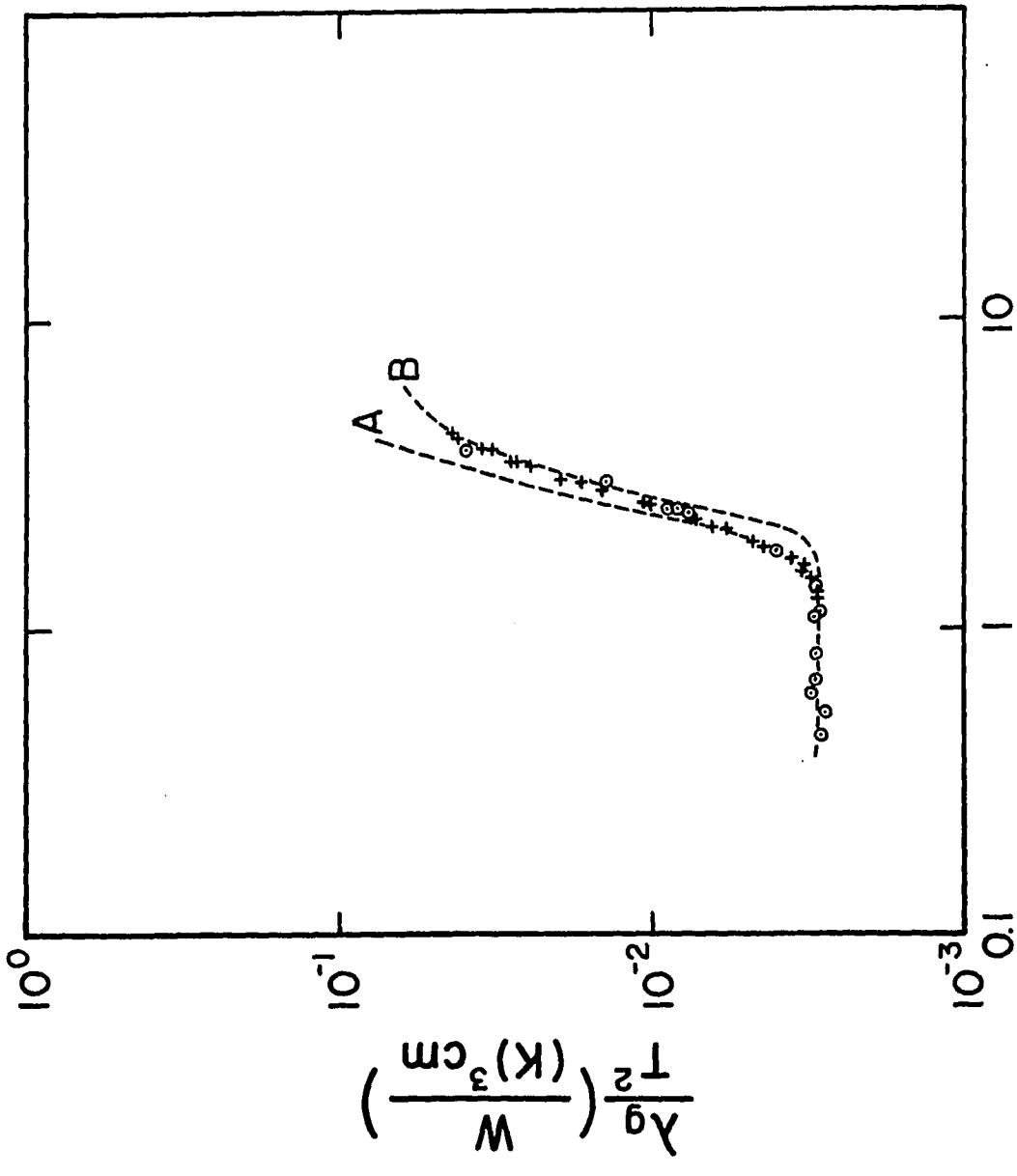
$\frac{\lambda_g}{T^2}\left(\frac{W}{(K)^3 cm}\right)$
10^0
10^{-1}
10^{-2}
10^{-3}
0.1
1
10
T(K)
A
B

Fig. 21

about 1.4°K. Thus, the lattice conductivity turns into a quadratic dependence on T below 1.4°K. This quadratic dependence characterizes the predominance of the carrier-phonon scattering, while the strong temperature dependence of the lattice conductivity above 1.4°K is due to the peripheral phonon-isotope and peripheral phonon-boundary scatterings plus some peripheral phonon-all phonon scattering.

Generally, the interpretation of lattice conductivity starts from Callaway's phenomenological theory[58] in which the relaxation effect from the three-phonon normal process is taken into account. Let τ_N^{-1} be the relaxation frequency due to the three phonon normal process and τ^{-1} be the combined resistive scattering frequency of phonon by other processes such as phonon-boundary, phonon-carrier, phonon-isotope and phonon-phonon Umklapp process. According to the theory, the lattice conductivity is given by

$$\lambda_g = \frac{k_B}{2\pi^2 S}\left(\frac{k_B T}{\hbar}\right)^3 \left(A_1 + \frac{A_2^2}{A_3}\right) \tag{93}$$

with

$$A_1 = \int_0^{\bar{T}} \frac{1}{\tau^{-1}+\tau_N^{-1}} \frac{x^4 e^x}{(e^x-1)^2}\, dx$$

$$A_2 = \int_0^{\bar{T}} \frac{\tau_N^{-1}}{\tau^{-1}+\tau_N^{-1}} \frac{x^4 e^x}{(e^x-1)^2}\, dx$$

and

$$A_3 = \int_0^{\bar{\Theta}} \frac{\tau^{-1}\tau_N^{-1}}{\tau^{-1}+\tau_N^{-1}} \frac{x^4 e^x}{(e^x-1)^2}\, dx$$

Thus the total lattice conductivity will depend sensitively upon the relative magnitudes of τ_N^{-1} and τ^{-1}. If $\tau_N^{-1} >> \tau^{-1}$ ($\tau << \tau^{-1}$) we have the regime of strong (weak) mixing.

To study the contribution of the peripheral phonon to the heat conduction, one may use Blewer's estimate[28] of the enclosed phonon contribution and write

$$\lambda_g^P = \lambda_g - \lambda_g^{en} \tag{94}$$

where λ_g^{en} = lattice conductivity due to enclosed phonon is about $.40\ T^3 J_3 (\Theta_1^*/T) \frac{mW}{Kcm}$ and Θ_1^* is taken 29^oK.

If one assumes that $\tau_N^{-1} << \tau^{-1} = \tau_{iso.}^{-1} + \tau_b^{-1}$ where phonon-isotope scattering,

$$\tau_{iso.}^{-1} = dx^4T^4 \simeq 4 \times 10^{-23}\ q^4(1/S), \quad x = \frac{\hbar sq}{kT} ,$$

and phonon-boundary scattering

$$\tau_b^{-1} = b \simeq .8 \times 10^6\ 1/S ,$$

then from the weak-mixing equation for peripheral phonons λ_g^P, is given by

$$\lambda_g^P = \frac{k_B}{2\pi^2 S}\left(\frac{k_B T}{\hbar}\right)^3 \int_{\frac{1}{T}}^{\infty} \frac{1}{b+dx^4T^4} \frac{x^4 e^x}{(e^x-1)^2}\, dx \qquad (95)$$

with Θ_1^* identified by the first type cutoff (see Section of Chapter III). The calculated term λ_g^P yields values for $\lambda_g = \lambda_g^P + \lambda_g^{en}$ which above 2.5°K exceed the measured value as can be seen in Fig. 21. To match the experimental values below 2.5°K the cutoff temperature $\Theta_1^* \sim 24$°K was chosen. Equation (95) shows that lattice conductivity λ_g^P, will increase exponentially. This, of course, is different from what is observed. The "temperature exponent" of the lattice conductivity temperature dependence, $\frac{d\ \ell n\ \lambda_g}{d\ \ell n\ T}$ can be determined experimentally through a special procedure and is shown in Fig. 22. This exponent reaches a maximum value of 2.5°K and thus may suggest that strong mixing of the phonon may not be negligible above T ~ 2.5°K.

To our knowledge there is no direct measurement indicating the strong-mixing in the phonon system of antimony. However, the second sound observation[59] in bismuth found that the three-phonon normal processes scattering frequency is about $4.5 \times 10^4\ T^4$ 1/s. If one assumes that the 3-phonon normal scattering of antimony has the same frequency as that of the bismuth, we could expect a strong mixing of phonon system above T ~ 3°K, indeed for $\tau_N^{-1} = 3.7 \times 10^6$ 1/s at T ≈ 3°K, while $\tau_b^{-1} = .8 \times 10^6$ 1/s and $\tau_{iso.}^{-1} \sim 2.62 \times 10^6$ 1/s at $q = 1.6 \times 10^7$ 1/cm for $q \approx 2k_{F_e} \sim 1.6 \times 10^7$ 1/cm.

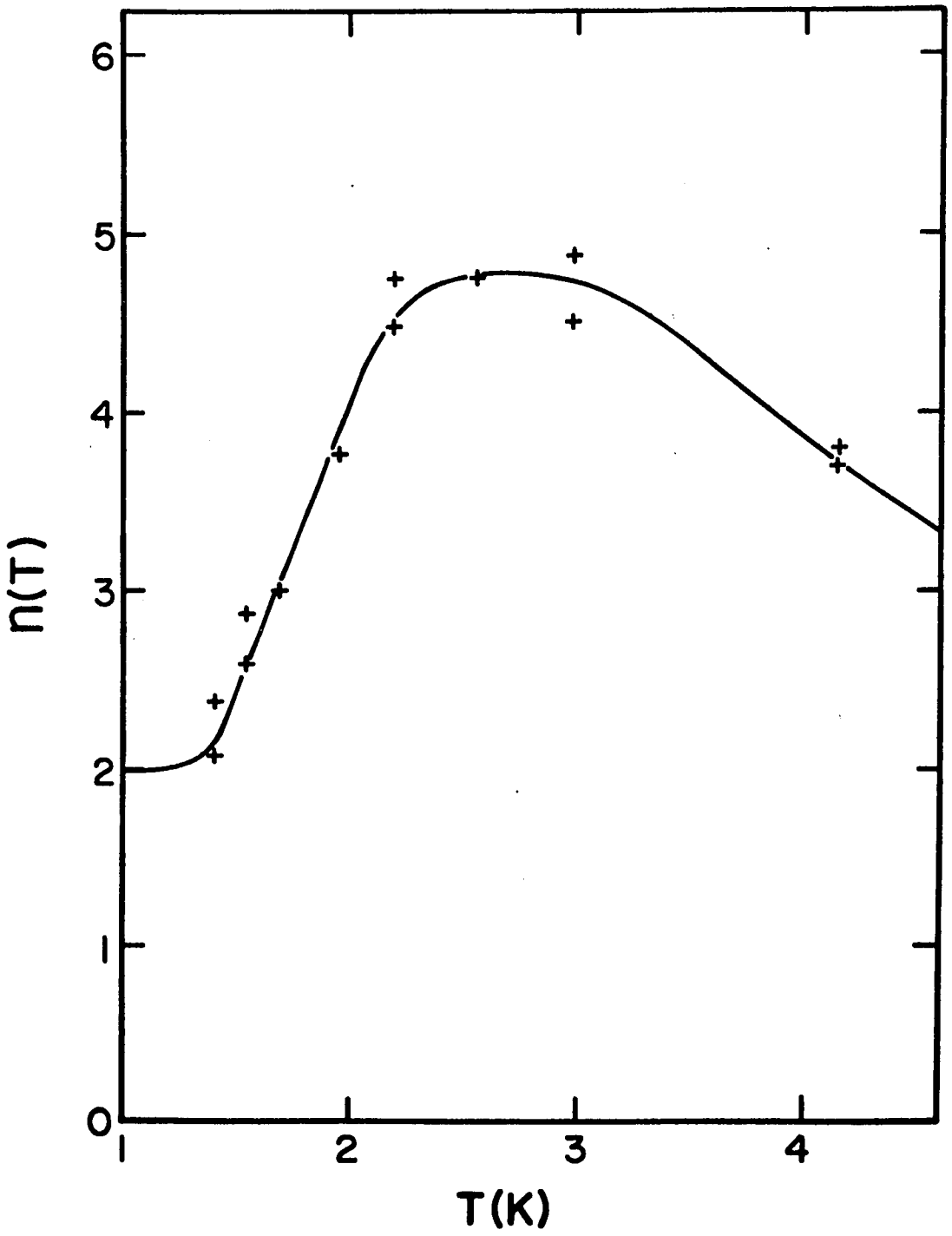

Fig. 22

With the assumption of strong-mixing in phonon system, the lattice conductivity, λ_g^P is then given by

$$\lambda_g^P = \frac{k_B^4 T^3}{2\pi^2 S \hbar^3} \frac{[J_4(\infty) - J_4(\frac{\Theta_1^*}{T})]^2}{b[J_4(\infty) - J_4(\frac{\Theta_1^*}{T})] + dT^4[J_8(\infty) - J_8(\frac{\Theta_1^*}{T})]} \tag{96}$$

The measured values λ_g above 2.5°K are found to match the values $\lambda_g^P + \lambda_g^{en}$ where λ_g^P are calculated with Eq. (96) using $\Theta_1^* \simeq 24^\circ K$.

We note also that the observed value of Θ_1^* are different from that measured in N-E and E effects (see the section on Nernst-Ettingshausen effect), even though they correspond to the same phonon cutoff. The explanation is that the predominant heat carriers of peripheral phonons are those phonons with the smaller wave vector values which have small phonon-isotope scattering frequencies. Therefore, with more weight being given to those smaller wave vector phonons would yield a smaller cutoff. On the other hand, the important energy carriers of enclosed phonon dragged by the electron and hole are those phonons with maximal wave vector or maximal specific heat. The weight being on the larger wave vector will yield a corresponding larger cutoff temperature (see Section C).

The measured values of λ_g of this study below 1.4°K also shows a nearly quadratic temperature dependence (see Fig. 21). It is in agreement with Blewer, et al., measurement. This quadratic dependence indeed displays the predominance of carrier-phonon scattering in the phonon system. However, according to the estimation from Blewer, et al., the deformation potential of carrier from this enclosed phonon conduction is lower than those obtained from the electrical or electronic thermal conduction. The likely explanation may be found in the distinction between longitudinal phonon-carrier interaction and transverse-phonon interaction. The former which is the stronger interaction yields the electrical and electronic thermal resistances. The latter which is weaker interaction dominates in the lattice conduction (see the Appendix G). This difference between longitudinal and transverse phonons should appear in other transport coefficients.

Thermal and Electrical Magnetoresistance

It is not easy to measure carrier thermal magnetoresistance in the high magnetic field limit because of a big reduction of electronic thermal conduction due to magnetic field and of a large lattice conduction. The carrier thermal conductivity λ_e is the difference $\lambda_e = \lambda - \lambda_g$. Since saturation ($\lambda_e << \lambda_g$) occurs at a relative small field, λ_e is measurable only over a rather limited field range. The result of the thermal magnetoconductivity, $\lambda_{11}(H) = (\lambda_{11}(H))_T - \lambda_g$, is shown in Fig. 23 for temperature dependence

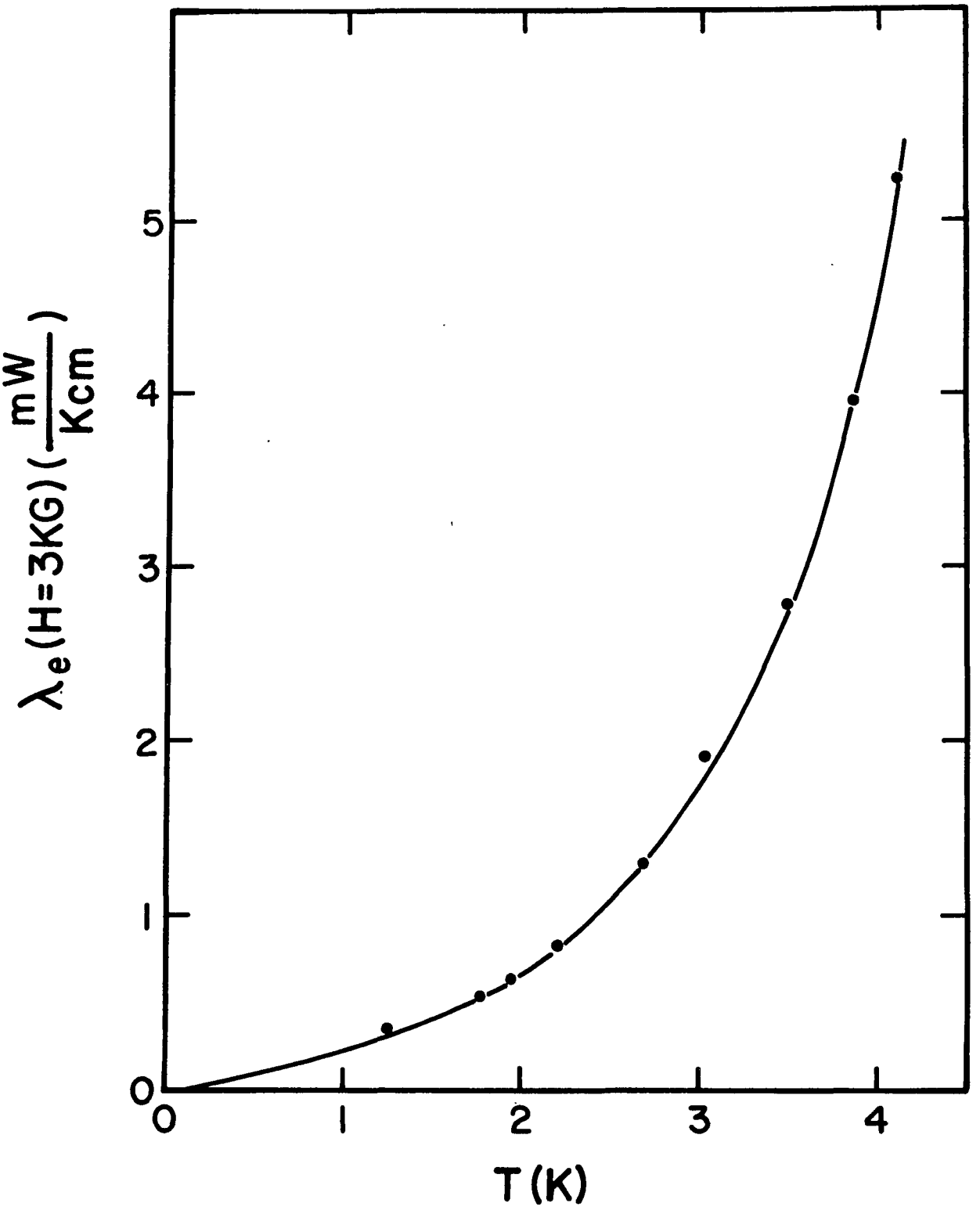

Fig. 23

and in Fig. 24 for typical field dependences, where $(\lambda_{11}(H))_T$ is the measured value of longitudinal thermal conductivity at magnetic field H. The thermal magnetoresistance shows an apparent quadratic field dependence, and there is no evidence of "diffusion size effect" (such as occurred in electrical magnetoresistance). Since under longitudinal temperature gradient, the electron and hold tend to drift transversely in opposite directions; there are no reasons for a "diffusive concentration gradient" to exist. One may interpret thermal magnetoresistance in a straightforward manner in terms of Sondheimer-Wilson theory as modified by Grenier, et al.[19,20] The thermal magnetoconductivity, $\lambda_{11}(H)$ is then given by

$$\lambda_{11}(H) = L_o \text{ nec } T\left(\frac{a_e H_{\lambda e}}{H^2+H_{\lambda e}^2} + \frac{a_h H_{\lambda h}}{H^2+H_{\lambda h}^2}\right) \tag{97}$$

with the aid of Righi-Leduc effect $\lambda_{12}(H)$

$$\lambda_{12}(H) = L_o \text{ nec } TH\left(\frac{1}{H^2+H_{\lambda h}^2} - \frac{1}{H^2+H_{\lambda e}^2}\right) \tag{98}$$

where

L_o is the Lorenz number or 2.45×10^{-8} $(J^2/coul^2K^2)$

n is the carrier concentration 5.45×10^{19} $1/cm^3$

$H_\lambda = m^*c/e\ \tau_\lambda$ with τ_λ, the relaxation time of the carrier in thermal conduction.

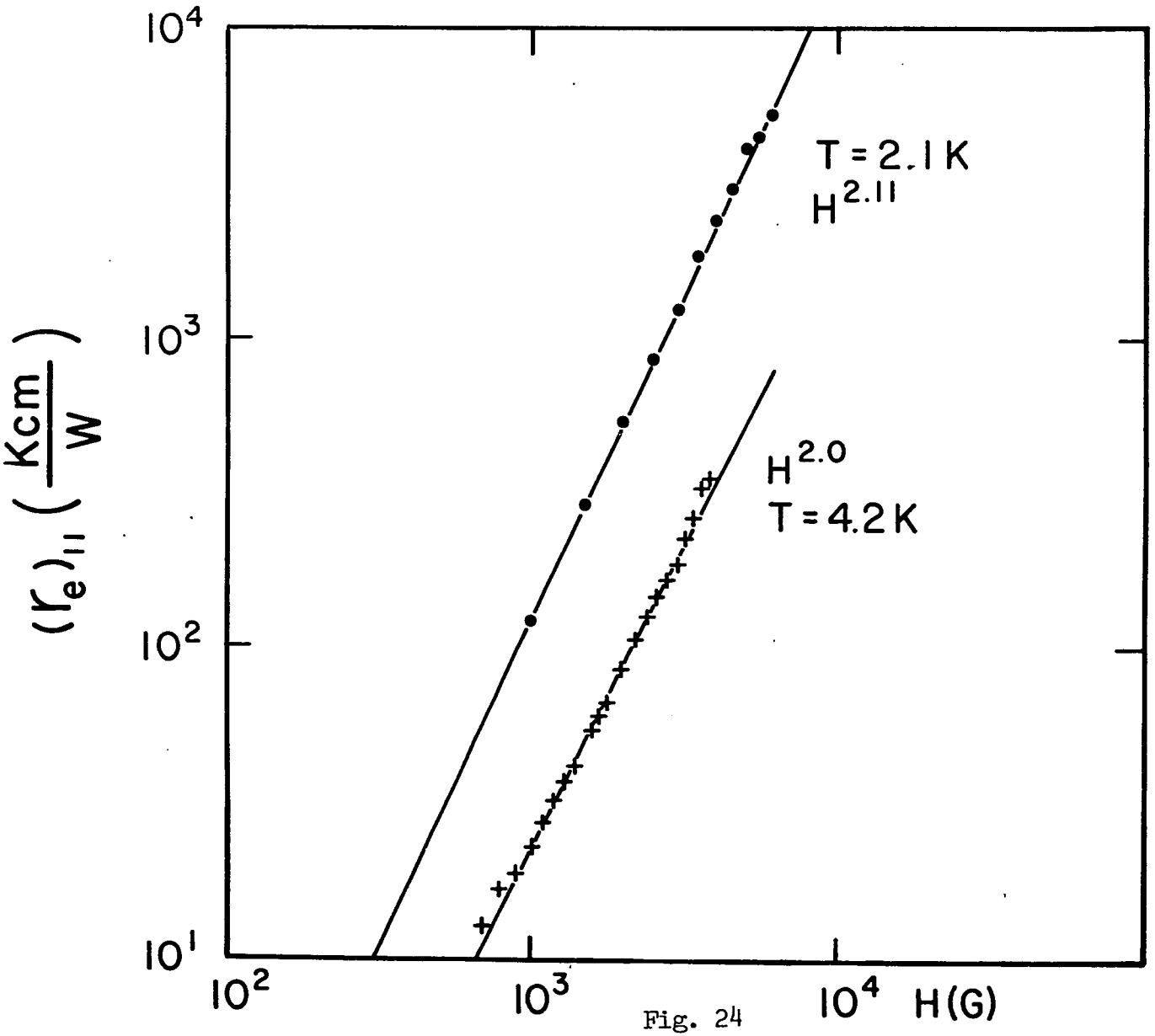
10^4
10^3
10^2
10^1
$(r_e)_{11}\left(\frac{Kcm}{W}\right)$
T = 2.1 K
$H^{2.11}$
$H^{2.0}$
T = 4.2 K
10^2
10^3
10^4 H(G)

Fig. 24

In particular, as H = 0, Eq. (97) becomes

$$\lambda_e = \lambda_{11}(0) = L_o \text{ nec } T\left(\frac{a_e}{H_{\lambda e}} + \frac{a_h}{H_{\lambda h}}\right) \tag{99}$$

From Eqs. (97), (98), and (99) we can obtain $H_{\lambda e}$, $H_{\lambda h}$, a_e and a_h (a_e and a_h are anisotropic parameters, and are independent of temperature).

The results of these calculations are shown in Fig. 25 as $H_{\lambda e}$ vis T^3 in Fig. 26 as $H_{\lambda h}$ vis T^3. Following Wilson's theory,[49] $H_{\lambda e,h}$ is given by

$$H_{\lambda e,h} = H^o_{\lambda e,h} + H^{id}_{\lambda e,h}$$

and $H^o_{\lambda e,h}$ is residual saturated field;

$$H^{id}_{\lambda e} = \frac{aL_o N n h^2 \varepsilon_e^2}{32\pi e \xi_e^2 \rho S} \left(\frac{T}{\Theta_D}\right)^3 J_5\left(\frac{\Theta^*_e}{T}\right) \left\{1 + 2\left(\frac{T}{\Theta^*_e}\right)^2 \left[\frac{2\pi^2}{3} - \frac{1}{3}\frac{J_7\left(\frac{\Theta^*_e}{T}\right)}{J_5\left(\frac{\Theta^*_e}{T}\right)}\right]\right\} \tag{100}$$

$$H^{id}_{\lambda h} = \frac{9L_o N n h^2 \varepsilon_h^2}{64\pi e \xi_h^2 \rho S} \left(\frac{T}{\Theta_D}\right)^3 J_5\left(\frac{\Theta^*_h}{T}\right) \left\{1 + 2\left(\frac{T}{\Theta^*_h}\right)^2 \left[\frac{2\pi^2}{3} - \frac{1}{3}\frac{J_7\left(\frac{\Theta^*_h}{T}\right)}{J_5\left(\frac{\Theta^*_h}{T}\right)}\right]\right\} \tag{101}$$

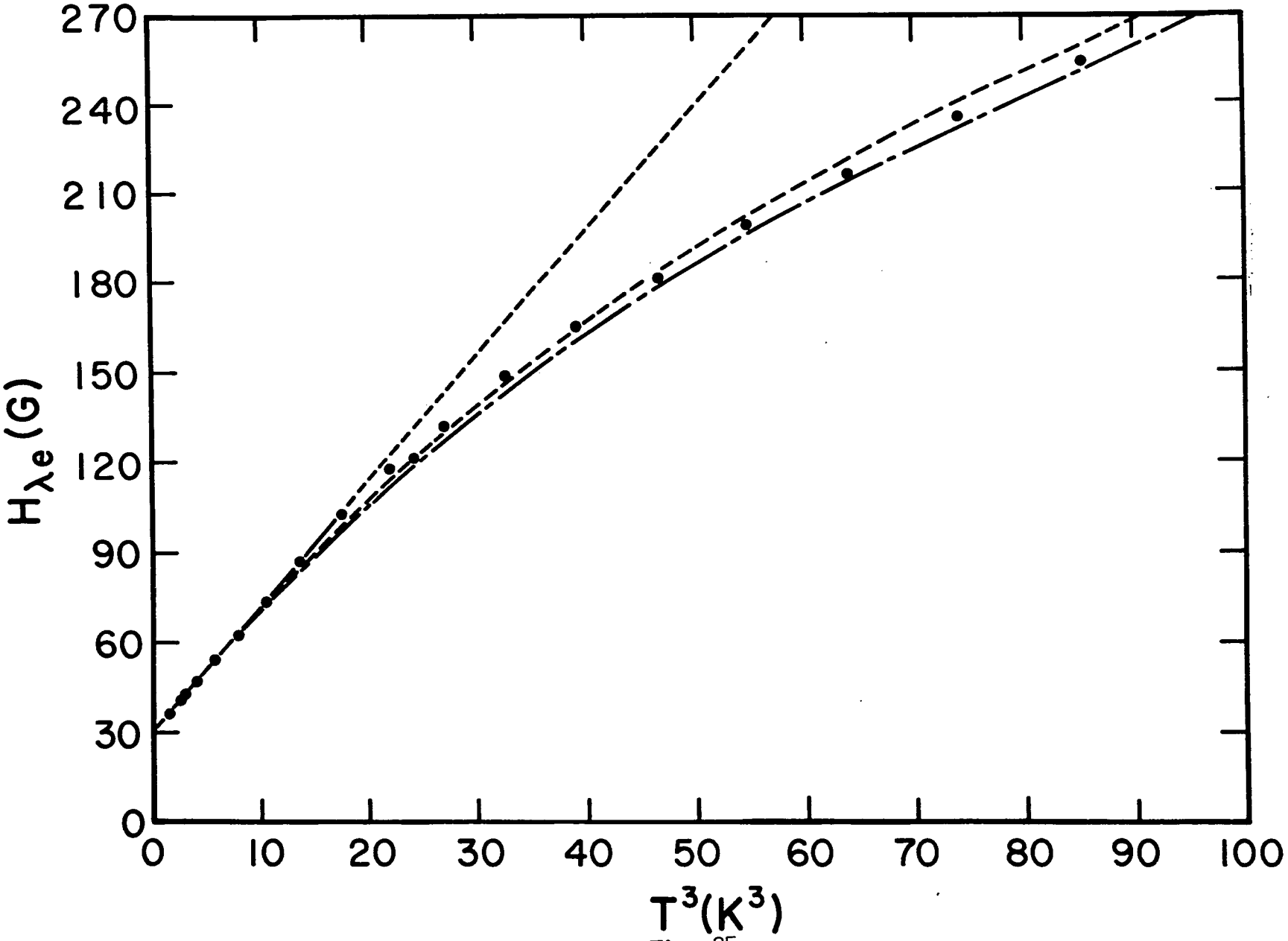
270
240
210
180
150
120
90
60
30
0
$H_{\lambda e}$ (G)
0
10
20
30
40
50
60
70
80
90
100
$T^3(K^3)$

Fig. 25

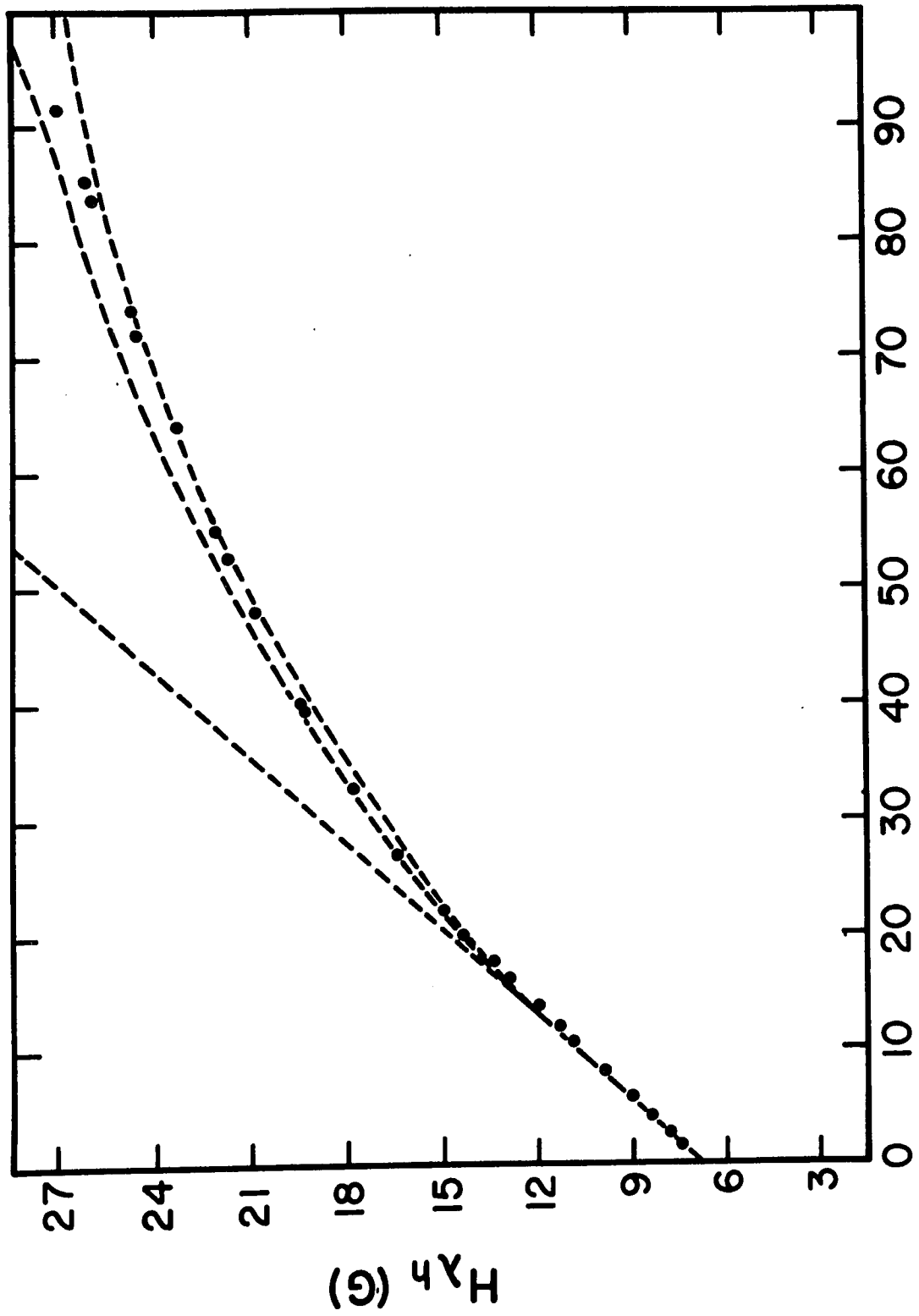

Fig. 26

The slope of $H_{\lambda e}^{id}$ against T^3 yields the deformation for electron about 3.0 eV and the bending of the curve of displays the characteristics of Debye integral $J_5(\frac{\Theta_e^*}{T})$ with the second type cutoff (see Section C of Chapter III and Fig. 25) and $\Theta_e^* \sim 28.5^oK$, close to the calculated value 30.8^oK.[28] The cutoff temperature, Θ_h^* for $H_{\lambda h}^{id}$ is about 26^oK. The apparent discrepancy between observed values of cutoff and the theoretically calculated values is not clear yet. However, it may be due to the anisotropic scattering and non-parabolic dispersion of carrier distributions.

It will be worthwhile knowing the thermal mean free path of electron, and comparing the values obtained by thermal magnetoresistance measurement and by RFSE.[53] If one is allowed to use isotropic model, the MFP of electron, therefore is given by

$$(\ell_e)_T = \frac{64.33}{T^3 J_5(\frac{\Theta_e^*}{T})} \text{ (cm)} \tag{102}$$

where $\Theta_e^* = 28.5^oK$, while it is given by the RFSE[53] as

$$(\ell_e)_T = \frac{.22}{T^2} \text{ (cm)} \tag{103}$$

Table IV shows the numerical values of mean free paths of electron due to the electron-phonon small angle scattering at various temperatures. The discrepancy at the lower temperature is not clear yet. It might be due to the

difference in extrapolation of the measured values.

Table IV

The Mean Free Path of an Electron (cm)

T	This Work Transport Property	Gantmakher RFSE
1.5	.153	.098
2	.065	.055
2.5	.034	.035
3	.021	.024
3.5	.015	.018
4	.011	.014

The measured values of magnetoresistance for sample #17 are shown in Fig. 8 plotted as in function of temperature at H = 20 kG and in Fig. 27 plotted as a function of magnetic field at T ~ 4.22°K. In Fig. 8, curve D shows the adiabatic magnetoresistance, curve A shows the isothermal magnetoresistance, while curves E and F present the magnetoresistances measured when sample was in the liquid helium bath. The details of size, surface effects and field dependence have been discussed in Chapter I. In this section we will study the carrier-phonon scattering and drag effects in the bulk magnetoresistance.

The magnetoresistances of semimetals, such as Sb and Bi, have been theoretically studied by Gurevich, et al.[42] and Kagan, et al.[48] Kagan, et al., have come to the theoretical conclusion that "in case of compensated metals with closed Fermi surfaces, the magnetic field itself produces a unified

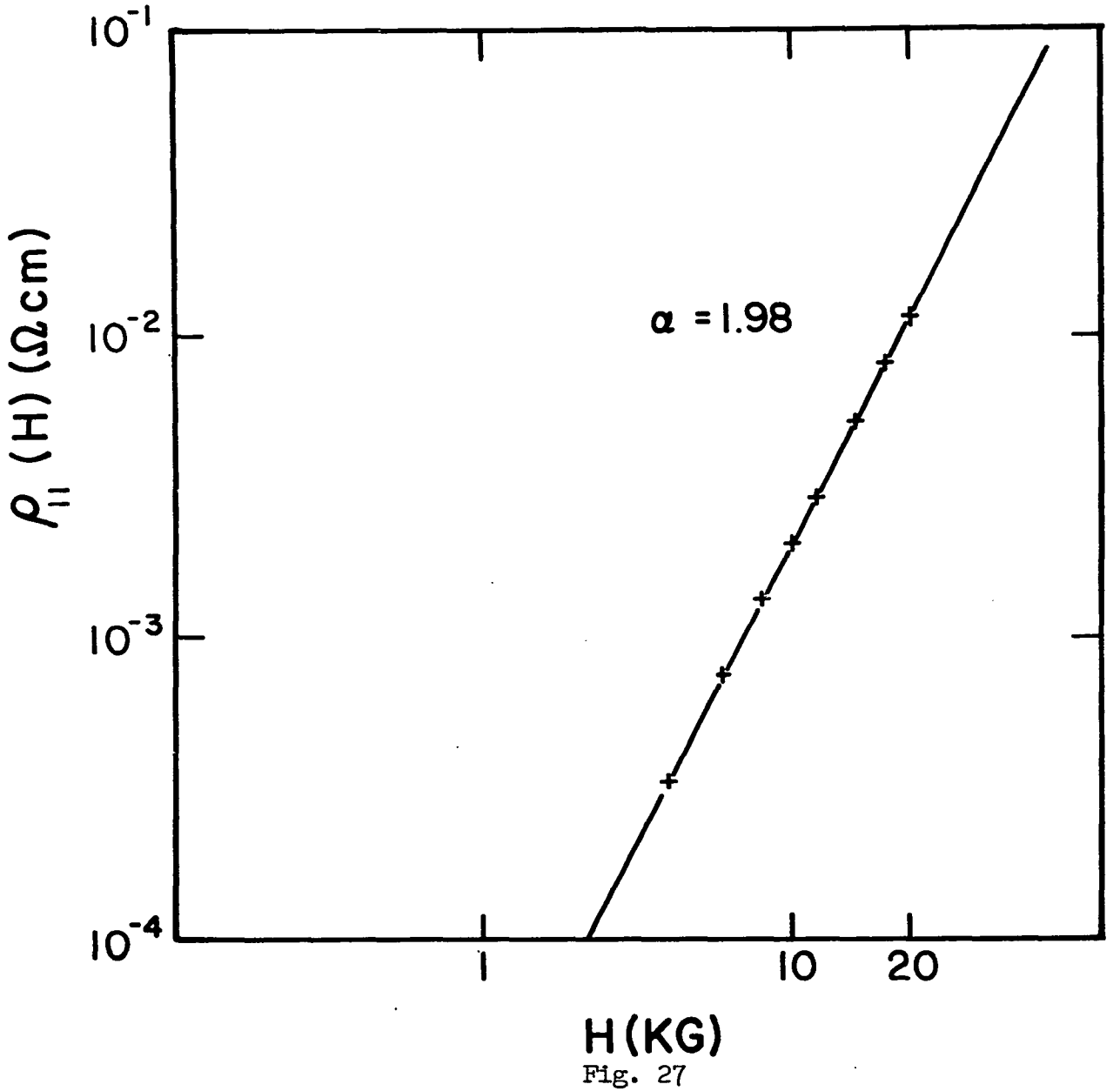

Fig. 27

drift of electrons and holes, which in turn stimulates phonon drift. The stronger the phonon dragging the less effective the scattering and the larger the transverse resistance. Thus, dragging can manifest itself in magnetoresistance of all metals with closed Fermi surfaces." If one assumes that the dragging efficiency is unity, the electron-phonon scattering should have no contribution to the magnetoresistance, thus one should have magnetoresistance independent of temperature because the main contribution to magnetoresistance is from carrier-impurity scattering which does not depend on temperature. The isothermal magnetoresistance in Fig. 28 shows a slight temperature dependence (at least compared with the zero field resistivity). This arises because the dragging efficiency is not one hundred per cent, even though the efficiency is still about 90% or even higher in antimony. As one noted in the section on lattice conductivity, the total scattering frequency of "enclosed" phonons arises almost entirely from phonon-carrier scattering. Therefore, the calculated efficiency,

$$\gamma = \frac{(\tau^{-1})_{pe}}{(\tau^{-1})_{total}} \quad ,$$

should be nearly unity.

The drag effect cannot be "turned off" in a natural system, even if the system is under the adiabatic conditions. The transverse drift of holes and electrons exerts force on

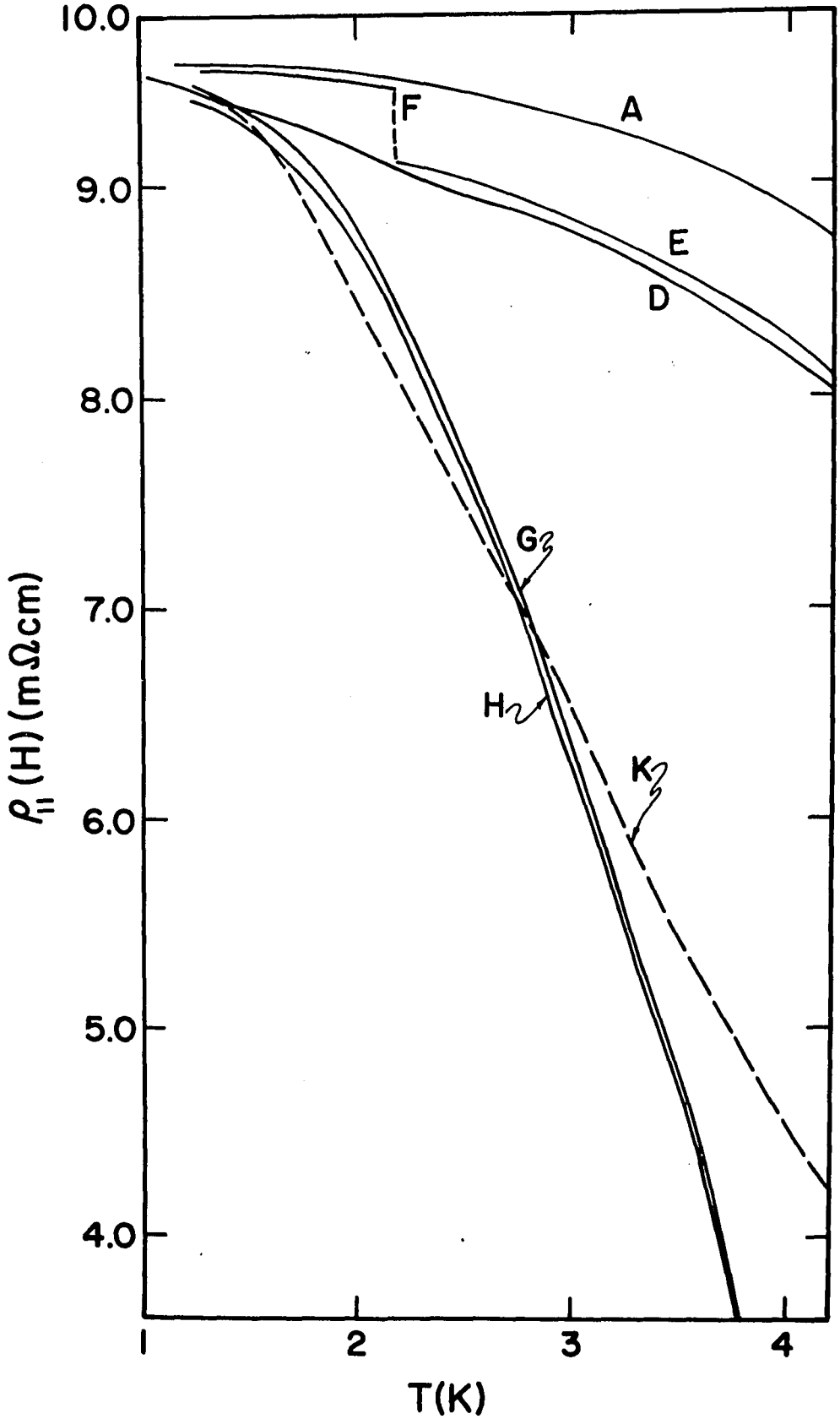

Fig. 28

the enclosed phonons and thereby creates a transverse concentration gradient of enclosed phonons, that is, a gradient of temperature appears. This in turn gives rise to a return diffusive heat flow, $\lambda_g G_2$, in which peripheral as well as enclosed phonons may participate. Thus even under adiabatic conditions, dragging of enclosed phonons still occurs because the return heat flow due to the peripheral phonons cancels this "drag heat" current, this situation can be seen by reference to Eq. (75) in the section on theoretical consideration of transport coefficients.

Based on the above picture and Eq. (75) with the known values of λ_g^{en}, λ_g, C_e (specific heat of carrier) and C_g^* (specific heat of enclosed phonon), one can obtain the term of magnetoconductivity $(\sigma_{e-p})_{11}$ due to the electron-phonon interaction in antimony. The calculated values of $(\sigma_{e-p})_{11}$ are shown in Fig. 29 plotted as a function of temperature. It is obvious that $(\sigma_{e-p})_{11}$ still obeys Bloch-Gurneisen T^5 law. $(\sigma_{ep})_{11}$ deviates from T^5 law at $T \sim 2.6^oK$. The slope of $(\sigma_{ep})_{11}$ against T^5 at lowest temperature gives the deformation potential approximately 2.9 eV for electron. This observed value seems to match with the value deduced from thermal conductivity. The cutoff of $(\sigma_{ep})_{11}$ is about 26^oK which is lower than the expected value 30.8^oK.[28] It may be due to the estimation without including the detailed scattering mechanisms for phonons.

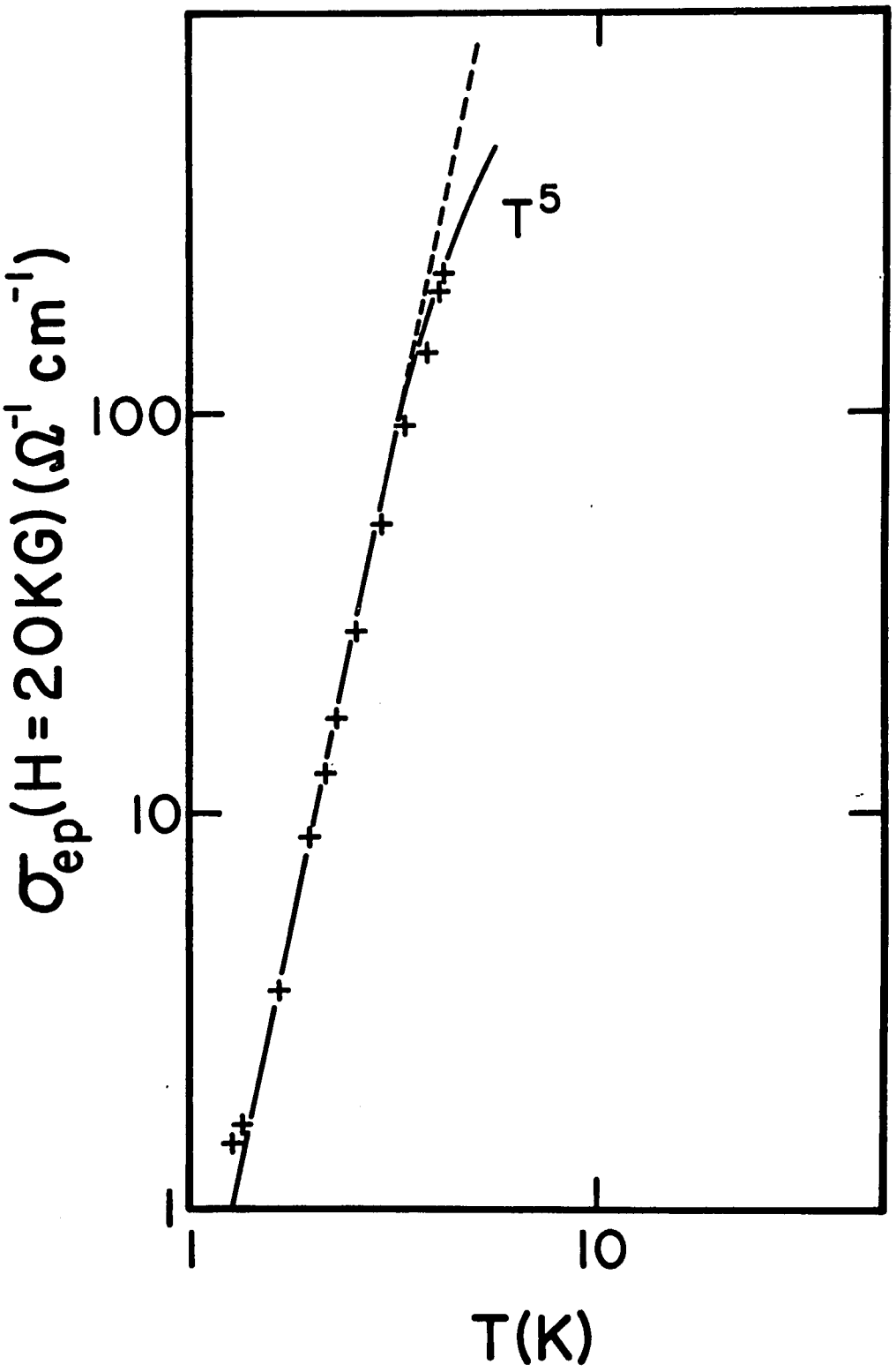

Fig. 29

Finally, the Wiedemann-Franz law and the Lorenz number are also interesting in this study. The effective Lorenz number which is defined as

$$L_n = \frac{H_{\sigma e}}{H_{\lambda e}} = L_o \frac{\sigma_{11}(H)T}{\lambda_{11}(H)}$$

is shown in Fig. 30. Curve A shows the observed value with skin effect; curve B displays the bulk values of L_n; curve C presents the bulk values of L_n in the non-drag limit. One can obviously see the difference between curves B and C, which is due to the difference of $H_{\sigma e}^{id}$ in both cases. The ideal Lorenz number which is defined as

$$L_n^{id} = \frac{H_{\sigma e}^{id}}{H_{\lambda e}^{id}}$$

is shown in Fig. 31. The interesting feature is the quadratic dependence of temperature. This quadratic dependence confirms that the small angle scattering mechanism dominates the thermal magnetoresistance and yields the electrical magnetoresistance. The slope yields the $\textcircled{H}_e^*$ about 25°K.

The comparison of specimens from two different sources is of limited value; but the comparison of the ideal parts is useful because the ideal parts are the intrinsic properties (of antimony). There is not enough data to do this comparison, the following is just showing the residual mobility ratio and the asymptotic ratio of the ideal part from

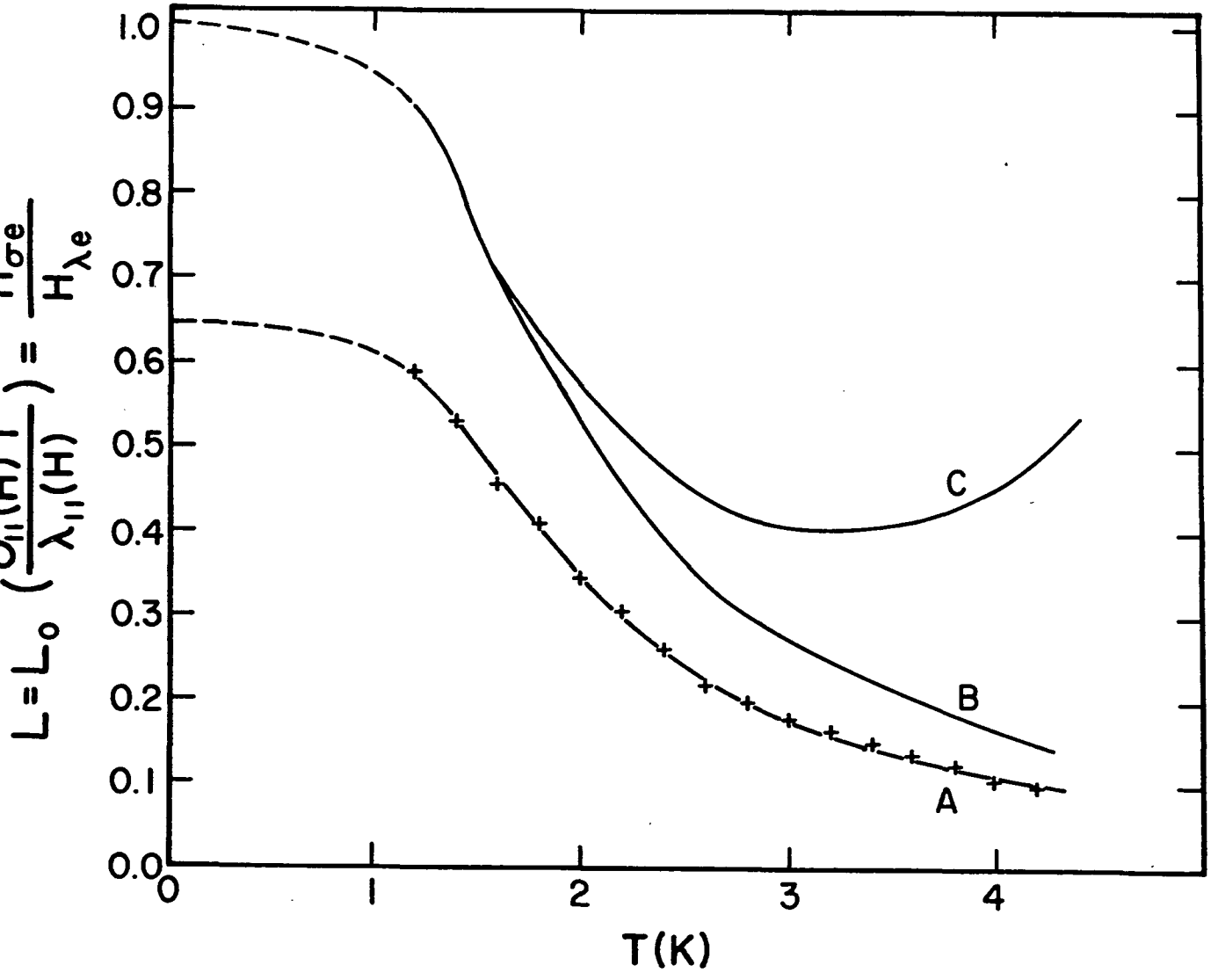
$L = L_o \left(\frac{\sigma_{11}(H)\,T}{\lambda_{11}(H)}\right) = \frac{H_{\sigma e}}{H_{\lambda e}}$
1.0
0.9
0.8
0.7
0.6
0.5
0.4
0.3
0.2
0.1
0.0
0
1
2
3
4
T(K)
A
B
C

Fig. 30

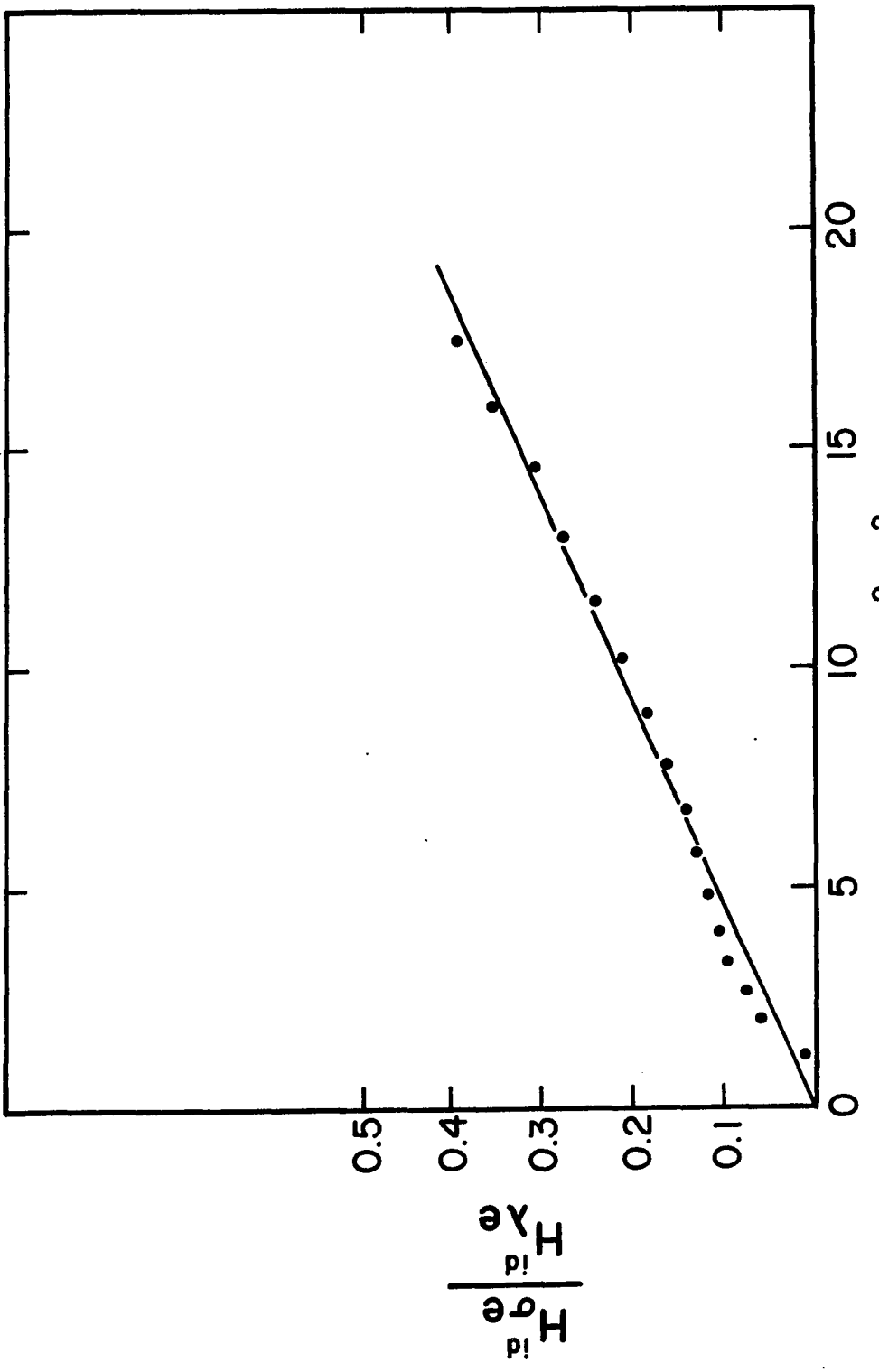

Fig. 31

several different measurements.

Table V

T		Rao, et al. & Bresler, et al.[3]	Bogod[4]	Long[5]	This Work
4.2°K	μ_h	1.16×10^2 mks	5.6×10^2	15.87×10^2 (1)	9.61×10^2
	μ_e	.20	.56	3.09	.88
	$R = \frac{\mu_h}{\mu_e}$	5.8	10	5.16	10.88
2.1°K		1.26	10.5	17.24	12.29
		.21	.56	3.36	2.63
	R	6	18.8	5.16	4.68
1.6°K		1.26 (2)		17.54	12.76
		.22		3.40	2.94
	R	5.73		5.16	4.34

(1) at 4.0°K

(2) at 1.7°K

(3) only for 4.0°K, see Ref. 10

(4) Ref. 3

(5) Ref. 20

The ratio of mobility between hole and electron is another important feature to study scattering mechanism. It was found that the ratio decreases as temperature approaches zero. It can be understood that the dominant mechanism at lower temperature range is electron-impurity scattering in

which the mean free path of carrier can be written as[49]

$$\frac{1}{\ell} = \frac{4\pi^3 m^*}{Nh^4} \sum_{st} P_s P_t U_{st} \qquad (104)$$

where P_i is the concentration of atoms besides antimony of type i. In one sample with homogeneous purity, the term of interaction $\sum_{st} P_s P_t U_{st}$ should be a constant and independent of temperature. Therefore the mobility of carrier at the impurity scattering range is

$$\mu_i = \frac{e\,\ell_i}{m_i^* U_F} \alpha \left(\frac{1}{m_i^*}\right)^2 \frac{a_i}{(P_f)_i}$$

$$\left(\frac{\mu_h}{\mu_e}\right) \sim 5.0$$

for isotropic case and

$$\left(\frac{\mu_h}{\mu_e}\right) \sim 3.8$$

for anisotropic scattering.

It was found that the mobility ratio for impurity scattering limit is about 4.3. This value is lower than the expected value by 15%, should this discrepancy be due to the anisotropic scattering at residual scattering limit and boundary scattering. It was also found that as temperature increases, the mobility ratio increase and this ratio should match with the ratio of ideal part. The ratio for ideal part is about 10, the difference between observed value and

theoretical expectation is because of the drag effect in ideal conductivity and (because) of the difference of the volume (in k-space) of the Fermi surfaces for electron and hole.

Nernst-Ettingshausen and Ettingshausen Effects

From the viewpoint of studying electron-phonon simple drag and mutual drag effects, the Nernst-Ettingshausen and Ettingshausen effects at high field limit are the two most important transport coefficients. Direct measurements of the adiabatic Nernst-Ettingshausen $\langle \varepsilon'_{21} \rangle$ and Ettingshausen coefficients $\langle \pi'_{21} \rangle$ are shown in Fig. 6 in Chapter I. The size and surface effects have been also discussed in that section. We will discuss the detailed properties of bulk kinetic coefficient ε''_{21} and π''_{21} in this section.

Nernst-Ettingshausen coefficient ε''_{21} has been studied by Long, et al.,[20] Blewer, et al.,[28] and Bresler, et al.,[10] at liquid helium temperature. Blewer, et al., formulated a simple equation for this coefficient related to the electronic density of states and lattice specific heat, which is consistent with the one derived from both Guenault's "current balance" model[60] and the "energy transfer" model (see Appendix H). Their equation is

$$\varepsilon''_{21} = \frac{\pi^2 k_B^2 cT}{3H} \left[Z_o + \gamma \frac{12\pi^2}{5} \frac{N}{k_B \Theta_D} \left(\frac{T}{\Theta_D} \right)^2 \right] \qquad (105)$$

where

Z_o is the electronic density of states

H_D is the Debye temperature

N is the number of atoms in a unit volume

γ is the "drag efficiency"

More generally, Eq. (105) should be rewritten as

$$\varepsilon''_{21} = \frac{\pi^2 k_B^2 cT}{3H} \left[Z_o + \gamma \frac{9N}{\pi^2 k_B \Theta_D} \left(\frac{T}{\Theta_D}\right)^2 J_4\left(\frac{\Theta^*}{T}, \frac{1}{T}\right)\right] \qquad (106)$$

This bulk coefficient is seen to involve not only the electronic specific heat but also 1/3 of the specific heat of those phonons which are capable of interacting with carriers by means of the normal process (see Fig. 11). The cutoff temperature of ε''_{21} is therefore identified with the first type cutoff (see Section C). The coefficient of ε''_{21} and its transformation from ε'_{21}, $\varepsilon''_{21} = \sigma_{22}\varepsilon'_{21}\lambda_{11}$, have been discussed in more detail in Chapter I. Let's note that the calculated value $\varepsilon''_{21} = \langle\sigma_{11}\rangle\langle\varepsilon'_{21}\rangle\lambda_{11}$ is not corresponding to the bulk one. However, the calculated value $\pi''_{21} = \langle\sigma_{11}\rangle\langle\pi''_{21}\rangle \lambda_g$ is corresponding to the bulk one, which we will discuss further.

The calculated values of effective electronic density of states,

$$Z_{eff} = Z_o + \frac{\gamma 9N}{\pi^2 k_B \Theta_D} \left(\frac{T}{\Theta_D}\right)^2 J_4\left(\frac{\Theta^*}{T}, \frac{1}{T}\right) \quad ,$$

from Nernst-Ettingshausen and Ettingshausen coefficients along with the data from Long, et al., Blewer, et al., and Crosby[61] are shown in Fig. 32.

The analysis of our data on π''_{21} by using the above Eq. (106) yields the values

$$Z_o = .731 \times 10^{33} \text{ erg}^{-1}\text{cm}^{-1}$$

$$\Theta_D = (221 \pm 2.0)^\circ K \quad \text{assuming } \gamma = .95$$

$$\Theta_1^* \simeq 29^\circ K \ .$$

The effective Debye temperature Θ_1^*, is in agreement with the expected scattering cutoff. The assumption $\gamma = .95$ is made in agreement with the predominance of the phonon-carrier scattering found in the lattice conduction. As a consequence the value for Θ_D is found almost in agreement with the value obtained from specific measurement[62]; even though the 5% excess value may be significant. The value found for Z_o is also of the order expected from the specific heat measurement, but it is difficult to dismiss the more than 20% discrepancy between these values.

There are a number of possible reasons for this apparent difference.

1. The accuracy of the measurement of Ettingshausen effect is less than that of the Nernst-Ettinghausen effect

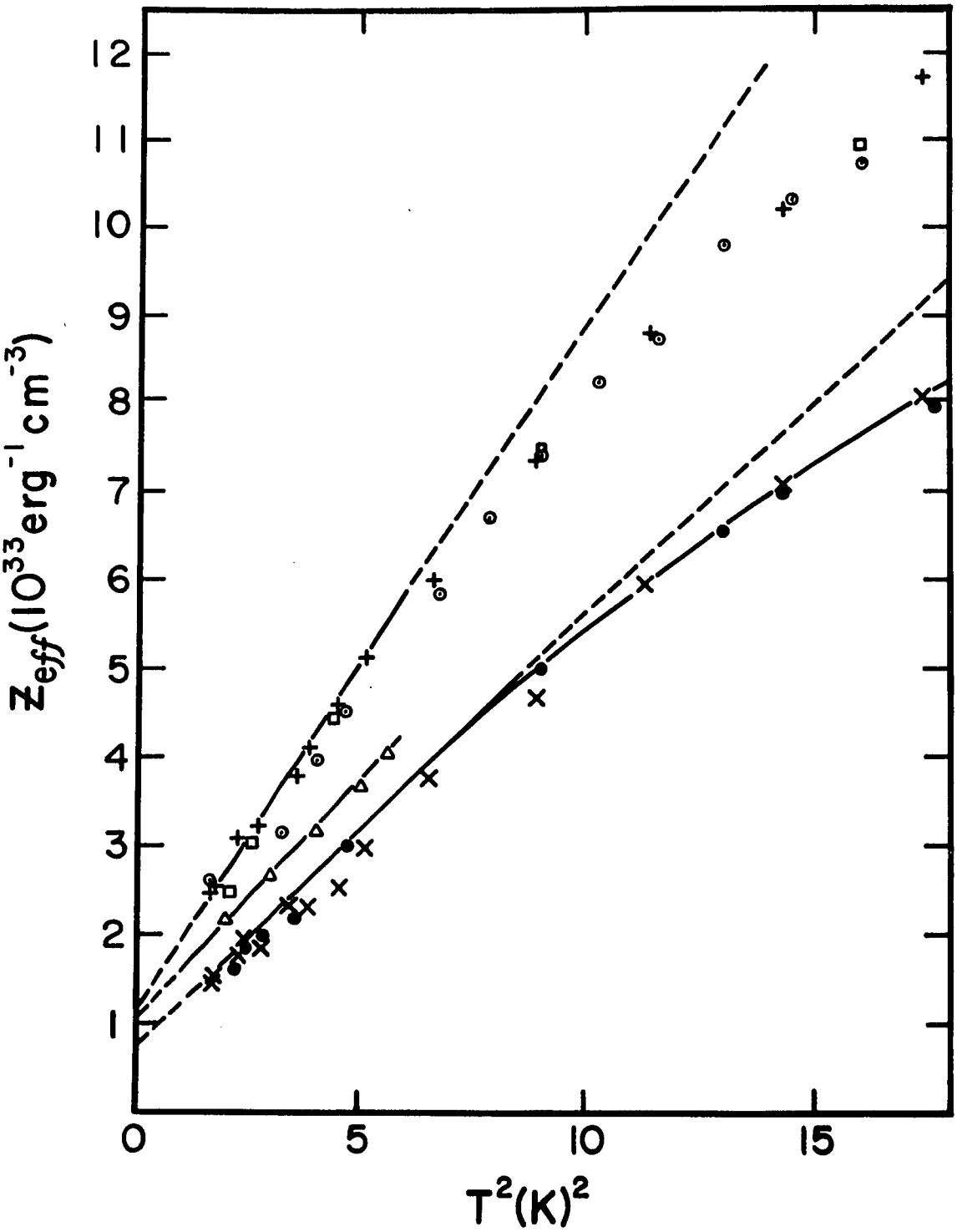

Fig. 32

because of basic experimental difficulties, thus a possibility of large error in extrapolation is made from these data.

2. The isotropic approximation in the electron and phonon distributions might arise this discrepancy even to first order of approximation. In a quadratic approximation,[28] one should expect that Eq. (106) would hold.

3. The N-E and Ettingshausen effect would depend on the bare mass of the electron, whereas the specific heat mass is that of the quasi particle or dressed electron, therefore $Z_o = Z_{sp.ht.} \frac{m_{b.e.}}{m_{q.p.}}$ is expected to be smaller than the specific heat density of states. Following the theoretical estimate, the relative increase $\alpha = \frac{m_{q.p.} - m_{b.e.}}{m_{b.e.}}$ is given by

$$\alpha \approx \frac{\varepsilon^2 G_o(\xi_F)}{\rho S^2} \tag{107}$$

where ε is the deformation potential, $G_o(\xi_F)$ the density of states, ρ the density and S the velocity of sound. A numerical estimate yields $\alpha \sim 3\%$ or less, a value confirmed by the cyclotron mass experiments of Herrod, et al.[63] Other estimates using the measured value α for Cu^{64} together with the ratio of the proper parameters between copper and antimony yield $\alpha < 4\%$, in agreement with other estimates, but these numbers are all too small to account for the 20% discrepancy.

4. A more likely reason for the discrepancy in Z_o and Θ_D can be, in addition to anisotropy, the different contributions of the transverse and longitudinal phonons. These differences appear to be responsible for some of the apparently different values obtained for the deformation potentials (see Appendix G). The transverse phonons interact more weakly with the carriers than do the longitudinal phonons and may have a smaller γ (drag efficiency). They have a smaller Θ_D and a larger specific heat, and the competitive contribution of both longitudinal and transverse phonons in the drag may yield a more complex behavior than predicted in Eq. (106).

5. Another likely reason for the apparent discrepancy found for these values may also be due to an overestimation of the surface current; and it will be worthwhile to study, with improved accuracy, the influence of the surface current in relation to Ettingshausen and N-E effects.

In conclusion, the N-E measurement presents a strong simple drag effect; the Ettinghausen measurement shows a strong mutual drag effect. The determination of effective electronic density of states from the bulk coefficients of both effects displays lower than that obtained from specific heat measurements. The explanation of this discrepancy is not clear, and there are several factors which should be investigated carefully.

REFERENCES

1. S. Tosima and T. Hattori, J. Phys. Soc. Japan 19, 2022 (1964).
2. T. Hattori, J. Phys. Soc. Japan 23, 19 (1967).
3. Yu. A. Bogod and V. B. Krasovitskii, Zh. Eksp. Teor. Fiz. 63, 1036 (1972); JETP 36, 544 (1973); Yu. A. Bogod, B. I. Verkin, and V. B. Krasovitskii, Zh. Eksp. Teor. Fiz. 61, 275 (1971); JETP 34, 142 (1972).
4. B. N. Aleksandrov, V. V. Dukin, L. A. Maslova and S. V. Tsivinskii, Zh. Eksp. Teor. Fiz. 61, 243 (1971); JETP 34, 125 (1972).
5. Yu. A. Bogod, V. V. Eremenko and L. K. Chubova, Phys. Stat. Solidi 28, K155 (1968); Yu. A. Bogod, V. B. Krasovitskii, Phys. Stat. Solidi (b) 49, K189 (1972).
6. S. Tanuma and Y. Ishizawa, Tech. Rept. I.S.S.P. A217 (1966).
7. M. Ya. Azbel, Zh. Eksp. Teor. Fiz. 44, 983 (1963); JETP 17, 667 (1963).
8. M. Ya. Azbel and V. G. Peschauskii, Zh. Eksp. Teor. Fiz. 49, 572 (1965); JETP 22, 399 (1966).
9. G. I. Babkin and V. Ya. Kravchenko, Zh. Eksp. Teor. Fiz. 60, 695 (1971); JETP 33, 378 (1971).
10. M. S. Bresler and N. A. Red'ko, Zh. Eksp. Teor. Fiz. 61, 287 (1971); JETP 34, 149 (1972).
11. V. Ya. Kravchenko and E. I. Rashba, Zh. Eksp. Teor. Fiz. 56, 1713 (1969); JETP 29, 918 (1969).

12. All of our samples have nearly square cross section and d = 4A/P represents a good approximation on either the thickness c or width b of the samples, and the linear behavior applies irrelevantly of which the sample surfaces contribute to the layer current effect.

13. See for example Herbert B. Callen, Phys. Rev. 73, 1349 (1948); ibid 85, 16 (1952). When Onsager's reciprocal relations are used to generalize Kelvin's relation $\pi = T\varepsilon$ to the case of an applied magnetic field, the tensor relation obtained and more specifically $\pi_{21}(H) = T\varepsilon_{12}(-H)$ are also known as Bridgmann relation.

14. P. L. Kapitza, Zh. Eksp. Teor. Fiz. 11, 1 (1941); J. Phys. USSR 4, 181 (1941); for a review on this effect, see for example G. L. Pollack, Rev. Mod. Phys. 41, 48 (1969).

15. Servomet Type SMD, Metals Research Instrument Corporation.

16. Grade 69 zone refined bar, Cominco Products, Inc., Spokane, Washington.

17. Yu. S. Gorodetskii and V. V. Peshkov, Otkrytiya Izobret. Prom. Obraztsy Tovarnye Znaki 50, 64 (1973), Patent (reference taken from Chem. Abst.).

18. J. P. Jan, Solid State Phys. 5, (1957), F. Seitz and D. Turnbull, eds., Academic Press, Inc., New York, 1957.

19. C. G. Grenier, J. M. Reynolds and J. R. Sybert, Phys. Rev. 132, 58 (1963).

20. J. R. Long, C. G. Grenier and J. M. Reynolds, Phys. Rev. 140, A187 (1965); C. G. Grenier, J. R. Long, J. M. Reynolds and N. H. Zebouni, Low Temp. Phys. LT9, B802, Plenum Press, New York (1965).

21. This so-called layer model as defined here under certain restrictions and approximations could be applied to damaged surface layers. It empirically fits only part of the experimental results.

22. The so-called skin model defined here arbitrarily considers the surface current not to have any direct effect on the bulk transport coefficients. It seems that some of the properties of diffusion size layer current may correspond to this model.

23. Model 2768 Rubicon Instruments, Minneapolis-Honeywell Co.

24. Allen-Bradley 50 Ω, 1/10 W.

25. The so-called adiabatic condition used here corresponds to $w_2 = 0$.

26. It is most probable that the roughness and surface damage of the lapped samples would vary from sample to sample and that light etching as in samples #5-#8 or etching as in samples #9-#12 will show some remnance of this unequal lapping. Examination of Fig. 3 seems indeed to show that some of the scatter of points in the etched samples seems related to the scatter in the data of the samples in the rough surface state.

27. e.g. K. Seeger, Semiconductor Physics, Springer Verlap, New York, 1973.

28. R. S. Blewer, N. H. Zebouni, and C. G. Grenier, Phys. Rev. 174, 700 (1968).

29. In the helium I bath the hot side of the sample will set itself at the boiling temperature of the bath so that the cool side will cool down the bath below the boiling point. Therefore heat flow will largely depend on the poor conduction of helium I, thus the nearly adiabatic behavior.

30. L. J. Challis, J. Phys. C, Solid State Phys. 7, 481 (1974).

31. Since the thermal conductivities parallel and perpendicular to the magnetic field are nearly in the ratio of the zero field and lattice conductivities we expect $|G_2| >> |G_3|$. We may neglect temperature variation in the z-direction if $|T(y,0) - T(y,\frac{c}{2})| << |T(y,0) - T_o|$. The lowest order solution of $\nabla\cdot\vec{w}^* = 0$ in z is

$$T(y,z) - T_o = T(y)\cos(\alpha z\sqrt{\frac{\lambda_g}{\lambda_{33}}})$$

where T(y) is the solution to (28). Thus

$$\frac{T(y,0) - T(\frac{c}{2},0)}{T(y,0)-T_o} \approx \frac{1}{2}(\frac{\alpha c}{2})^2\frac{\lambda_g}{\lambda_{33}}$$

Now at the λ-point, $\frac{1}{2}\left(\frac{\alpha c}{2}\right)^2 \sim 1$ and $\frac{\lambda_g}{\lambda_{33}} \sim 5 \times 10^{-3}$. Therefore our condition for the neglect of G_3 is satisfied.

32. The inclusion of Joule heating leads to the same temperature gradient as (30), but modified by a factor which is approximately $\left(1 + \frac{c\rho_{11}J_1}{\pi_{21}}\right)$. Under the usual conditions of this experiment $J_1 \sim 10^{-2}$ A/cm^2 the second term is less than 0.01 and therefore Joule heating has a negligible effect on Δ.

The inclusion of the Thomsen term considerably complicates the problem since $T(y,z) - T_o = -[T(-y,z) - T_o]$. The solution appears to be altered mainly by the replacement of $\pm\alpha$ by

$$\frac{\Lambda}{2}\sqrt{\alpha^2 + \left(\frac{\Lambda}{2}\right)^2} \quad \text{where} \quad \Lambda = \left(\varepsilon_{12} - \frac{\partial \pi_{12}}{\partial T}\right)\frac{J_1}{\lambda_g} .$$

At 1.6 K we find $\Lambda/2 \sim 3 \times 10^{-3}$ cm^{-1} while $\alpha \sim 10$ cm^{-1}. In the final analysis we are able to neglect these effects because no dependence of ρ_{11}(He) upon J_1 was detectable.

33. Equation (34) was derived for an idealized situation in which there is no surface conduction. The presence of either layer or skin conductance leads to a Δ value which does not differ sensibly from that of the idealized situation.

34. R. C. Johnson and W. C. Little, Phys. Rev. 130, 596 (1963).

35. The thermal transport processes in liquid He I are known to be complex. Undoubtedly convection is present and as well we may have boiling on one lateral face of the crystal and not on the other. Such a physical situation cannot be described in a way which lends itself to the type of analytical treatment employed here.

36. L. M. Falicov and P. J. Lin, Phys. Rev. 141, 562 (1966).

37. L. R. Windmiller, Phys. Rev. 149, 73 (1966); N. B. Branat, N. Ya. Minima and Chu Chen-Kang, Soviet Phys - JETP 24, 73 (1967).

38. H. J. Mackey, Dissertation, Louisiana State University, 1963 (unpublished).

39. K. Sugihara, T. Takezawa, T. Tsuzuku, Y. Hishiyama and A. Ono, J. Phys. Chem. Solids 33, 1475 (1972).

40. G. N. Rao, N. H. Zebouni, C. G. Grenier and J. M. Reynolds, Phys. Rev. 133, A141 (1964).

41. Ko Sugihara, J. Phys. Soc. Japan 27, 356 (1969).

42. L. E. Gurevich and I. Ya. Korenblit, Sov. Phys. - Solid State 9, 932 (1967).

43. J. M. Ziman, Electron and Phonon, Oxford University Press, London, 1960.

44. J. E. Parrot, J. Phys. F: Metal Phys. 1, 657 (1971); F. W. Sheard, J. Phys. F: Metal Phys. 3, 1963 (1973).

45. See e.g. Ref. 42, 43, 44.

46. Take Fermi energies of electron $\xi_e = 14.1 \times 10^{-14}$ erg and of hole $\xi_h = 18.2 \times 10^{-14}$ erg. See Ref. 28.

47. It is valid within the first order approximation and with the assumption that phonon-phonon interaction is very weak.

48. Yu. Kagan and Y. N. Flerov, JETP Letter 20, 384 (1974).

49. A. H. Wilson, The Theory of Metals, Cambridge, 2nd edition. See also Ref. 28.

50. G. K. White and S. B. Woods, Phil. Mag. 3, 342 (1958).

51. R. E. B. Makinson, Proc. Camb. Phil. Soc. 34, 474 (1938).

52. P. G. Klemens, Aust. J. Phys. 7, 64 (1954).

53. V. F. Gantmakher and V. I. Dolgopolov, Sov. Phys. - JETP 33, 1215 (1971).

54. R. B. Dingle, Proc. Roy. Soc. A201, 545 (1950).

55. N. A. Red'ko and S. S. Shalyt, Sov. Phys. - Solid State 10, 1233 (1968).

56. D. K. C. MacDonald, Thermoelectricity: An Introduction to the Principle, John Wiley and Son, Inc., New York, 1962.

57. P. E. Nielsen and P. L. Taylor, Phys. Rev. B10, 4061 (1974).

58. J. Callaway, Phys. Rev. 113, 1046 (1959); 122, 787 (1961).

59. V. Narayanamurti and R. C. Dynes, Phys. Rev. Letters 28, 1461 (1972).

60. A. M. Guenault, J. Phys. F: Metal Phys. 1, 273 (1971).

61. R. C. Crosby, private communication.

62. See e.g. D. C. McCollum and W. A. Taylor, Phys. Rev. 156, 782 (1967); H. V. Culbert, Phys. Rev. 157, 560 (1967). See also Ref. 28.

63. R. A. Herrod and R. G. Goodrich, Phys. Letters 33A, 331 (1970).

64. M. J. G. Lee, Phys. Rev. B2, 250 (1970).

APPENDIX A

Equations of Damaged Layer Model

As is noted in Chapter I the basic assumptions for the damaged layer model have been made. In this appendix we will derive several equations of the effective transport coefficients based on those assumptions (see Chapter I).

As used in Chapter I, δ_y, σ_{11sy} and δ_z, σ_{11sz} are the thicknesses and electrical conductivities of the damaged layers perpendicular to y- and z-axis respectively (see Fig. 1 in Chapter I). We will calculate the effective transport coefficients within the first order approximation of δ_y/b and δ_z/c or σ_b/σ_{11sy} and σ_b/σ_{11sz}.

(i) Electrical Magnetoconductivities $\langle\sigma_{11}\rangle$ and $\langle\sigma_{22}\rangle$

The kinetic equations of transport properties have been listed in Eq. (1) of Chapter I, which are written as

$$\vec{J} = \hat{\sigma}\,\vec{E}^* - \hat{\varepsilon}''\vec{G} \tag{A1a}$$

$$\vec{W}^* = -\hat{\pi}''\vec{E}^* + \hat{\lambda}''\vec{G}. \tag{A1b}$$

For isothermal transverse conductivity measurement, $\vec{G} = 0$. In case of antimony with magnetic field along high symmetry axis, we can neglect Hall coefficient, that is, $E_2 = 0$ and $E_3 = 0$. If we assume there are no end effects for simple consideration, then the electrical current densities through bulk and layers are given by:

$$J_{1b} = \sigma_{11b}E_1 \tag{A2a}$$

$$J_{1sy} = \sigma_{11sy}E_1 \tag{A2b}$$

$$J_{1sz} = \sigma_{11sz}E_1 \tag{A2c}$$

but
$$\langle J_1 \rangle \simeq J_{1b}(1-\frac{2\delta_y}{b})(1-\frac{2\delta_z}{c})+J_{1sy}\frac{2\delta_y}{b}+J_{1z}\frac{2\delta_z}{c}$$

with
$$\langle J_1 \rangle = \langle \sigma_{11} \rangle E$$

so
$$\langle \sigma_{11} \rangle \sim \sigma_{1b}+\frac{2\delta_y}{b}(\sigma_{11sy}-\sigma_{11b})+\frac{2\delta_z}{c}(\sigma_{11sz}-\sigma_{11b})$$

or
$$\frac{\langle \sigma_{11} \rangle}{\sigma_{11b}} = 1+\frac{2\delta_y}{b}(\frac{\sigma_{11sy}}{\sigma_{11b}}-1)+\frac{2\delta_z}{c}(\frac{\sigma_{11sz}}{\sigma_{11b}}-1). \qquad (A3)$$

Equation (A3) can be easily obtained by just considering five conductors in parallel.

For $\langle \sigma_{22} \rangle$ calculation, we will follow the same assumptions made in the above, except that the electrical field along y-axis is no longer homogenous. Assume the electric gradient E_2 in y-layers is E_2^1 and in bulk and the z-layers is E_2^2, then the electrical current densities are:

$$J_{2b} = \sigma_{22b}E_2^2 \qquad (A4a)$$

$$J_{2sz} = \sigma_{22sz}E_2^2 \qquad (A4b)$$

$$J_{2sy} = \sigma_{22sy}E_2^1. \qquad (A4c)$$

The continuity equation also gives

$$\langle J_2 \rangle = J_{2sy} = J_{2b}(1-\frac{2\delta_z}{c})+J_{2sz}\frac{2\delta_z}{c} \qquad (A5)$$

or
$$\sigma_{22sy}E_2^1 = [\sigma_{22b}+(\sigma_{22sz}-\sigma_{22b})\frac{2\delta_z}{c}]E_2^2.$$

The effective conductivity $\langle \sigma_{22} \rangle$ is defined as

$$\langle J_2 \rangle = \langle \sigma_{22} \rangle E$$

where

$$E_2 = E_2^2(1-\frac{2\delta_y}{b})+E_2^1\frac{2\delta_y}{b}$$

so

$$\langle \sigma_{22} \rangle = \frac{\sigma_{22b}+(\sigma_{22sz}-\sigma_{22b})\frac{2\delta_z}{c}}{1+(\frac{\sigma_{22b}+(\sigma_{22sz}-\sigma_{22b})\frac{2\delta_z}{c}}{\sigma_{22sy}}-1)\frac{2\delta_y}{b}}$$

or

$$\langle \sigma_{22} \rangle \approx \frac{\sigma_{22b}+(\sigma_{22sz}-\sigma_{22b})\frac{2\delta_z}{c}}{1+(\frac{\sigma_{22b}}{\sigma_{22sy}}-1)\frac{2\delta_y}{b}}$$

or

$$\frac{\langle \sigma_{22} \rangle}{\sigma_{22b}} = \frac{1+(\frac{\sigma_{22sz}}{\sigma_{22b}}-1)\frac{2\delta_z}{c}}{1+(\frac{\sigma_{22b}}{\sigma_{22sy}}-1)\frac{2\delta_y}{b}}. \qquad \text{(A6)}$$

The other effective transport coefficients which are modified by the damaged layer currents can be obtained in the same way.

(ii) Nernst-Ettingshausen Coefficient $\langle \varepsilon'_{21} \rangle$

The performance of $\langle \varepsilon'_{21} \rangle$ is to measure the transverse potential as longitudinal heat current is applied to the sample under the adiabatic condition, i.e. $W_2 = 0$.

$$\langle \varepsilon'_{21} \rangle = \frac{\langle E_2 \rangle}{\langle W_1 \rangle} = \frac{\langle E_2 \rangle}{\lambda_g \langle G_1 \rangle},$$

as sketched in Fig. 1 in Chapter I. Suppose the electric field in the damaged layer along the y-axis is E_2^1, and that in the bulk part or z-layers is E_2^2. The kinetic equation (1) gives:

$$J_2 = \sigma_{22} E_2 - \varepsilon''_{21} G_1$$

where

$$E_1 = 0,\ G_2 = 0,\ E_3 = G_3 = 0.$$

Considering in a y-z plane, J_2 is a function of (y,z). G_1 is homogeneous everywhere in this plane, so is ε''_{21}. Therefore, according to the condition of measurement $I_2 = 0$. So,

$$J_{2b} = \sigma_{22b} E_2^2 - \varepsilon''_{21} G_1 \tag{A7a}$$

$$J_{2sz} = \sigma_{22sz} E_2^2 - \varepsilon''_{21} G_1 \tag{A7b}$$

$$J_{2sy} = \sigma_{22sy} E_2^1 - \varepsilon''_{21} G_1 \tag{A7c}$$

or

$$[\sigma_{22b} + \frac{2\delta_z}{c}(\sigma_{22sz} - \sigma_{22b})]E_2^2 = \varepsilon''_{21} G_1$$

and

$$\sigma_{22sy} E_2^1 = \varepsilon''_{21} G_1$$

since

$$\langle E_2 \rangle = E_2^1(1 - \frac{2\delta_y}{b}) + E_2^1(\frac{2\delta_y}{b})$$

thus

$$\langle \varepsilon'_{21} \rangle = \varepsilon'_{21} \frac{1 + \frac{2\delta_y}{b}(\frac{\sigma_{22b}}{\sigma_{22sy}} - 1)}{1 + \frac{2\delta_z}{c}(\frac{\sigma_{22sz}}{\sigma_{22b}} - 1)}$$

or

$$\frac{\langle \varepsilon'_{21} \rangle}{\varepsilon'_{21}} = \frac{\sigma_{22b}}{\langle \sigma_{22} \rangle}. \tag{A8}$$

The calculation for $\langle \varepsilon'_{12} \rangle$ is similar to the previous one, and $\langle \varepsilon'_{12} \rangle$ is given by

$$\langle \varepsilon'_{12} \rangle = \varepsilon_{12} \frac{\sigma_{11b}}{\langle \sigma_{11} \rangle}$$

or

$$\frac{\langle \varepsilon'_{12} \rangle}{\varepsilon'_{12}} = \frac{\sigma_{11b}}{\langle \sigma_{11} \rangle}. \tag{A9}$$

(iii) Ettingshausen Coefficient $\langle \pi'_{21} \rangle$

The Ettingshausen coefficient $\langle \pi'_{21} \rangle$ is measured directly under the conditions $W_1=W_2=J_2=0$ with the applied electrical current J_1 along the bisectrix axis. Since Righi-Leduc effect is so small that there is no measurable transverse temperature difference, even the stray heat current along the 1-axis may be large. Hence $\langle G_2 \rangle / \langle J_1 \rangle$ yields $\langle \pi'_{21} \rangle$.

According to kinetic equations, we can write down these six equations for bulk and layers electrical as well as thermal current densities as

$$J_{1b} = \sigma_{11b}E_1 - \varepsilon''_{12}G_2^1 \tag{A10a}$$

$$J_{1sy} = \sigma_{11sy}E_1 - \varepsilon''_{12}G_2^2 \tag{A10b}$$

$$J_{1sz} = \sigma_{11sz}E_1 - \varepsilon''_{12}G_2^1 \tag{A10c}$$

$$W_{2b} = -\pi''_{21}E_1 + \lambda''_{22b}G_2^1 \tag{A10d}$$

$$W_{2sy} = -\pi''_{21}E_1 + \lambda_{22sy}G_2^2 \tag{A10e}$$

$$W_{2sz} = -\pi''_{21}E_1 + \lambda_{22sz}G_2^1 \tag{A10f}$$

where G_2^1 is the temperature gradient in the bulk or z-layers. G_2^2 is the temperature gradient in the y-layers (see Fig. 1 in Chapter I). E_1 is homogeneous, $E_2=E_3=G_1=G_3=0$ (neglect Joule heating and Thomson effect).

As is noted in the condition of measurement,

$$W_{2b}(1 - \frac{2\delta_z}{c}) + W_{2sz}\frac{2\delta_z}{c} = 0$$

$$W_{2sy} = 0.$$

Thus

$$G_2^1 = \frac{\pi''_{21}E_1}{\lambda''_{22b} + \frac{2\delta_z}{c}(\lambda''_{22sz} - \lambda''_{22b})} \tag{A11}$$

$$G_2^2 = \frac{\pi''_{21}E_1}{\lambda''_{22sy}} \tag{A12}$$

$$< G_2 > = G_2^1(1 - \frac{2\delta_y}{b}) + G_2^2\frac{2\delta_y}{b}$$

or

$$< G_2 > = \pi''_{21}E\frac{\lambda''_{22sy} + (\lambda''_{22b} - \lambda''_{22sy})\frac{2\delta_y}{b}}{\lambda''_{22sy}[\lambda''_{22b} + (\lambda''_{22sz} - \lambda''_{22b})\frac{2\delta_z}{c}]}. \tag{A13}$$

Substitute Eqs. (A11) and (A12) into kinetic equations, we obtain

$$< J_1 > = \{\sigma_{11} - \frac{\varepsilon''_{12}\pi''_{21}}{\lambda''_{22sy}}[\frac{\lambda''_{22sy} - (\lambda''_{22b} - \lambda''_{22sy})\frac{2\delta_y}{b}}{\lambda''_{22b} + (\lambda''_{22sz} - \lambda''_{22b})\frac{2\delta_z}{c}}]\}E. \tag{A14}$$

Therefore

$$< \pi'_{21} > = \frac{\pi''_{21}}{\sigma_{11}\lambda''_{22sy}}(\frac{\lambda''_{22sy}+(\lambda''_{22b}-\lambda''_{22sy})\frac{2\delta_y}{b}}{\lambda''_{22b}+(\lambda''_{22sz}-\lambda''_{22b})\frac{2\delta_z}{c}}$$

$$\{1- \frac{\varepsilon''_{12}\pi''_{21}}{\lambda''_{22sy}\sigma_{11}}[\frac{\lambda''_{22sy}+(\lambda''_{22b}-\lambda''_{22sy})\frac{2\delta_y}{b}}{\lambda''_{22b}+(\lambda''_{22sz}-\lambda''_{22b})\frac{2\delta_z}{c}}]\}^{-1}.$$

As is noted that

$$\lambda'' = \lambda_g + \frac{\varepsilon''_{12}\pi''_{21}}{\sigma_{11}(H)},$$

since

$$X = \frac{\varepsilon''_{12}\pi''_{21}}{\lambda''_{22}\sigma_{11}} = -\frac{\sigma^a_{11} - \sigma_{11}}{\sigma_{11}},$$

then X is very small. Thus

$$\langle \pi'_{21} \rangle \simeq \pi'_{21} \frac{\sigma_{11b}}{\langle \sigma_{11} \rangle}. \tag{A15}$$

The Eq. (A14) also gives

$$\langle \sigma^a_{11} \rangle = \langle \sigma_{11} \rangle - \frac{\varepsilon''_{12}\pi''_{21}}{\lambda''_{22sy}} \frac{[\lambda''_{22sy}+(\lambda''_{22b}-\lambda''_{22sy})\frac{2\delta_y}{b}]}{[\lambda''_{22b}+(\lambda''_{22sz}-\lambda''_{22b})\frac{2\delta_z}{c}]}$$

$$\simeq \langle \sigma_{11} \rangle - \frac{\varepsilon''_{12}\pi''_{21}}{\lambda''_{22b}}. \tag{A16}$$

Therefore

$$\langle \sigma^a_{11} \rangle - \langle \sigma_{11} \rangle = \sigma^a_{11} - \sigma_{11} \tag{A17}$$

which also follows the assumption that

$$\langle \sigma_{11} \rangle = \sigma_{11b}+(\sigma_{11sy}-\sigma_{11b})\frac{2\delta_y}{b} +(\sigma_{11sz}-\sigma_{11b})\frac{2\delta_z}{c}$$

$$\langle \sigma^a_{11} \rangle = \sigma^a_{11}+(\sigma^a_{11sy}-\sigma^a_{11b})\frac{2\delta_y}{b} +(\sigma^a_{11sz}-\sigma^a_{11b})\frac{2\delta_z}{c}.$$

Equation (A17) leads directly to the conclusion which has been discussed in great detail in Chapter I

$$\frac{\langle \rho_{11} \rangle - \langle \rho^a_{11} \rangle}{\langle \rho_{11} \rangle} \simeq \frac{\rho_{11} - \rho^a_{11}}{\rho^2_{11}} \langle \rho_{11} \rangle. \tag{A18}$$

Equation (A18) has been discussed in detail in Chapter I.

APPENDIX B

Thermal Conductivity Measurement

In this investigation we use three methods to measure thermal conductivity. They are designated: "absolute" method, potentiometric method and so called "$\delta\dot{Q}$" method.

(i) "Absolute" method, which follows the definition of thermal conductivity, is given this designation because the temperature difference is the absolute temperature of the resistance thermometers. This method may be less reliable because it involves the uncertainties of two calibrations.

(ii) Potentiometric method is a more reliable method in measuring the thermal conduction. It involves first passing a heat current, $\dot{Q}$, through the specimen giving rise to the temperature distribution in the specimen shown schematically by the "$\dot{Q}$ on" curve in Fig. B1. The resistances $R_1(T_1)$ and $R_2(T_2)$ are noted. After the main heater is turned off, then the auxiliary heater is turned on and adjusted so that $R_1(T_1)$ is reproduced, the temperature distribution is the straight line designated by $\langle T_1 \rangle$ in Fig. B1. $R_2(\langle T_1 \rangle)$ is also noted. From these two readings, $R_2(T_2)$ and $R_2(\langle T_1 \rangle)$, and using calibration curve $R_2(T)$, we can determine the temperature difference $\Delta T = T_2 - \langle T_1 \rangle$. This method has one advantage over (i) in that only one calibration curve $R_2(T)$ is used. In general, $T_1 \neq \langle T_1 \rangle$, the difference between them is usually no more than a few

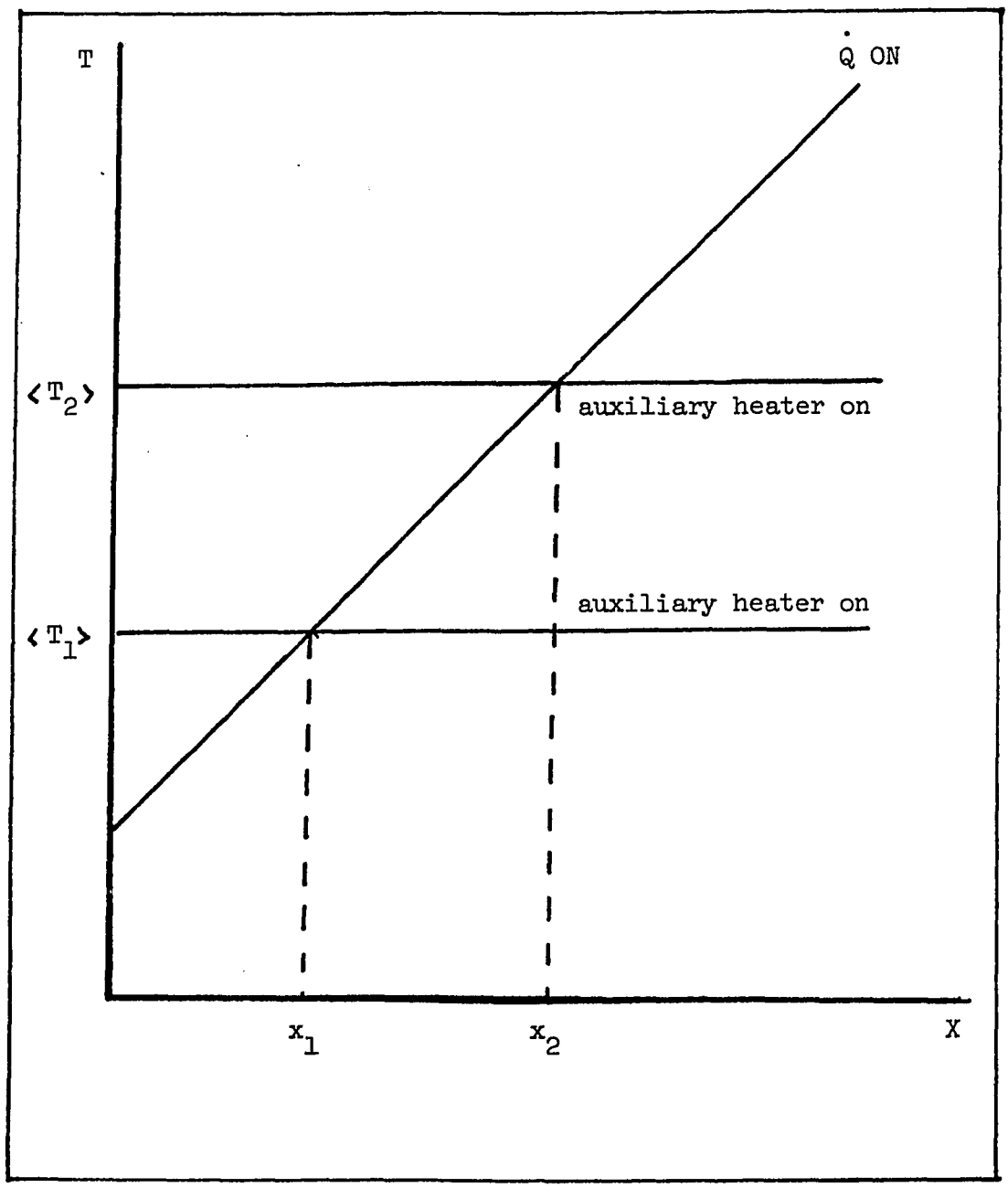
T
$\dot{Q}$ ON
$\langle T_2 \rangle$
auxiliary heater on
auxiliary heater on
$\langle T_1 \rangle$
x_1
x_2
X

Fig. B1

tenths of a mK and the correction to the value of ΔT is made with $R_1(T)$ calibration curve. We can also determine ΔT by using the auxiliary heater to raise the temperature of the specimen to $\langle T_2 \rangle$ and the computation procedure is as above. The difference of (ΔT) from these determinations is less than 0.1 mK, which is less than 0.5% of the temperature difference, ΔT.

(iii) The last method called "$\delta\dot{Q}$" method involves a rather extended procedure and analysis. The equations of this method will be discussed in the next appendix. This method is most useful for samples with high conductivities. In these situations, methods (i) and (ii) are less reliable because ΔT is very small and the mean temperature $\langle T \rangle$ rises markedly above the bath temperature T_o. First, one has to adjust the electrical currents passing through every Wheatstone bridge element, which includes 2 carbon resistors as thermometers and 2 decade resistors boxes so that the output voltage of this bridge (or the difference of the voltages across two thermometers) is constant for a small step change of specimen temperature raised by the auxiliary heater. Then after the resistor currents have been adjusted so that there is no change in the bridge voltage (see Fig. C1) with the stepping of the auxiliary heater, several small heat currents, $\delta\dot{Q}$, are applied to the sample and the changes of the bridge voltage noted. The slope of unbalanced voltage against the heat current is proportional to the thermal

resistivity. From the calibration curve* of the carbon resistor and the balance conditions of the bridge, one will obtain some parameters which will be discussed in the next appendix. With the parameter A*, and the slope, m, one gets the thermal resistivity of sample, γ_T,

$$\gamma_T = \frac{m}{A^*} \frac{a}{L}$$

where a is the cross section of the sample, L is the length between two thermometers. If at any temperature we assume $\gamma_T \propto T^{-n}$, then $n = \frac{d \ln \gamma_T}{d \ln T}$. Let a temperature difference, $T_2 - T_1$, be established by a heat current, $\dot{Q}$. Then if the currents through the resistors (thermometers) varied so that a step by the auxiliary heater produces a null change in the bridge voltage, then

$$n = \frac{B^* \langle T \rangle}{A^*(T_2 - T_1)}$$

where $\langle T \rangle = \frac{(T_2+T_1)}{2}$. This equation is justified in the next appendix.

---

*The carbon resistors used in this investigation are Allen-Bradley 50 1/10 W. The calibration curves were fit Clement-Quninel formula for three different temperature regions (i.e. 4.2 K-3.2 K; 3.2 K-2.3 K; 2.1 K-1.2 K). The RMSD is always less than 0.5 mK for the calibration temperatures.

APPENDIX C

Bridge Equations

In Appendix B we described the procedures for measuring thermal conductivity including the "$\delta\dot{Q}$" method which uses a resistance bridge. In this appendix this method will be analyzed in detail.

Heat flow is usually assumed to follow the equation:

$$\frac{\dot{Q}}{a} = \lambda(T) \frac{dT}{dx} \tag{C1}$$

where $\dot{Q}$ is the heat current; a is the area of cross section of sample; $\lambda(T)$ is thermal conductivity.

Let's assume that $\gamma(T) = 1/\lambda(T)$, where $\gamma(T)$ is thermal resistivity, thus

$$\frac{dT}{dx} = \gamma(T) \frac{\dot{Q}}{a}. \tag{C2}$$

The "$\delta\dot{Q}$" method is employed in this investigation to compliment the standard methods (i) and (ii) of Appendix B. It is used when the sample conductance is very high, say greater than that of the auxiliary heater mounting. The value of thermal resistivity obtained is associated with the bath temperature T_o, thus the "$\delta\dot{Q}$" method enables the determination of γ at temperature 0.1^{o} to 0.2^{o} lower than the conventional methods.

The thermometer resistors R_1 and R_2 are elements of a wheatstone bridge shown schematically in Fig. C1. R_1' and R_2' are adjustable resistors. The null detector (Keithley

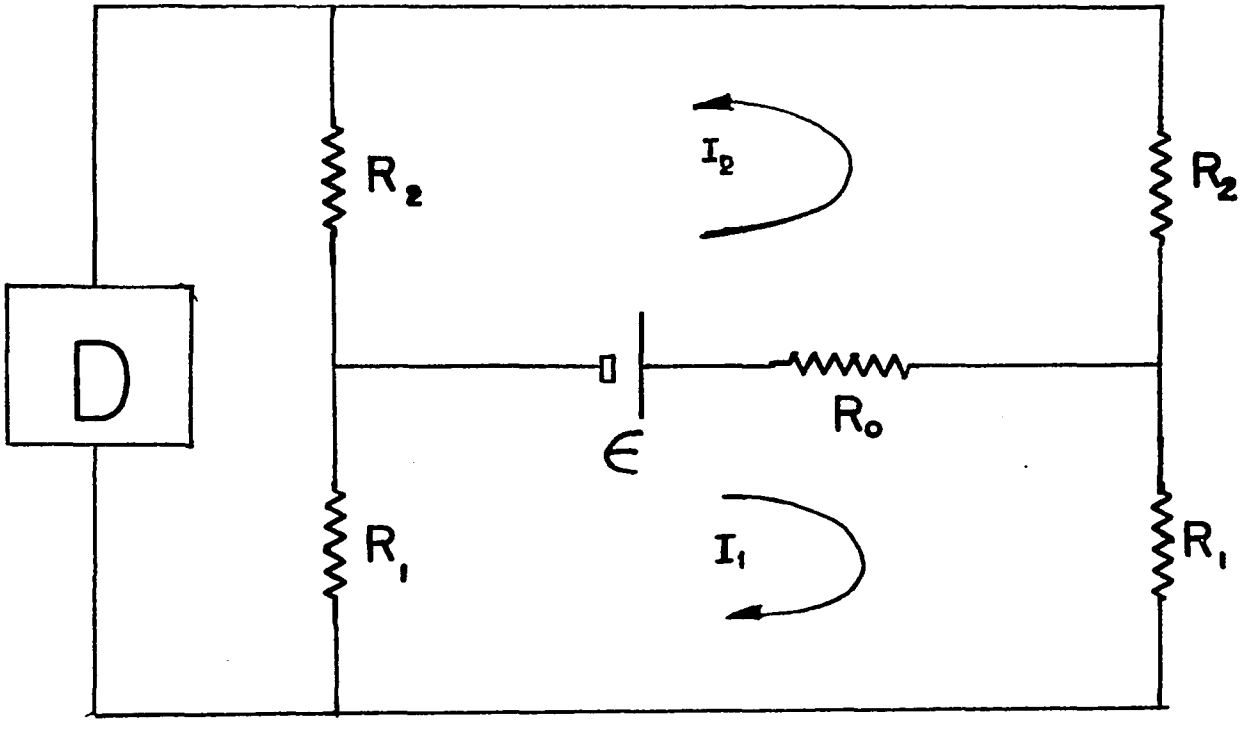

Fig. C1

147 nanovoltmeter) is assumed to have infinite input impedance. The loop currents flowing in the bridge system are I_1 and I_2. From Kirchhoff's law, one will obtain

$$\begin{aligned} \varepsilon &= (R_o + R_1 + R_1')I_1 + R_oI_2 \\ \varepsilon &= R_oI_1 + (R_o + R_2 + R_2')I_2. \end{aligned} \tag{C3}$$

If the voltage drop across R_1 is V_1, across R_2 is V_2, therefore

$$V_2 - V_1 = I_2R_2 - I_1R_1 \tag{C4}$$

where

$$\begin{aligned} I_1 &= \frac{\varepsilon(R_2+R_2')}{\Delta}, \quad I_1 = \frac{\varepsilon(R_1+R_1')}{\Delta} \\ \Delta &= R_o(R_1+R_1'+R_2+R_2')+(R_1+R_1')(R_2+R_2') \end{aligned} \tag{C5}$$

therefore

$$V_2-V_1 = \frac{\varepsilon}{\Delta}(R_2R_1' - R_1R_2')$$

the variation of $V_2 - V_1$ with respect to temperature is more interesting than $V_2 - V_1$ itself, and

$$\delta(V_2-V_1) = \frac{\varepsilon}{\Delta}(R_1'\delta R_2 - R_2'\delta R_1) - \frac{V_2-V_1}{\Delta}\delta\Delta$$

for a simple case with $R_o >> R_1, R_2$ $\quad \frac{\delta\Delta}{\Delta} \simeq \frac{\delta R_1+\delta R_2}{R_1+R_1'+R_2+R_2'}$

$$\delta(V_2 - V_1) = i_2\,\delta R_2 - i_1\delta R_1 \tag{C6}$$

where

$$i_1 = I_1\alpha_1 + \frac{(V_2-V_1)}{R_1+R_1'+R_2+R_2'} \qquad \alpha_1 = \frac{R_2'}{R_2+R_2'} \tag{C6a}$$

$$i_2 = I_2\alpha_2 - \frac{(V_2-V_1)}{R_1+R_1'+R_2+R_2'} \qquad \alpha_2 = \frac{R_1'}{R_1+R_1'}. \tag{C6b}$$

The resistances of thermometers may be expressed by Taylor expressions at the reference temperature T_1 and T_2 and at a constant magnetic field,

$$\delta R_{1,2} = \left(\frac{\partial R_{1,2}}{\partial T}\right)_{T_{1,2}} (\delta T_{1,2}) + \frac{1}{2}\left(\frac{\partial^2 R_{1,2}}{\partial T^2}\right)_{T_{1,2}} (\delta T_{1,2})^2 + \ldots.$$

Then

$$\delta(V_2-V_1) = A^*\delta(T_2-T_1)+B^*\delta\langle T\rangle+C^*\left[(\delta\langle T\rangle)^2+\left(\frac{\delta(T_2-T_1)}{2}\right)^2\right] + D^*\delta\langle T\rangle\delta(T_2-T_1) \tag{C7}$$

where

$$\delta T_1 = -\delta(T_2-T_1)/2 + \delta\langle T\rangle$$

and

$$\delta T_2 = +\delta(T_2-T_1)/2 + \delta\langle T\rangle$$

$$A^* = \frac{1}{2}\left[i_2\left(\frac{\partial R_2}{\partial T}\right)_{\langle T_2\rangle} + i_1\left(\frac{\partial R_1}{\partial T}\right)_{\langle T_1\rangle}\right]$$

$$B^* = \frac{1}{2}\left[i_2\left(\frac{\partial R_2}{\partial T}\right)_{\langle T_2\rangle} - i_1\left(\frac{\partial R_1}{\partial T}\right)_{\langle T_1\rangle}\right] \tag{C7a}$$

$$C^* = \left[i_2\left(\frac{\partial^2 R_2}{\partial T^2}\right)_{\langle T_2\rangle} - i_1\left(\frac{\partial^2 R_1}{\partial T^2}\right)_{\langle T_1\rangle}\right]$$

$$D^* = \frac{1}{2}\left[i_2\left(\frac{\partial^2 R_2}{\partial T^2}\right)_{\langle T_2\rangle} + i_1\left(\frac{\partial^2 R_1}{\partial T^2}\right)_{\langle T_1\rangle}\right]$$

for empirical purposes, the second order terms are negligible, then

$$\delta(V_2-V_1) \simeq A^*\delta(T_2-T_1) + B^*\delta\langle T\rangle. \tag{C7b}$$

Now, let's consider measuring the thermal conductivity by determining the slope of the $\delta(V_2-V_1)$vis $\dot{Q}$ curve.

In considering this problem we must take into account the thermal contact resistance at the junctions between the sample and the copper post as well as the auxiliary heater and the sink. If one passes an amount of heat current $\dot{Q}$ through the specimen, the temperatures of the two thermometers T_1 and T_2 are given by

$$T_1 = T_o + (\Gamma + R)\dot{Q} + \gamma(\langle T\rangle)\frac{x_1\dot{Q}}{a} \tag{C8}$$

$$T_2 = T_o + (\Gamma + R)\dot{Q} + \gamma(\langle T\rangle)\frac{x_2\dot{Q}}{a} \tag{C9}$$

where T_o is the bath temperature, Γ is the contact resistance between sample and the copper auxiliary heater mounting, R is the thermal resistance of auxiliary heater mounting to the bath, and a is the cross sectional area of the sample. So

$$\delta(T_2-T_1) = \gamma(\langle T\rangle)\frac{L}{a}\dot{Q}$$

$$\delta\langle T\rangle = \langle T\rangle - T_o = (\Gamma + R)\dot{Q} + \gamma(\langle T\rangle)\langle x\rangle\frac{\dot{Q}}{a}$$

where $L = x_2 - x_1$ and $\langle x\rangle = (\frac{x_1 + x_2}{2})$.

In general, to the second order

$$\delta(V_2-V_1) = A^*\delta(T_2-T_1)+B^*\delta\langle T\rangle+C^*\{(\delta\langle T\rangle)^2+(\frac{\delta(T_2-T_1)}{2})^2\}$$
$$+D^*\delta\langle T\rangle\delta(T_2-T_1).$$

The resistor currents I_1 and I_2 are adjusted so that $B^* = 0$

and thereby the C* term gives a negligibly small contribution.

$$\delta(V_2-V_1) = \gamma(\langle T\rangle)\frac{L}{a}\dot{Q}\{A^*+D^*\delta\langle T\rangle\}$$

but if $(\Gamma+R)$ is comparable with $\gamma(\langle T\rangle)\frac{x_1}{a}$, $\delta\langle T\rangle$ will not be negligible so that

$$\gamma(\langle T\rangle) = \gamma(T_o) + \frac{\partial\gamma}{\partial T}\delta\langle T\rangle$$

$$\delta(V_2-V_1) = A^*\gamma(T_o)\frac{L}{a}\dot{Q}[1+(\frac{1}{\gamma}\frac{\partial\gamma}{\partial T})_{T_o}\delta\langle T\rangle][1+\frac{D^*}{A^*}\delta\langle T\rangle].$$

In general both bracketed terms are less than unity. Measurements of $\delta(V_2-V_1)$ vs $\dot{Q}$ display a discernible deviation from linearity. Therefore the linear term must be extracted from the data by means of a quadratic least square fit. Typically for sample #17 in zero field $\delta(V_2-V_1)/\dot{Q} \simeq 20$ μv/mW and the standard deviation was < 0.1 μv for $0 \lesssim \dot{Q} \lesssim 1.5$ mW. This method, like (i) of Appendix B, suffers the disadvantage that A*, B*, C* and D* involve temperature derivatives of both R_1 and R_2 and thereby the errors of both calibrations.

The determination of the exponent of temperature dependence involves changing the mean temperature of the specimen by a step of auxiliary heater as the sample heater on. Thus

$$T_2 - T_1 = \gamma(\langle T\rangle)\frac{L}{a}\dot{Q} \qquad (C11)$$

where $L = x_2 - x_1$ and

$$\frac{\delta(T_2-T_1)}{T_2-T_1} = \frac{\delta\gamma}{\gamma} = \frac{1}{\gamma}\left(\frac{\partial\gamma}{\partial_T}\right)_{\langle T\rangle} \delta\langle T\rangle . \qquad (C12)$$

In any case

$$\delta(V_2-V_1) = [A^*(T_2-T_1)\left(\frac{1}{\gamma}\left(\frac{\partial\gamma}{\partial T}\right)_{\langle T\rangle}\right)+B^*]\delta\langle T\rangle. \qquad (C13)$$

Now if one adjusted $\delta(V_2-V_1) = 0$ for the mean temperature of a specimen changed by auxiliary heater, then

$$B^* = -A^*(T_2-T_1)\left(\frac{1}{\gamma}\frac{\partial\gamma}{\partial T}\right)_{\langle T\rangle}.$$

Since

$$\gamma = aT^{-n}$$

then

$$n = \frac{B^*\langle T\rangle}{A^*(T_2-T_1)}. \qquad (C15)$$

APPENDIX D

Kapitza Resistance

The model used in Chapter II is based on the bulk sample with homogeneous properties. Even though that treatment can be extended to those samples with either skin layers or damaged layers on the surfaces.

As noted in Chapter I the difference between bulk and skin type magnetoresistance is only a factor q_1, or,

$$\rho_{11b} = q_1 \langle \rho_{11} \rangle .$$

Therefore, the degree of adiabaticity Δ has no difference between bulk and skin type material. That is,

$$\Delta_s = \frac{\langle \rho_{11} \rangle - \langle \rho_{11}(He) \rangle}{\langle \rho_{11} \rangle - \langle \rho_{11}^a \rangle} = \frac{q_1(\rho_{11b} - \rho_{11b}(He))}{q_1(\rho_{11b} - \rho_{11b}^a)} = \Delta .$$

As a consequence, we come to the conclusion that there is no influence of the diffusion layer on the determination of Kapitza resistance.

As is stated in Chapter I, the assumptions for damaged layer model include: (1) π''_{21} and ε''_{21} are the same in both the layer and the bulk part; (2) the thickness of the layer, δ, is large enough so that uniform transport tensors can be defined. With these assumptions we will see that the influence of damaged layer on the determination of Kapitza resistance is also negligible.

If one neglects Joule heating and Thomson effect, the solution of differential Eq. (28) in the text is still the

same type. It is given by, for the damaged layer,

$$\left(\frac{dT}{dy}\right)_1 = - \frac{\pi_{21b} J_{1b}}{\lambda_g} \frac{\alpha}{M} \cosh\alpha y \qquad (D1)$$

$$\left(\frac{dT}{dy}\right)_2 = - \frac{\pi_{21sy} J_{1sy}}{\lambda_g} \frac{\alpha}{M} \cosh\alpha y \qquad (D2)$$

where $\left(\frac{dT}{dy}\right)_1$ is the temperature gradient in the bulk and z-layers, $\left(\frac{dT}{dy}\right)_2$ is the temperature gradient in the y-layers. (Compare Eqs. (D1) and (D2) with (A11) and (A12).)

But the (dT/dy) is homogeneous in the xz-plane. The following is to determine the effective E-field in the x axis (bisectrix-axis in sample #17). The microscopic circuit along x-direction is shown in Fig. D1. The measured voltage drop between A and B is V (the length of AB is L). If the resistance in the slab is γ, the voltage generated by temperature gradient dT/dy is e, the current flows in this slab is i, then

$$V = i_j \gamma_j + e_j \qquad (D3)$$

where

$$i_j = J(yz)dydz$$

$$\gamma_j = \rho(yz)\frac{L}{dydz}$$

$$e_j = - \varepsilon_{12}(yz)\left(\frac{\partial T}{\partial y}\right)L \qquad \frac{V}{L} = E$$

$$E(yz) = \rho_{11}(yz)J(yz) - \varepsilon_{12}(yz)\left(\frac{\partial T}{\partial y}\right)$$

or

$$E(yz) = \rho_{11}(yz)J(yz) + \frac{\varepsilon_{12}(yz)\pi_{21}(yz)J(yz)\alpha}{\lambda_g M}\cosh\alpha y$$

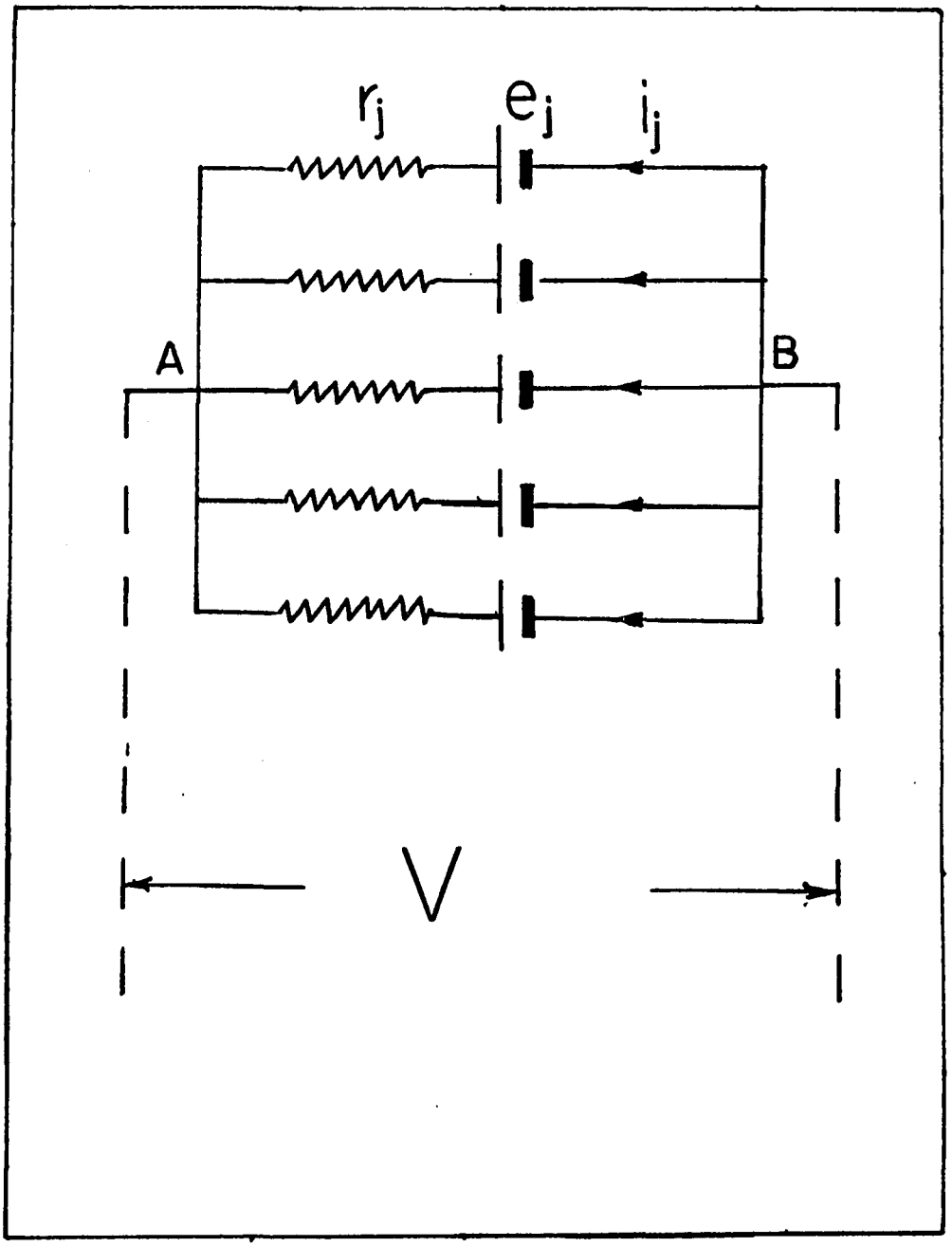

Fig. D1

$$J(yz) = \frac{E(yz)}{(1 + \frac{\varepsilon_{12}(yz)\pi_{21}(yz)}{\rho_{11}(yz)\lambda_g M}\alpha\cosh\alpha y)\rho_{11}(yz)} \tag{D4}$$

or

$$\sigma_{11}(He)(yz) = \frac{\sigma_{11}(yz)}{1 + \frac{\varepsilon_{12}(yz)\pi_{21}(yz)}{\rho_{11}(yz)\lambda_g M}\alpha\cosh\alpha y} .$$

To the first order approximation

$$\langle \sigma_{11}(He)\rangle = \langle \sigma_{11}\rangle - \frac{2\varepsilon''_{12}\pi''_{21}}{\lambda_g Mb}\int_{-\frac{b}{2}}^{\frac{b}{2}} \alpha\cosh\alpha y dy \tag{D5}$$

$$\langle \sigma_{11}(He)\rangle = \langle \sigma_{11}\rangle - \frac{2\varepsilon''_{12}\pi''_{21}}{\lambda_g Mb}\sinh\frac{\alpha b}{2}$$

thus

$$\langle \sigma_{11}(He)\rangle = \langle \sigma_{11}\rangle + \frac{2\sinh\frac{\alpha b}{2}}{Mb}(\langle \sigma_{11}\rangle^a - \langle \sigma_{11}\rangle)\frac{\lambda''_{11}}{\lambda_g}$$

$$\Delta_{layer} = \frac{\langle \rho_{11}\rangle - \langle \rho_{11}(He)\rangle}{\langle \rho_{11}\rangle - \langle \rho^a_{11}\rangle} = \frac{\langle \rho_{11}(He)\rangle}{\langle \rho^a_{11}\rangle}\frac{\lambda''_{11}}{\lambda_g}\left[\frac{c}{b}\left(\frac{\alpha b}{2}\right)^2 + \frac{\alpha b}{2}\coth\frac{\alpha b}{2}\right]^{-1} \tag{D6}$$

$$\simeq \Delta_b .$$

The difference between Δ_{layer} and Δ_b is thus negligible.

The solution of the differential Eq. (28) in Chapter II is approximate. If we are to obtain the exact solution for Eq. (23), we must know the boundary conditions exactly. So far, the Kapitza resistance of antimony is not well known. What we can do is to find a solution closer to the real physical case.

If Eq. (28) includes Joule and Thomson heat, it is rewritten as

$$\lambda_g \frac{\partial^2 T(y)}{\partial y^2} - (T \frac{\partial \varepsilon_{12}}{\partial T}) J_1 \frac{\partial T(y)}{\partial y} - \frac{T(y)-T_o}{\frac{c}{2}R_K} = \rho_{11} J_1^2. \quad \text{(D7)}$$

The general solution of (D7) is

$$T_g(y) - T_o = e^{\beta y}[A \sinh \alpha' y + B \cosh \alpha' y] \quad \text{(D8)}$$

where

$$\beta = \frac{T}{2\lambda_g} \frac{\partial \varepsilon_{12}}{\partial T} J_1$$

$$\alpha' = [\frac{2}{cR_K\lambda_g} + (T \frac{\partial \varepsilon_{12}}{\partial T} \frac{J_1}{\lambda_g})^2]^{1/2}.$$

The particular solution of (D1) is chosen as

$$T_P(y) - T_o = \frac{c}{2} R_K \rho_{11} J_1^2. \quad \text{(D9)}$$

Therefore, the complete solution is

$$[T(y) - T_o] = e^{\beta y}[A\sinh\alpha' y + B\cosh\alpha' y] + \frac{c}{2}R_K\rho_{11}J_1^2. \quad \text{(D10)}$$

One has to be aware that $[T(y) - T_o]$ is no longer antisymmetric about $y = 0$ due to the term of Joule heating.

It is proper to assume that the Ettingshausen heat is only passing through y surfaces, i.e.

$$\pm[\frac{T(\pm \frac{b}{2})-T_o}{R_K}] = -\pi_{21}J_1 - \lambda_g \frac{\partial T}{\partial y}\Big|_{y=\pm\frac{b}{2}}. \quad \text{(D11)}$$

If set

$$M(\alpha') = \frac{1}{R_K\lambda_g} \sinh \frac{\alpha' b}{2} + \alpha' \cosh \frac{\alpha' b}{2} \quad \text{(D12)}$$

and

$$P(\alpha') = \frac{1}{R_K \lambda_g} \cosh \frac{\alpha' b}{2} + \alpha' \sinh \frac{\alpha' b}{2}. \tag{D13}$$

The equation of $M(\alpha')$ is exactly the same as M, defined in the text, except α' is replaced by α. Then, the parameters A and B are given by

$$A = \frac{1}{\lambda_g M(\alpha') P(\alpha')}\left[P(\alpha')\left(\pi_{21} J_1 \cosh\frac{\beta b}{2} + \frac{c}{2}\rho_{11} J_1^2 \sinh\frac{\beta b}{2}\right)\right.$$

$$\left. + \beta \cosh \frac{\alpha' b}{2}\left(\pi_{21} J_1 \sinh\frac{\beta b}{2} - \frac{c}{2}\rho_{11} J_1^2 \cosh\frac{\beta b}{2}\right)\right] \tag{D14}$$

$$B = \frac{1}{\lambda_g M(\alpha') P(\alpha')}\left[M(\alpha')\left(\pi_{21} J_1 \sinh\frac{\beta b}{2} + \frac{c}{2}\rho_{11} J_1^2 \cosh\frac{\beta b}{2}\right)\right.$$

$$\left. + \beta \sinh\frac{\alpha' b}{2}\left(\pi_{21} J_1 \cosh\frac{\beta b}{2} + \frac{c}{2}\rho_{11} J_1^2 \sinh\frac{\beta b}{2}\right)\right]. \tag{D15}$$

Now, the temperature gradient (dT/dy) is given by

$$\frac{dT}{dy} = \beta e^{\beta y}[A \sinh\alpha' y + B \cosh\alpha' y]$$

$$+ \alpha' e^{\beta y}[A \cosh\alpha' y + B \sinh\alpha' y]$$

and the total actual electric field is given by

$$E_1 = \rho_{11} J_1 - \varepsilon_{12}\left(\frac{dT}{dy}\right).$$

From now on the later calculations will follow the equations listed in Chapter II step by step. And finally, the equation of Δ is given by

$$\Delta = \frac{\langle \rho_{11} \rangle - \langle \rho_{11}(He) \rangle}{\langle \rho_{11} \rangle - \langle \rho_{11}^a \rangle} \tag{D16}$$

$$= \frac{\langle \rho_{11}(He) \rangle}{\langle \rho_{11} \rangle} f(A, B, \alpha', \beta, J)$$

where

$$f(A,B,\alpha',\beta,J) = \frac{1}{b}\{[\frac{1}{\alpha'+\beta}\sinh\frac{(\alpha'+\beta)b}{2} - \frac{1}{\alpha'-\beta}\sinh\frac{(\alpha'-\beta)b}{2}]*$$

$$[\frac{\beta A}{\pi_{21}J_1} + \frac{\alpha B}{\pi_{21}J_1}] + [\frac{1}{\alpha'+\beta}\sinh\frac{(\alpha'+\beta)b}{2} + \frac{1}{\alpha'-\beta}\sinh\frac{(\alpha'-\beta)b}{2}]*$$

$$[\frac{\beta B}{\pi_{21}J_1} + \frac{\alpha A}{\pi_{21}J_1}]\} \qquad \text{(D17)}$$

if Joule heating and Thomson effects are neglected (i.e. $\beta = 0$, $J_1 = 0$ in (D17)) then

$$f = [\frac{c}{b}(\frac{\alpha b}{2})^2 + (\frac{\alpha b}{2})\coth\frac{\alpha b}{2}]^{-1}.$$

It is exactly the same as Eq. (34).

For our experimental values, we found that Joule heating, $\rho_{11}J^2$, is about 10^{-6} W/cm^3 and Thomson effect, $T(\varepsilon_{12} - \frac{\partial\pi_{12}}{\partial T})J_1$, is about 10^{-7} W/cm^2. They are smaller than the Ettingshausen heat which is about 10^{-4} W/cm^3. Therefore, both of the Joule and Thomson heating are negligible in antimony for a small current J.

APPENDIX E

Misalignment and Spurious Effects

The misalignment of potential leads and thermometers as well as the presence of thermal emf's in the potential leads generally give rise to spurious effects of the measured transport coefficients. There is obviously a need to minimize or even to eliminate these effects.

The spurious effects in the Ettingshausen coefficient measurement are removed by simply reversing the current and/or field directions. The longitudinal temperature gradient arising from Joule heating of sample and its current leads is independent of both current and magnetic field direction. The transverse temperature gradient from Righi-Leduc (if it exists) of Joule heating will reverse as field reverses. The transverse temperature gradient yielded by Ettingshausen will reverse when either current or field reverses. Thus, suppose $(\nabla T)_m$ is the measured gradient, $(\nabla T)_E$ is the Ettingshausen gradient, $(\nabla T)_R$ is the Righi-Leduc effect, and $(\nabla T)_L$ is the longitudinal gradient due to misalignment of thermometers. Then

$$(\nabla T)_m(H,I) = (\nabla T)_E(H,I) + (\nabla T)_R(H,I) + (\nabla T)_L(H,I)$$

$$(\nabla T)_m(H,-I) = (\nabla T)_E(H,-I) - (\nabla T)_R(H,-I) - (\nabla T)_L(H,-I)$$

$$(\nabla T)_m(-H,-I) = (\nabla T)_E(-H,-I) - (\nabla T)_R(-H,-I) + (\nabla T)_L(-H,-I)$$

$$(\nabla T)_m(-H,I) = (\nabla T)_E(-H,I) + (\nabla T)_R(-H,I) - (\nabla T)_L(-H,I).$$

Summing above four equations, one obtains

$$(\nabla T)_E = \frac{1}{4}[(\nabla T)_m(H,I)+(\nabla T)_m(H,-I)+(\nabla T)_m(-H,-I)+(\nabla T)_m(-H,I)].$$

If one used "bridge" method to measure the temperature difference by reading the unbalanced voltage of a Wheatstone bridge, it is necessary to eliminate the spurious thermal emf in the potential leads of thermometers. This can be accomplished by using an auxiliary heater to reproduce the mean temperature of the specimen, which was recorded when the sample current was on. The desired bridge voltage is the difference between the readings with sample current on and auxiliary heater on.

In the measurement of Nernst-Ettingshausen effect, the direction of the heat current cannot be reversed. The method employed to minimize any possible spurious voltages is to reverse the magnetic field and by use the auxiliary heater as described above since spurious thermal emfs exist in the potential leads. The spurious voltages in N-E measurement will include the thermal emf in potential leads and in sample. Suppose

$V_2(\pm H,\dot{Q})$ is the measured transverse voltage with the heater on and the field in the forward/reverse direction.

$V_2(\pm H,0)$ is the measured transverse voltage with the heater off, auxiliary heater on and the field in the forward/reverse direction.

The actual voltage from the Nernst-Ettingshausen effect is

$$V_2 = \frac{1}{2}\{[V_2(+H,\dot{Q})-V_2(+H,0)]-[V_2(-H,\dot{Q})-V_2(-H,0)]\}$$

Since Righi-Leduc effect is immeasurably small at high field, there is no transverse temperature gradient and thereby no thermoelectric gradient is generated. Furthermore, since temperature of the two potential leads change only slightly, the total thermal emf in those leads remains unchanged.

The other misalignment in longitudinal measurements is negligible and will not be discussed further.

APPENDIX F

Experimental Details at Zero Magnetic Field

Measurement of Ideal Resistivity and Thermoelectric Power

The experimental procedures and experimental apparatus used in zero field measurement were not discussed in the main text. The thermal conductivity measurements were discussed in Appendix B, so that this appendix will be limited to the description of the techniques for measuring the very small voltages encountered in zero field.

The cryogenic system used in this investigation is similar to that used previously in this lab.* The apparatus used to measure the very small voltage differences encountered in the zero field investigation was a Keithley Model 800 picovoltmeter. Block diagram of the circuit is shown in Fig. F1.

"The operation of the model 800 is based on the superconducting coil modulator technique put forth by C. Satterthwaite and R. Ries. This technique consists of using a time-varying mutual inductance to generate an a.c. voltage proportional to a d.c. current. The device described by Satterthwaite and Ries is a current sensing device; the model 800, however, uses it as an error detector in a feedback system, and a very sensitive, accurate voltmeter is the result."[1]

---

*G. N. Rao, Dissertation, Louisiana State University, 1963; J. R. Long, Dissertation, Louisiana State University, 1965.

[1]Instruction Manual of Keithley Model 800 Picovoltmeter.

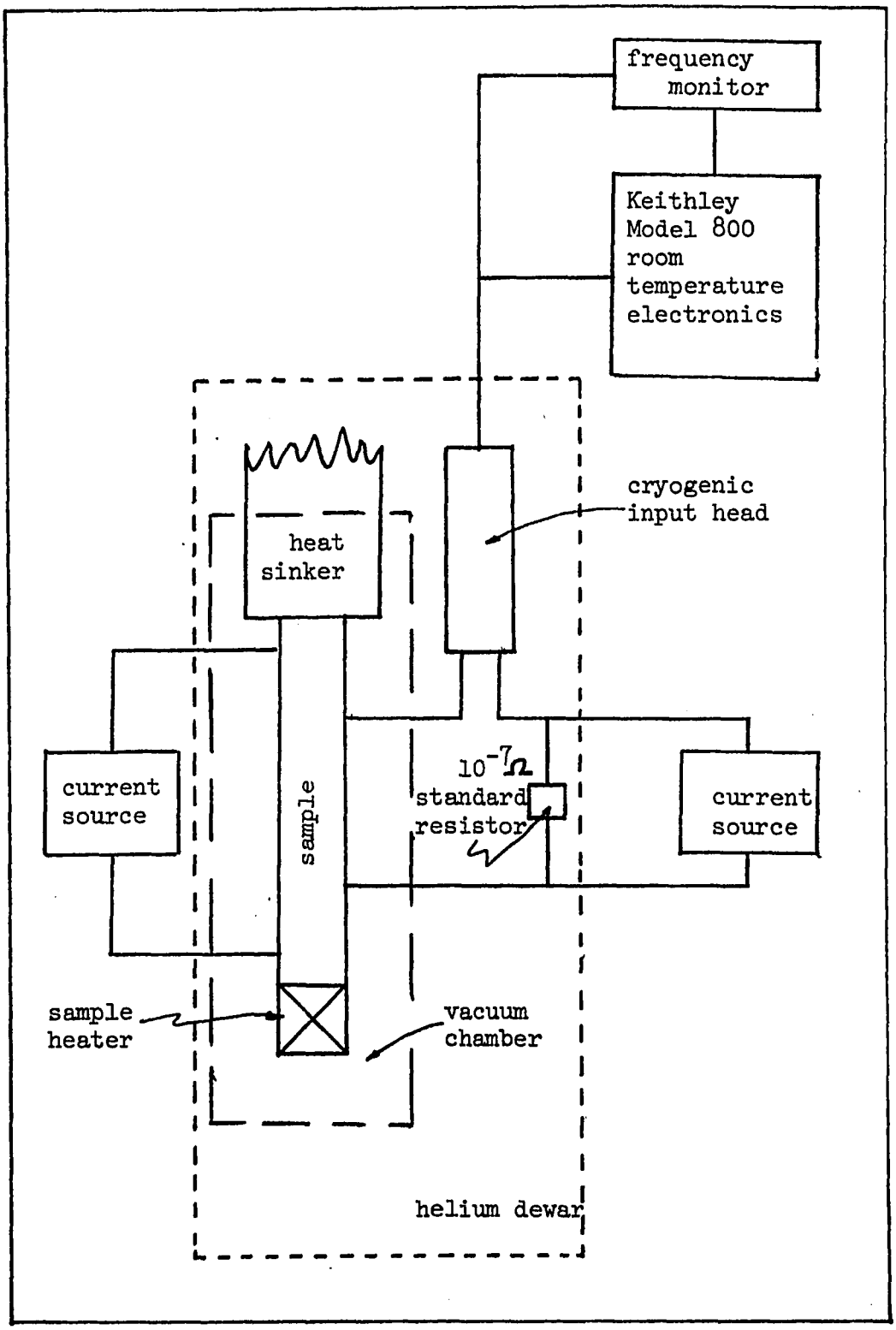
frequency monitor
Keithley Model 800 room temperature electronics
heat sinker
cryogenic input head
current source
sample
$10^{-7}\Omega$ standard resistor
current source
sample heater
vacuum chamber
helium dewar

Fig. F1

Therefore we can use it as a null detector since its sensitivity is about 5 pv. Detail information and theoretical basis can be found in the original article.*

The primary currents J and W were applied along the bisectrix 1-direction. The electrical currents, sufficient to give a measured longitudinal potential difference 1 nv for ideal resistivity measurement, were usually about 7 ma to 15 ma. The applied heat current were sufficient to give a longitudinal temperature difference of 20 mK yielding a longitudinal thermoelectric potential difference, varying from 5 to 20 nv.

The potential differences thus generated by sample currents (electrical or heat) are balanced by voltage developed by passing current through a 10^{-7} Ω standard resistor (see Fig. F1). The model 800 picovoltmeter used a null detector. We used 88/12 PbSb solder, since it is a superconductor below 6.6 °K.+ The potential leads in these measurements were niobium wires. Even with these precautions, there were spurious resistances in the circuit. The likely sources of these resistances are the sample-solder and solder-leads junctions. Such resistances appeared in the junctions reduce the sensitivity of the model 800 picovoltmeter since it is a current sensing device. With

---

*R. P. Ries and C. B. Satterthwaite, Rev. Sci. Instr. 38, 1203 (1967).

+Handbook of Chemistry and Physics, 46th ed., The Chemical Rubber Co. (1965).

the sample heater off the specimen was raised from the bath temperature to the mean temperature observed when the sample heater was on. The picovoltmeter showed no detectable change, thus spurious thermal emfs seem to be absent.

APPENDIX G

Carrier-Longitudinal Phonon and Carrier-Transverse Phonon Interaction

In order to study the difference between transverse and longitudinal phonon-carrier interaction, as pointed out by Klemens,* we start from the comparison of λ_g with λ_e^{id}.

Generally, if we neglect three-phonon normal process scattering, the "enclosed" phonon lattice conductivity which is the dominant term of lattice conductivity below 1.4°K in antimony is given by

$$\lambda_g^{eN}(T) = \frac{k_B^3}{\pi} \frac{\rho\hbar}{(3\frac{m_e^*}{a_e}\varepsilon_e^2 + 6\frac{m_h^{*2}}{a_h}\varepsilon_h^2)} T^2 J_3(\frac{\textcircled{H}_1^*}{T}). \qquad (G1)$$

According to the experimental result,

$$\lambda_g^{eN}(T) \sim .00312\ T^2\ \frac{W}{^oKcm}$$

for low temperature limit.

In the limit of low temperature, the ideal electronic thermal conductivity is $\lambda_e^{id} \propto T^{-2}$. As pointed out by Klemens,* it is preferable to compare $\lambda_g (=\lambda_g^{eN})$ with the values of $\lambda_e^{id}(T)$. But since the electron-phonon scattering dominates in phonon system in Sb, it is better to use the thermal conduction of electron for this comparison purpose.

---

*P. G. Klemens, Solid State Phys. 7 (1958); F. Seitz and D. Turnbull, eds. (Academic Press, New York, 1958).

The measured value of ideal electronic thermal conductivity (of electron) is about (see thermal magnetoresistance)

$$\lambda_e^{id}(T) = 10.2\ T^{-2}\ \frac{W}{^oKcm}. \qquad (G2)$$

While the relationship between $\lambda_g (=\lambda_g^{eN})$ and $\lambda_e^{id}(T)$ depends on the nature of the interaction of electron with lattice waves in the different branches of polarization, the deformation potential term will combine in either form $\Sigma_j \varepsilon_j^2$ or $\Sigma_j \varepsilon_j^{-2}$ (where j denotes the different branches), for this determined the relation between $\Sigma_j \varepsilon_j^2$ and $\Sigma_j \varepsilon_j^{-2}$. The former appears in the electronic ideal thermal conduction; the latter shows in the lattice conduction.

Makinson has assumed equal interaction between electron and all branches of polarization, i.e.

$$\varepsilon_L^2 = \varepsilon_T^2 = \frac{1}{3}\varepsilon^2.$$

Therefore,

$$\frac{\lambda_g^{eN}(T)}{\lambda_e^{id}(T)} = 313\ \left(\frac{T}{\Theta_D}\right)^4 \left(\frac{N}{n}\right)^{4/3} \qquad (G3)$$

in the limit of low temperature, where N is the number of atoms in the unit volume, n is the carrier density.

In the simplest form the Bloch theory requires that

$$\varepsilon_L^2 = \varepsilon^2 \qquad \varepsilon_T^2 = 0$$

for complete spherical symmetry. Under this assumption, one obtains*

$$\frac{\lambda_g^{eN}(T)}{\lambda_e^{id}(T)} = \frac{313}{3}\left(\frac{T}{\Theta}\right)^4 \left(\frac{N}{n}\right)^{4/3}. \qquad (G4)$$

The factor 3 in (G4) arises because $(\Sigma\ \varepsilon_j^{-2})^{-1} = \frac{\varepsilon_L^2}{3} = \frac{\varepsilon^2}{3}$. As is noted elsewhere that $N = 3.31 \times 10^{22}$ 1/cm^3, $N = 5.45 \times 10^{19}$ 1/cm^3, and $\Theta_D = 210°K$ for Sb with these numbers and Eqs. (G2), (G3), and (G4) we get

$$\frac{\lambda_g^{eN}}{\lambda_e^{id}(T)} = .825 \times 10^{-3}\ T^4 \text{ in "Makinson" limit} \qquad (G5)$$

$$\frac{\lambda_g^{eN}}{\lambda_e^{id}(T)} = .275 \times 10^{-3}\ T^4 \text{ in "Bloch" limit.} \qquad (G6)$$

In comparison these two calculated values with measured value, $.306 \times 10^{-3}\ T^4$, one will find that the ratio of $\lambda_g^{eN}/\lambda_e^{id}$ tends to the result of the "Bloch" limit (or $\varepsilon_L^2 = \varepsilon^2$, $\varepsilon_T^2 = 0$). Thus, we can conclude that the longitudinal phonon-carrier scattering has stronger interaction than transverse phonon-carrier scattering does.

APPENDIX H

Phenomenological Models for Phonon Drag Thermoelectric Power and Nernst-Ettingshausen Effect

In the past few years several phenomenological models have been proposed for the description of the thermoelectric effects, e.g. TEP and Nernst-Ettingshausen effects. They are referred as: "force balance" model,[1] "energy transfer" model[2] and "current balance" model.[3]

A. "Force balance" model

This model is based on the assumption of strong phonon-carrier interaction. Suppose a conductor under a temperature, dT/dx, and consider phonons as quasi-particles, then, at a given temperature, these quasi-particles will exert a pressure on any other particle which can interact with phonons. If phonon energy-density is u(T) and isotropic, then the pressure from phonon exerted on carrier (electron, etc.) is given by

$$p = \frac{1}{3}u(T). \tag{H1}$$

If temperature gradient is presented, then this will give rise to a pressure gradient, or force, F_x, on electron given by

$$F_x = -\frac{\partial p}{\partial x} = -\frac{1}{3}\frac{\partial u}{\partial T}\frac{dT}{dx}. \tag{H2}$$

If no current is permitted to flow, an electric field, ε_x, acting on the electrons will be required to balance the force, F_x, of Eq. (H2). If electron density is n, then we simply have

$$ne\ E_x + F_x = 0$$

i.e.

$$ne\ E_x = \frac{1}{3}C_g^* \frac{dT}{dx}$$

or

$$\varepsilon_g(0) = \frac{C_g^*}{3ne} \tag{H3}$$

where

$$C_g^* = C_g(\frac{\Theta^*}{T}) \text{ instead of } C_g = C_g(\frac{\Theta}{T}).$$

Using this model, Blewer, et al., formulated a simple equation for $\varepsilon''_{12}(H)$ which is given in Eq. (105).

As is noted in Eq. (1) in Chapter I,

$$\vec{J} = \hat{\sigma}\vec{E}^* + \hat{\varepsilon}''\vec{\nabla}T. \tag{H4}$$

Under high field asymptotic condition, the classical mobility of every carrier is almost equal to Hall mobility, therefore Eq. (H4) takes this simple form

$$J_x = (\frac{C}{H})F_y \tag{H5}$$

where F_y is the effective driving force acting on the carrier system with

$$F_y = (n_h - n_e)eE_y + \nabla_y(P_{el} + P_g). \tag{H6}$$

E is the electrostatic field, P_{el} and P_g are the "pressure" of the electron and phonon "gas" respectively. Under the assumption of isotropic pressure, the pressure $P = \Omega$ (grand canonical potential per unit volume), then

$$J_x = \frac{C}{H}[(n_h - n_e)eE_y + \frac{\partial\Omega}{\partial\mu}\nabla_y\mu + \frac{\partial(\Omega_{el} + \Omega_g)}{\partial T}\nabla T]$$

and

$$\frac{\partial \Omega_{el}}{\partial T} = C_{el}$$

$$\frac{\partial \Omega_{g}}{\partial T} = C_{g}^{*}.$$

Thus

$$\varepsilon''_{12} = -\frac{C}{H}(C_{el} + \frac{\gamma}{3} C_{g}^{*}). \qquad \text{(H7)}$$

Equation (H7) is the same as Eq. (73) derived from Boltzmann equations.

B. "Energy transfer" model

Ziman formulated the TEP in the following way: Assumed there is only electron-phonon interactions, the phonon system will try to come into equilibrium with the displaced electron system, i.e. the phonon system itself will tend to be displaced in its own momentum space. But such a displacement of the phonon system corresponds to a "drift" of the phonons in real space - that is, it corresponds to a heat current. Suppose the drift velocity of the phonons is the same as the drift velocity of the electrons in an electric field (see Section 2, Chapter III), that is

$$V = \frac{\mu e \ell}{P} E.$$

If C_g^* is the specific heat of those phonon interacted with electron, there will be a lattice heat current

$$W_g \sim C_g^* T(\frac{1}{\mu} V). \qquad \text{(H8)}$$

Thus, there will be a Peltier coefficient

$$\pi_g(0) = \frac{W_g}{J} \sim \frac{C_g^* T}{ne} \qquad \text{(H9)}$$

or "dragged" thermoelectric power

$$\varepsilon_g(0) \sim \frac{C^*_g}{ne}. \tag{H10}$$

In fact, the "energy transfer" model is an extension from the concept of Boltzmann equation.

Based on this "energy transfer" idea, we can easily obtain the Nernst-Ettingshausen and Ettingshausen coefficients.

As is noted in Section 2, Chapter II, at the high field (asymptotic) limit, the transverse drift velocities of both carrier (electron and hole) and phonon are

$$\frac{1}{\hbar} V_y^{\pm} = \frac{1}{\hbar} U(\omega) = \frac{CE}{H}. \tag{H11}$$

Therefore, there is a flow of Ettingshausen heat current, that is

$$(W_g)_y = \frac{1}{3} \frac{CE}{H} C^*_g T.$$

And the Ettingshausen coefficient is

$$\pi''_{21g}(H) = \frac{T}{3} \frac{C}{H} C^*_g \tag{H12}$$

and Nernst-Ettingshausen coefficient is

$$\varepsilon''_{21g}(H) = \frac{1}{3} \frac{C}{H} C^*_g. \tag{H13}$$

If we take the scattering mechanisms into account, we should multiply a factor, called efficiency of drag, in these two coefficients. That is,

$$\pi''_{21g} = \frac{\gamma}{3} \frac{C}{H} C^*_g T \tag{H14}$$

and

$$\varepsilon''_{21g} = \frac{\gamma}{3}\frac{C}{H}C^*_g. \tag{H15}$$

For the total Nernst-Ettingshausen and Ettingshausen coefficients, they are given by

$$\varepsilon''_{21} = \frac{C}{H}(C_{el} + \frac{\gamma}{3}C^*_g) \tag{H16}$$

$$\pi''_{21} = \frac{C}{H}T(C_{el} + \frac{\gamma}{3}C^*_g) \tag{H17}$$

where

$$C^*_g = 9Nk_B(\frac{T}{\Theta_D})^3 J_4(\frac{\Theta^*_1}{T}).$$

C. "Current balance" model

This model was proposed by Guenault in 1971. It is based on the fact that there is no net current passing through the metal during the measurement of TEP. Therefore, we may write

$$J_{tot} = J_s + J_e + J_g = 0 \tag{H18}$$

where J_e is the electric current density arising from carrier diffusion mechanism; J_g is produced by the phonon drag mechanism, and J_s is the current density, produced in the steady state to counteract $J_e + J_g$ driven by the Seebeck voltage.

Since the diffusion mechanism is of less interest, the discussion here will be limited only to the study of the drag contribution. In considering the phonon drag contribution to the TEP, we start from the basic equation of J_g in this model, which is given by

$$\vec{J}_g = \sum_q - \left(\frac{\partial N_q}{\partial t}\right)_{\text{carrier-phonon}} e(\vec{\ell}_{\vec{k}'} - \vec{\ell}_{\vec{k}}). \qquad \text{(H19)}$$

This phenomenological equation for J_g can be understood as an effect which the carrier-phonon drag effect "enlarges" the mean free path of carriers, therefore it raises an extra current in addition to the diffusive current. Then,

$$\begin{aligned} \varepsilon_g(0) &= \frac{e}{3\sigma(0)} \cdot \frac{\tau_k}{m} \sum_q \left(\frac{\partial N_q^o}{\partial T}\right)_{\text{scatt}} \hbar\omega_q \gamma(q) \\ &\sim \frac{C_g^*}{3ne} \langle \gamma \rangle. \end{aligned} \qquad \text{(H20)}$$

$\langle \gamma \rangle$ is the overall average of dragging efficiency of phonon system. Equation (H20) is similar to the Eq. (H3) or (H10).

The "current balance" model can be used as well to derive the equation for the Nernst-Ettingshausen coefficient. As is noted that

$$(J_y)_{\text{total}} = (J_s)_y + (J_e)_y + (J_g)_y = 0$$

where

$$(J_s)_y = \sigma_{22}(H) E_y \qquad \text{(H21)}$$

$(J_e)_y$, following Ziman's equation[4] is given by

$$(J_e)_y = \frac{1}{e} \frac{\pi^2 k_B^2 T}{3} \left[\frac{\partial \sigma_{21}(\varepsilon)}{\partial \varepsilon}\right]_{\varepsilon=\zeta} (-\nabla T) \qquad \text{(H22)}$$

as in high field asymptotic,

$$\sigma_{21} = (n_h - n_e) e c \frac{1}{H}, \quad \left(\frac{\partial n_{he}}{\partial \varepsilon}\right) = \mp Z_{h,e}.$$

Hence

$$(J_e)_y = -\frac{C}{H}\left(\frac{\pi^2 k_B^2 T}{3} Z_o\right)(-\nabla T) \qquad \text{(H23)}$$

where (H23) describes the diffusion current in N-E effect. $(J_g)_y$, following Eq. (H19), is given by

$$(J_g)_y = \frac{1}{3}\Sigma(\frac{\partial N_q^o}{\partial T})\gamma(q)S(\hbar q)(\mu_H)(-\nabla T)$$

for a high field asymptotic condition,

$$\mu_H = \frac{C}{H}$$

$$(J_g)_y = \frac{1}{3}\sum_q -(\frac{\partial N_q^o}{\partial T})\gamma(q)\hbar\omega_q \frac{C}{H}(-\nabla T). \qquad \text{(H24)}$$

From Eq. (H21), (H23) and (H24) one obtains

$$\varepsilon''_{21} = \frac{C}{H}(C_{el} + \frac{\gamma}{3} C_g^*) \qquad \text{(H25)}$$

where γ is drag efficiency.

All models yield the same result in the case of isotropic distributions of carriers and phonons and strong carrier-phonon interaction. However, the "current balance" model can be directly extended to other cases. In particular, the parameter $\gamma(q)$ allows to fit for general scattering mechanisms of phonon system.

---

[1] e.g. D. K. E. MacDonald, Thermoelectricity: An Introduction to the Principles (New York, John Wiley, 1962); R. S. Blewer, N. H. Zebouni, and C. G. Grenier, Phys. Rev. 174, 700 (1968).

[2] e.g. J. M. Ziman, Principle of the Theory of Solids (Cambridge University Press, London, 1964).

[3] e.g. A. M. Guenault, J. Phys. F: Metal Phys. 1, 373 (1971).

[4] J. M. Ziman, Electrons and Phonons (Oxford University Press, London, 1960).

VITA

Ching-Long Tsai was born May 25, 1945 in Kaohsiung, Taiwan, Republic of China, and was raised and educated in the elementary school in that area. In July 1964, after his graduation from Provincial Tainan First Senior High School, he passed the entrance examination and entered National Taiwan Normal University. In July 1968, he received his Bachelor Degree in physics and was an assistant in the Department of Physics of the same institute for one year to practice his teaching in physics. In September 1971, he entered the graduate school of Louisiana State University and in May 1973 graduated with the degree of Master of Science in physics. In June 1973, he married the former Yueh-Meei Peng. He is presently a candidate for the degree of Doctor of Philosophy in the Department of Physics and Astronomy of Louisiana State University.

EXAMINATION AND THESIS REPORT

Candidate: Ching Long Tsai

Major Field: Physics

Title of Thesis: Surface and Bulk Transport Coefficients in Antimony

Approved:

Major Professor and Chairman

Dean of the Graduate School

EXAMINING COMMITTEE:

Date of Examination:

July 23, 1976